The Dissertation Committee for David Matthew Trombly
certifies that this is the approved version of the following dissertation:

Modification of Surfaces Using Grafted Polymers: A Self Consistent Field Theory Study

Committee:

Venkat Ganesan, Supervisor

Nicholas Peppas

Pengyu Ren

Isaac Sanchez

Thomas Truskett

Modification of Surfaces Using Grafted Polymers: A Self Consistent Field Theory Study

by

David Matthew Trombly, B.S.

DISSERTATION

Presented to the Faculty of the Graduate School of

The University of Texas at Austin

in Partial Fulfillment

of the Requirements

for the Degree of

DOCTOR OF PHILOSOPHY

THE UNIVERSITY OF TEXAS AT AUSTIN

August 2011

Dedicated to the memory of my grandmother, Antonet Barbich Senini. Her great sacrifice and hard work to find a better life in America and her constant encouragement of her children and grandchildren to strive for excellence in academics have inspired me throughout my education.

Acknowledgments

I am deeply grateful for the support and help of the people who made this thesis and the work entailed in accomplishing it possible over the last five years.

First and foremost, I would like to offer my heartfelt thanks to my adviser, Professor Venkat Ganesan. Without his support, ideas, feedback, encouragement, patience, honesty, and occasional prodding, these projects would not have been completed. It has been a pleasure to be mentored by and to collaborate with him over the last five years. I appreciate him funding my degree and making possible the exclusive focus on my research that was required during these years.

I would also like to thank Dr. Victor Pryamitsyn for the huge contributions he made to this work and its success. I am especially appreciative of the key insights and ideas he contributed to each of my projects, his patience in passing on his thorough knowledge of polymer physics, and the conversations we enjoyed about life and the world. A special thank you also to Dr. Manas Shah for being a resource for questions and advice. I am also very appreciative of Landry, Chetan, Paresh, Thomas, and the other members of the Ganesan group for their help with my research, feedback about my projects, and support in making the work more enjoyable.

I am very appreciative of the teachers and mentors I have had throughout my schooling, and especially to my dissertation committee for being a source of insight and feedback.

I would like to thank Brandon and Daniel for being such great friends while we shared in this season of life. I would also like to thank Gerrit, Melissa, John, Jessica, Paul, Joyie, Wes, Jeff, Mel, and Jeremy for their friendship and prayers, and for helping make this time more enjoyable.

I am extremely thankful to Pastor P.G. Mathew for the role he has played in my life. Thank you for your prayers and deep care, and for always being willing to speak the truth in love. I also am very appreciative to Pastor Juan Sanchez, Mr. Suman Jha, Mr. Gregory Perry, Dr. Richard Spencer, and the leaders and members of Grace Valley Christian Center and High Pointe Baptist Church for their support, counsel, encouragement, and prayers during my PhD and my entire life.

I would like to express my utmost appreciation to my parents for all they have done for me in my life, including their love, advice, understanding and support during my PhD. I am also so appreciative to Kristina, Juliana, the Robys, the Manderfields, and my grandparents for their love, patience, support, and prayers.

Words cannot express my appreciation for Sarah and how much her presence and support has meant to me over the last five years. Thank you for encouraging me to push forward, listening in the hard times, being patient

when I was not, and filling my life with love and happiness.

Finally, I thank and praise my Lord and Savior Jesus Christ for being with me and guiding me through every path of my life, including my PhD and time in Austin.

Modification of Surfaces Using Grafted Polymers: A Self Consistent Field Theory Study

Publication No. _____

David Matthew Trombly, Ph.D.
The University of Texas at Austin, 2011

Supervisor: Venkat Ganesan

This research focuses on the modeling of surfaces decorated by grafted polymers in order to understand their structure, energetics, and phase behavior. The systems studied include flat and curved surfaces, grafted homopolymers and random copolymers, and in the presence of solvent conditions, homopolymer melt conditions, and diblock copolymer melt conditions. We use self-consistent field theory to study these systems, thereby furthering the development of new tools especially applicable in describing curved particle systems and systems with chemical polydispersity.

We study a polymer-grafted spherical particle interacting with a bare particle in a good solvent as a model system for a polymer-grafted drug interacting with a blood protein in vivo. We calculate the energy of interaction between the two particles as a function of grafting density, particle sizes, and

particle curvature by solving the self-consistent field equations in bispherical coordinates. Also, we compare our results to those predicted by the Derjaguin approximation.

We extend the previous study to describe the case of two grafted particles interacting in a polymer melt composed of chains that are chemically the same as the grafts, especially in the regime where the particle curvature is significant. This is expected to have ramifications for the dispersion of particles in a polymer nanocomposite. We quantify the interfacial width between the grafted and free polymers and explore its correlation to the interactions between the particles, and use simple scaling theories to justify our results.

In collaboration with experimentalists, we study the behavior of the glass transition of polystyrene (PS) films on grafted PS substrates. Using the self consistent field theory methods described above as well as a percolation model, we rationalize the behavior of the glass transition as a function of film thickness, chain lengths, and grafting density.

Grafting chemically heterogeneous polymers to surfaces in melt and thin film conditions is also relevant for both particle dispersion and semiconductor applications. To study such systems, we model a random copolymer brush in a melt of homopolymer that is chemically identical to one of the blocks. We modify the self-consistent field theory to take into account the chemical polydispersity of random copolymer systems and use it to calculate interfacial widths and energies as well as to make predictions about the window in which perpendicular morphologies of diblock copolymer are likely to

form. We also explore the effect of the rearrangement of the chain ends on the surface energy and use this concept to create a simple modified strong stretching theory that qualitatively agrees with our numerical self-consistent field theory results.

We explicitly study the system that is most relevant to semiconductor applications - that of a diblock copolymer melt on top of a substrate modified by a random copolymer brush. We explore the morphologies formed as a function of film thickness, grafting density, chain length, and chain blockiness, and make predictions about the effect of these on the neutral window, that is, the range of brush volume fractions over which perpendicular lamellae are expected to occur.

Table of Contents

List of Figures

Chapter 1

Introduction

Many emerging technologies depend on grafting polymers to surfaces in order to tune the surfaces for applications. In this work, we advance this goal through several studies considering the physics of polymers grafted to surfaces. In particular, our goals are to 1) provide insight for experimentalists on how polymer grafted systems behave as a function of the diverse parameters that characterize these systems, and 2) develop fast and accurate modeling tools that can be used to characterize and understand grafted polymer systems more effectively.

1.1 Background and Motivation

Grafting polymers to surfaces is an effective way to modify them and improve their properties. This approach is used in a variety of applications, including drug [111, 157, 193] and nanocomposite [145] design, membranes, thin films,[145] and semiconductors and electronic materials. [70–72, 80, 129, 130, 151, 176, 194, 203]

A common goal in grafting polymers to surfaces is to change the manner by which these surfaces interact with other surfaces. This is often moti-

vated by the presence of strong van der Waals attractions between particles and particle surfaces, which lead to aggregation and/or segregation. [111, 157] Grafting polymers to the particle surfaces has been shown to be an effective approach to overcome such attractions. [111, 157, 193] For example, in drug delivery applications, experimentalists graft polymers to drugs in order to induce a repulsion between the drug and blood proteins. [111, 157, 193] This prevents thrombosis and uptake by the mononuclear phagocytic system, outcomes that are both catastrophic for effective delivery. [111, 157] Similarly, in nanocomposite applications, polymers are grafted to fillers to introduce a repulsion between the nanoparticles in order to disperse the particles in the polymer matrix, thereby improving the properties of the composite. [145] In membrane applications, experimentalists are currently researching a method of preventing the attraction of biological fouling agents by using polyethylene glycol (PEG) grafts.

A different, albeit related, goal of modifying surfaces using polymers is to modulate the interactions between the surface and a bulk polymer matrix. In nanoparticle applications, this goal is related to the previous one because the attraction and repulsion of the particles is directly connected to the energetics between the surfaces and the polymer matrix. In semiconductor applications where the self-assembly behavior of diblock copolymers has been proposed as a method to create small, perpendicularly aligned features, modification of the substrate with random or diblock copolymers has been shown to be an effective way of tuning the surface energy between the substrate and the blocks. [70–

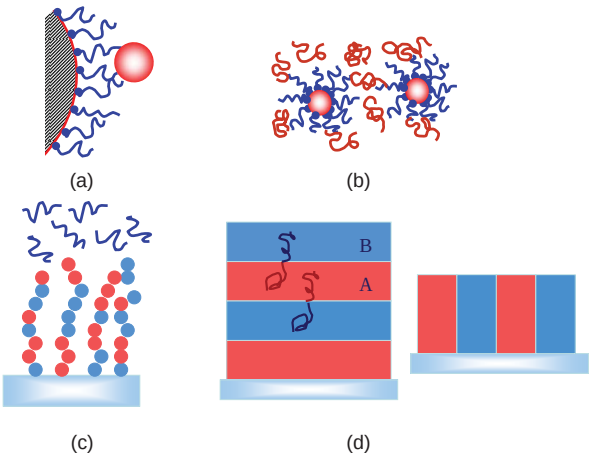

Figure 1.1: Schematics of the systems we propose to study; (a) a polymer-grafted drug interacting with a blood protein; (b) a polymer-coated nanoparticle in a nanocomposite; (c) a random copolymer brush interacting with a polymer melt; (d) diblock copolymer thin films with parallel (left) and perpendicular (right) alignments.

72, 80, 129, 130, 151, 176, 194, 203] Thus, instead of the parallel arrangement associated with a preference of one of the blocks for the substrate, the diblock copolymers have been shown to align perpendicularly.

Implicit in the discussion above is the diversity of polymers that have been used to modify surfaces, as well as the diversity of chemical milieus to which these polymers are exposed. Polymers that have been used as modifiers include homopolymers, mixed chemically different homopolymers, diblock copolymers, Y-shaped copolymers, random copolymers, and gradient copolymers. These polymers have been used in contexts ranging from solvent and melt conditions, chemically identical or different homopolymers, diblock

copolymers, or combinations thereof. These environments each have unique interactions with the grafted polymers.

The geometry of the systems in which polymers may be used to modify surfaces is also diverse. In many cases, the surfaces are flat or are large enough to be assumed as such. However, as the sizes of particles used in polymeric systems decreases to be on the order of the size of the polymers ($\sim$ 10 nm), the curvature of the particles becomes significant and may lead the system to behave differently.

The design of the next generation of specialty polymer materials will require a detailed molecular level understanding of the way the polymers and surfaces behave as well as details about their structure and energetics. In modeling such systems, our goal is to provide experimentalists with this qualitative understanding, especially in systems where the large number of system parameters make experimentally exploring the parameter space prohibitively time consuming.

Modeling of grafted polymer systems has a long history that has often borrowed concepts from other areas of physics. Initially, simple scaling theories were used to model these systems. [4, 33]These theorized that when the chains are grafted sparsely to the surface, they are able to maximize their configurational entropy by taking on a random walk configuration. However, when the chains become more densely grafted, they must stretch for steric reasons, leading to an extended configuration called a polymer brush. Using these ideas, researchers found expressions for the brush height as a function of the

grafting density and chain length. Atomistic simulations have also been used to describe grafted polymer systems, but these simulations tend to be rather expensive. In contrast, early researchers used field theories with analogies to quantum and classical mechanics to describe a polymer brush and found that it accurately predicted the correct behavior of these systems, especially in the limit of large grafting density. A first effort in this vein used a simplifying assumption to create a strong stretching theory to describe a polymer brush. [147] This was later extended to a more complete numerical self-consistent field theory. [53, 54]This theory has the advantage of being much less expensive than atomistic simulations while it has been shown very accurately describe the system in certain parameter regimes. Hence, the theory was used to model polymer brushes attached to flat plates in solvent and melt conditions as well as in a variety of chemical environments.

More recently, self-consistent field theory was used in order to assess the effect of curvature in polymer grafted particles in a solvent as well as a particle interacting with a grafted flat plate.[98, 99] However, work remained to be done in the context of a polymer-grafted particle interacting with a bare particle, the system that is relevant to the drug delivery application mentioned above, as well as a two polymer-grafted particles interacting in a melt, relevant to nanocomposite applications. Additionally, the use of self-consistent field theory to describe chemically polydisperse grafted systems has received very little attention. In this work, we seek to fill in these gaps by developing tools that will allow them to be modeling and provide insight to experimentalists.

We detail these endeavors, which function as chapters, below.

1.2 Outline of Dissertation

1.2.1 Interactions between polymer grafted particles and bare particles in a solvent

[205]

We use self-consistent field theory (SCFT) to study the interactions between a polymer-grafted spherical particle and a bare spherical particle and explore how these interaction energies depend on the radii of the two particles and the grafting density. We find that the magnitude of the interaction energies increases with the radii of both the grafted and bare particles and with increasing grafting density. We also find a universal scaling law for the interaction potential which exhibits a power-law dependence on both particle sizes, a linear dependence on grafting density, and a logarithmic dependence on interparticle distance with a range of interaction that scales with brush height. We compare our numerical results to those obtained using the Derjaguin approximation.

1.2.2 Interfacial widths and interactions of polymer grafted particles in polymer matrices

We study the interactions between polymer-grafted nanoparticles immersed in a chemically identical polymer melt using a numerical implementation of polymer mean-field theory. We focus on the interpenetration width between the grafted and free chains and its relationship to the polymer-mediated

interparticle interactions. To this end, we quantify the interpenetration width as a function of particle curvature, grafting density and the relative molecular weights of the grafted and free chains. We show the onset of wetting and dewetting as a function of these quantities and explain our results through simple scaling arguments to include the effects of curvature. Subsequently, we show that the interparticle potentials correlate both quantitatively with the trends displayed by the interpenetration widths.

1.2.3 Glass Transition Behavior of PS Films on Grafted PS Substrates

We develop a model to justify results from experimental collaborators probing the glass transition behavior of polystyrene (PS) films on grafted PS layers of the same chemical identity as a function of film thickness. The experimental results suggest that the T_g of PS films on brush substrates decreases with decreasing film thickness. The thickness dependence of T_g was observed to be more pronounced for the films on the shorter brushes with the high grafting density. We propose a qualitative rationalization of the observations by invoking both interfacial energy considerations as well as by adapting the percolation model for the glass transition of polymer films.

1.2.4 Interfacial widths and energies in grafted random copolymer brushes in a homopolymer melt

[206]

We use polymer self-consistent field theory to quantify the interfacial

properties of random copolymer brushes (AB) in contact with a homopolymer melt chemically identical to one of the blocks (A). We calculate the interfacial widths and interfacial energies between the melt and the brush as a function of the relative chain sizes, grafting densities, compositions of the random copolymer in the brush, and degree of chemical incompatibility between the A and B species. Our results indicate that the interfacial energies between the melt and the brush increase (signifying expulsion of the free chains from the brush) with increasing grafting density, chemical incompatibility between A and B components, and size of the free chains relative to the grafted chains. We also compare the interfacial energies of random copolymers of different sequence characteristics and find that, except for the case of very blocky or protein-like chains, blockiness of the copolymer has only little effect on interfacial properties. Our results for interfacial energies are rationalized based on the concept of an "effective volume fraction" of the brush copolymers, f_{eff}, which quantifies the chemical composition of the brush segments in the interfacial zone between the brush and melt copolymers. Using this concept, we modify the strong-stretching theory of brush-melt interfaces to arrive at a simple model whose results qualitatively agree with our results from self-consistent field theory. We discuss the ramifications of our results for the design of neutral surfaces.

1.2.5 Phase behavior of diblock copolymer thin films mediated by a grafted random copolymer brush

We model a diblock copolymer thin film in contact with a random copolymer brush using self-consistent field theory, focusing on the regime of parameters where lamellar morphologies have been observed. We study the morphologies formed as a function of the chemical composition of the brush, grafting density of the brush, relative chain lengths of the grafted and free species and the blockiness of the grafted chains. We find two novel features of templating behavior in the brush driven by the self-assembly of the diblock copolymer film. First, the ends of the grafted chains may rearrange themselves to create a more favorable interface, an effect which is present in both the parallel and perpendicular morphologies and increases for increasing blockiness. Second, the brush may splay laterally, an effect which is present only in the perpendicular lamellae. The latter feature leads to nontrivial free energy differences between the parallel and perpendicular lamellae. We explicitly find the parametric window for the stability of perpendicular lamellae and compare against the trends suggested by surface energy considerations. Such comparisons indicate that viewing the grafted surface purely in terms of the surface energies of the components of the diblock copolymer may leads to erroneous conclusions regarding the occurrence of parallel and perpendicular morphologies.

Chapter 2

Interactions between polymer-grafted particles and bare particles for biocompatibility applications

2.1 Introduction

Surface modification of drugs by grafting polymers is a widely used strategy for improving biocompatibility. Proteins in the blood quickly adsorb to foreign surfaces by Van Der Waals forces, leading either to coagulation and thrombosis or uptake by the mononuclear phagocyte system (MPS). [111, 157] Grafting a polymer layer unto the biomolecule introduces a repulsive force, potentially preventing thrombosis and, if desired, allowing for the targeting of the biomolecule to regions other than MPS organs. [193]

Many prior theoretical studies have examined the conformation and properties of polymers grafted on surfaces of various geometries. Polymers grafted on flat surfaces have been studied using scaling theory,[4, 33] self-consistent field theory (SCFT),[147, 235] Monte Carlo simulations,[23, 26] and molecular dynamics simulations.[152] The first studies used scaling theories to obtain expressions for brush height as a function of grafting density and the chain length, [4, 33] while later studies demonstrated a parabolic monomer density profile in the brush and also yielded expressions for the interaction energy

as a function of distance between two polymer-grafted flat plates. [147, 235]

For many biomedical applications, the biomolecule can be envisioned as a spherical drug, underscoring the need to understand the effects of curvature on the physics of grafted polymer layers. Curvature can be symbolized in terms of the relative size of the spherical particle and the grafted polymer layer, $R_{\text{grafted}}/H_{\text{brush}}$, where R_{grafted} is the radius of the polymer-grafted particle and H_{brush} is the average height of the polymer brush. Examples from the experimental literature pertaining to biomedical applications have reported a range of $R_{\text{grafted}}/H_{\text{brush}}$ from order 1 to 10, [73, 81, 193] confirming the need to model the effects of curvature.

Prior modeling of curved systems has extensively considered two limits of $R_{\text{grafted}}/H_{\text{brush}}$: $R_{\text{grafted}}/H_{\text{brush}} \gg 1$, which is the flat plate limit discussed above, and $R_{\text{grafted}}/H_{\text{brush}} \ll 1$, in which the polymer-grafted particle can be modeled as a star polymer. The latter scenario has been studied extensively using scaling theory, [32, 227] and MC. [116] Density profiles for this case have been shown to decay as a power law from the core of the star polymer and the interaction energy between two stars has been shown to have a logarithmic dependence on the interparticle distance. [32, 227]

Although for some applications the above limiting cases may apply, it is evident from the discussion of the experimental parameters above that situations where the characteristic lengths of the grafted particle and polymer chains are comparable emerge in many applications. In this intermediate regime, the physical features of polymers grafted on an isolated sphere or

cylinder have been studied using SCFT,[10, 31, 224] and molecular dynamics simulations.[153] In this context, Wijmans and Zhulina [224] used SCFT to obtain expressions for the brush height and also monomer density profiles. The latter exhibits a power-law dependence on the distance from the center of the particle that becomes more prominent with increasing curvature.

For modeling the biological applications discussed above, an understanding of the interactions arising between a polymer-grafted sphere and a bare sphere (representing the MPS proteins) is needed. The bare particle is also viewed as a sphere since the polymer-grafted particles and MPS proteins may both be comparable in size. [111, 193] In the context of interparticle interactions, we note that early work by Gast and coworkers used a modified Derjaguin approximation to estimate the energy of interaction between two diblock copolymer-grafted spheres of equal size. [117] Later work by Roan and Kawakatsu used SCFT in a bispherical coordinate system to explore the interaction between two equally-sized polymer-grafted spheres. They reported a repulsive force for large interparticle distances that became sharply attractive for small interparticle distances. [174] More recently, Kim and Matsen used SCFT with a modified numerical method to study the interaction between two brush-coated spheres of equal size and demonstrated that the interparticle potential is purely repulsive for all interparticle distances. [99] Kim and Matsen have also explored the case of a flat polymer-grafted surface interacting with a bare spherical particle, reporting monomer density profiles and the interaction energies as a function of interparticle distance. [98] The problem of two

polymer-grafted spheres of equal size has also been studied using Monte Carlo simulations and density-functional theory. [196]

In this paper, we use SCFT to further the research cited above by exploring the interaction between a polymer-grafted spherical particle (drug) and a bare spherical particle (protein). Explicitly, we consider situations in which the polymer-grafted particle cannot be viewed as a flat plate, but falls in the regime between the flat and star polymer limits. Furthermore, we extend prior studies by considering the physically applicable scenario in which the two spherical particles being studied are unequal in size. We explore various parameters relevant to such situations, with particular attention to the significance of curvature in the system.

The actual interaction between a polymer-coated drug and a blood protein consists of an attractive contribution between the particles and a repulsive contribution resulting from the grafted chains. By modeling only the repulsive interaction induced by the polymer chains, we seek to quantify the locus of parameters that would be necessary to prevent a net attraction for a given interparticle attraction. Additionally, in assuming that the protein behaves as a hard sphere, we assume that it will remain in a globular state while interacting with the brush. In reality, this assumption may not be true and could be lifted by also modeling the physics of the protein chain.

While most of our work was motivated by the objective of discerning the design parameters for biomedical applications, our results are expected to have significance for synthetic polymer applications, especially those focused on

assembling particles on curved grafted interfaces such as in spherical phases of diblock copolymers. [167, 221] In such contexts, by quantifying the interaction energies our results provide insights into the influence of curvature upon the location and organization of particles in self-assembled phases.

The outline of the paper is as follows: in Section 2.2 we summarize key details pertaining to the theory used in the paper. In Section 2.3 we present results in the form of density profiles and energies. Finally, in Section 2.4 we demonstrate an empirical scaling relationship for energy results and discuss the results in light of previous work.

2.2 Theory and Numerical Methods

We use self consistent field theory for tethered polymer chains [53] to describe an isolated polymer-grafted sphere as well as the interactions between a polymer-grafted sphere and a bare particle. The polymer is modeled as a Gaussian chain whose conformations are described by the continuous curve $\mathbf{R}_\alpha(s)$, where α represents different polymer chains and s is a continuous chain index coordinate running from 0 to N, where N is the chain length. Using this framework, in an implicit (good) solvent framework the partition function in the canonical ensemble can be written as[53]

$$Z = \int \prod_\alpha D\mathbf{R}_\alpha(s) \exp(-\beta U_0[\mathbf{R}_\alpha(s)] - \beta U_1[\mathbf{R}_\alpha(s)]) \delta(\mathbf{R}_\alpha(0) - \mathbf{r}_\perp), \quad (2.1)$$

where $\delta(\mathbf{r} - \mathbf{r}_\perp)$ denotes a two-dimensional delta function enforcing the fact that the ends of the grafted chains are located at the surface on which chains

are grafted (denoted by $\mathbf{r}_\perp$). U_0 corresponds to bonded interactions and in the Gaussian chain model is usually described by an elastic potential:[45]

$$\beta U_0[\mathbf{R}_\alpha(s)] = \frac{3}{2b^2}\sum_\alpha \int_0^N ds \left|\frac{\partial \mathbf{R}_\alpha(s)}{\partial s}\right|^2, \tag{2.2}$$

where b denotes the statistical segment length. U_1 represents the energy that arises from the repulsion of monomers due to the solvent-mediated excluded volume interactions and is modeled as[45]

$$\beta U_1[\mathbf{R}_\alpha(s)] = \frac{\upsilon}{2}\sum_\alpha \sum_\beta \int_0^N ds \int_0^N ds' \delta(\mathbf{R}_\alpha(s) - \mathbf{R}_\beta(s')), \tag{2.3}$$

where υ denotes the excluded volume parameter.

An arbitrary potential $w(\mathbf{r})$ can be introduced and used to transform the above theory into a field theory dependent on this potential. [54] The partition function then can be written as

$$Z = \int Dw \exp(-\beta H[w(\mathbf{r})]). \tag{2.4}$$

where H is the effective Hamiltonian of the system and is given as

$$H[w(\mathbf{r})] = \frac{1}{2B}\int d\mathbf{r}[w(\mathbf{r})]^2 - \sum_{j=1}^{n} \ln Q(\mathbf{r}_{\perp,j}; [iw]). \tag{2.5}$$

in which n denotes the number of grafted chains, assumed in general to be distributed non-uniformly on the surface. In eq. (2.5), length scales have been nondimensionalized by R_g, and the potential w and the continuous chain index s by N. With this nondimensionalization, the constant $B = \upsilon N^2/R_\mathrm{g}^\mathrm{d}$ emerges

as a dimensionless excluded volume parameter. Q is the partition function of a single grafted chain in the field $w(\mathbf{r})$ and is defined as

$$Q = \int d\mathbf{r} q_{\mathbf{r}_\perp}(\mathbf{r}, s = 1; [iw]). \tag{2.6}$$

In the above equation, the field $q_{\mathbf{r}_\perp}(\mathbf{r}, s; [iw])$, called a chain propagator, provides a statistical description of chain conformations, and satisfies the diffusion equation[54]

$$\begin{aligned} \frac{\partial q_{\mathbf{r}_\perp}(\mathbf{r}, s; [iw])}{\partial s} &= \nabla^2 q_{\mathbf{r}_\perp}(\mathbf{r}, s; [iw]) - w(\mathbf{r}) q_{\mathbf{r}_\perp}(\mathbf{r}, s; [iw]); \\ & \quad q_{\mathbf{r}_\perp}(\mathbf{r}, s = 0; [iw]) = \delta(\mathbf{r} - \mathbf{r}_\perp). \end{aligned} \tag{2.7}$$

The thermodynamic limit of this system corresponds to allowing the number of chains and the box size to approach infinity while maintaining a finite grafting density σ (defined as the number of chains per unit surface area of the grafted sphere). Taking this limit allows us to use a quenched average over the positions of the grafting sites in eq. (2.5) instead of a sum over grafting sites. The result is a modified expression for the effective Hamiltonian of the system:

$$H[w(\mathbf{r})] = \frac{1}{2B} \int d\mathbf{r} [w(\mathbf{r})]^2 - \sigma \int d\mathbf{r}_\perp \ln Q(\mathbf{r}_\perp; [iw]). \tag{2.8}$$

Note that σ has been nondimensionalized by R_g^2.

Replacing eq. (2.4) with the value of the exponent at its saddle point constitutes the approximation termed as self-consistent field theory (SCFT). The saddle point field $w^*(\mathbf{r})$ can be solved by taking a functional derivative of eq. (2.8) with respect to $w(\mathbf{r})$, resulting in the self consistency condition,

$$w^*(\mathbf{r}) = BC\phi(\mathbf{r}). \tag{2.9}$$

where $C = \rho_0 R_g^d / N$ ($\rho_0 = 1/a^d$ is the average monomer number density). The parameter C is assumed to be unity throughout, which is equivalent to redefining σ as σ/C and grouping BC in eq. (2.9). Similarly, all energies we report can also be seen as normalized by C. The volume fraction $\phi(\mathbf{r})$ (normalized by ρ_0) is found with

$$\phi(\mathbf{r}) = \frac{1}{C} \int_0^1 ds q_c(\mathbf{r}, s) q(\mathbf{r}, 1-s), \tag{2.10}$$

where the fields $q_c(\mathbf{r}, s)$ and $q(\mathbf{r}, s)$ are complementary chain propagators corresponding to the grafted and free ends of the chain, respectively. They each satisfy eq. (2.7) with initial conditions

$$q_c(\mathbf{r}, s=0) = \frac{\sigma \delta(\mathbf{r} - \mathbf{r}_\perp)}{q(\mathbf{r} = \mathbf{r}_\perp, s=1)} \tag{2.11}$$

and

$$q(\mathbf{r}, s=0) = 1. \tag{2.12}$$

The free energy of the system can then be approximated using the value of $H[w(\mathbf{r})]$ at the saddle point as

$$F(N,V,T) = -k_B T \ln Z = -\frac{1}{2B} \int d\mathbf{r} [w^*(\mathbf{r})]^2 - \sigma \int d\mathbf{r}_\perp \ln Q(\mathbf{r}_\perp; [iw^*]). \tag{2.13}$$

Computation of $F(N,V,T)$ requires the solution of equations (2.7) and (2.9) - (2.11) with the appropriate boundary conditions (discussed below). In order to fully capture the two-sphere nature of the drug-protein system, we solved the diffusion equation in a bispherical coordinate system using the alternating-direction implicit method described by Roan and Kawakatsu.

[174] We used a constant η mesh size of 0.02, a constant θ mesh size of $\pi/100$, and a value of Δs that allowed the solution to remain stable. A convergence criterion of 0.0001 on mean squared difference in potential $w^*(\mathbf{r})$ was used. For the isolated sphere, the corresponding equations were solved numerically using a Crank-Nicolson method. [1]

Typically, the conditions $q = 0$ and $q_c = 0$ (Dirichlet boundary conditions) are used on the surfaces of both the grafted and bare spheres to enforce the impenetrability of the polymers into the surfaces. [174] Because the polymers are unable to enter the bare sphere, we imposed the Dirichlet boundary condition at this surface. However, on the grafted sphere, consistency with the grafting constraint (2.11) requires that the Dirichlet boundary condition be imposed a small ϵ away from the grafting surface (inside the sphere). [39] Kim and Matsen pointed out that numerical errors arising from this feature can lead to spurious attractive interactions in the context of numerical solutions in the bispherical coordinate system. [99] To avoid such errors, we used Neumann boundary conditions, $\mathbf{n} \cdot \nabla q_c = 0$ and $\mathbf{n} \cdot \nabla q = 0$ at the grafted surface. This allowed the imposition of the boundary condition at the same location as the delta function initial condition and resulted in the purely repulsive potentials that are predicted by physical arguments. We comment on the relationship between the Neumann and Dirichlet boundary conditions in the results section.

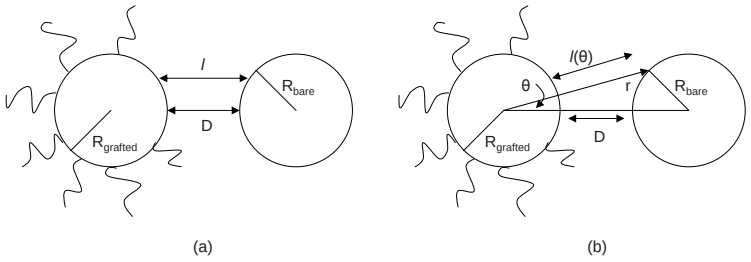

Figure 2.1: A schematic illustration of the chain compression used in (a) standard and (b) modified Derjaguin approximations for estimating the energy between a polymer-grafted sphere and a bare sphere.

2.2.1 Derjaguin Approximation

In this section, we derive the appropriate modified Derjaguin approximation (originally proposed by Kim and Matsen[99]) which provides an estimate of the interaction energy between a polymer-grafted sphere and a bare sphere. The notation used is defined in Figure 2.1. This approximation deduces the interaction energies by estimating the costs of compression of grafted chains due to the bare particle. The standard Derjaguin approximation assumes that compression is based on the perturbation of the brush height in the direction of the axis connecting the spheres, while the modified approximation assumes that compression is based on perturbation of the brush height in the radial direction. The latter yields much improved results for the related case of two brush-covered spheres of the same size. [99] We derive such a modified approximation for our system and report the values of free energy calculated using the standard and modified Derjaguin approximations in the main text.

Extending the previous work by Kim and Matsen, the energy of interaction is estimated as

$$F(D; R_{\text{grafted}}, R_{\text{bare}}) = \sigma \int_0^{\pi} d\theta 2\pi R_{\text{grafted}}^2 \sin\theta \Delta f(l(\theta); R_{\text{grafted}}, R_{\text{bare}}) \quad (2.14)$$

where $\Delta f(l(\theta); R_{\text{grafted}}, R_{\text{bare}}) = f(l; R_{\text{grafted}}, R_{\text{bare}}) - f(H_{\text{brush}}; R_{\text{grafted}}, R_{\text{bare}})$ where $f(l)$ denotes the energy cost of compressing one polymer chain radially. The latter is obtained using strong stretching theory (SST) or self-consistent field theory (SCFT). The details of obtaining $f(l)$ with SST can be found in Kim and Matsen's paper. These authors provide the expression for the height of the brush on a sphere

$$\frac{H_{\text{brush}}}{H_0} = \left(1 + \frac{3H_{\text{brush}}}{4R_{\text{grafted}}} + \frac{H_{\text{brush}}^2}{5R_{\text{grafted}}^2}\right)^{-1/3} \quad (2.15)$$

from SST. Here H_0 is the height of a brush on a flat plate with the same grafting density. To obtain H_0, we note that the normal SST prediction for brush height $H_{0,max}$ (corresponding to the maximum height of a parabolic brush) is given by SST as $H_{0,max} = (24B\sigma/\pi^2)^{1/3}$, where all variables have been nondimensionalized as described in the theory section of the main text. When the grafted and bare particles are both small, in order to describe the system more realistically, we adjust the SST expression for $H_{0,max}$ using eq. (2.19). Using the parabolic density profile from Milner and coworkers in this equation suggests that $H_0 = (H_{0,max}^2/5)^{1/2}$. For all other cases, we assume that $H_0 = H_{0,max}$.

Using the law of cosines, we have

$$\cos\theta = \frac{(l + R_{\text{grafted}})^2 + k^2 - R_{\text{bare}}^2}{2k(l + R_{\text{grafted}})}, \quad (2.16)$$

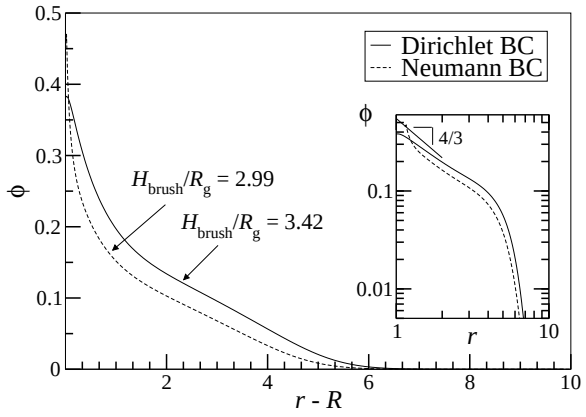

Figure 2.2: A comparison of volume fractions $\phi(r)$ of the grafted segment for Neumann and Dirichlet boundary conditions at the grafted surface using SCFT for a polymer-grafted sphere with $R/R_g = 1.0$ (Dirichlet) and $R/R_g = 1.14$ (Neumann), $\sigma = 3.335$, and $B = 100$. The inset compares volume fractions to the exponent predicted by Wijmans and Zhulina. [224]

where $k = R_{\text{grafted}} + D + R_{\text{bare}}$ is the center-to-center distance of the spheres. Using the above we can transform eq. (2.14) to an integral over l as

$$F(D; R_{\text{grafted}}, R_{\text{bare}}) = \\ 2\pi\sigma R_{\text{grafted}}^2 \int_D^{H_{\text{brush}}} dl \left[\frac{2k^3 - 2kl^2 - 2kR_{\text{grafted}}^2 - 2kR_{\text{bare}}^2 - 4klR_{\text{grafted}}}{(2kl + 2kR_{\text{grafted}})^2} \right] \Delta f(l). \tag{2.17}$$

In the limit of large R_{grafted} and R_{bare}, the above expression reduces to the standard Derjaguin approximation,

$$F(D; R_{\text{grafted}}, R_{\text{bare}}) = 2\pi\sigma \frac{R_{\text{grafted}} R_{\text{bare}}}{R_{\text{grafted}} + R_{\text{bare}}} \int_D^{\infty} dl \Delta f(l). \tag{2.18}$$

2.3 Results

2.3.1 Polymer-grafted sphere

Some justification is necessary for the use of the Neumann boundary condition instead of the more commonly used Dirichlet condition. Physically, the boundary condition $\mathbf{n} \cdot \nabla q = 0$ corresponds to a weak surface attraction between the polymer segments and the surface (with a magnitude of attraction that exactly counteracts the depletion effect typical of a Dirichlet boundary condition at the surface). [53] While this is in fact a likely feature for many situations involving polymers grafted on surfaces, the density profiles for polymers grafted onto an isolated spherical particle can be used to compare the differences (from a modeling viewpoint), if any, in using the Neumann verses Dirichlet boundary conditions.

Results from the use of these two boundary conditions at the grafted surface is demonstrated for a polymer-grafted sphere in Figure 2.2. In order to obtain these results, the depletion layer associated with the Dirichlet boundary condition is removed for the density profiles. The Neumann boundary condition is then imposed at the point where the Dirichlet condition achieves a maximum. In the inset, the power-law behavior predicted by Wijmans and Zhulina is demonstrated, although the exact exponent differs slightly from their analytical prediction. It is observed from Figure 2.2 that the use of the Neumann boundary condition changes the density profile only minimally relative to the Dirichlet boundary condition. As shown in the plot, brush heights are also comparable. Moreover, below we demonstrate that the brush

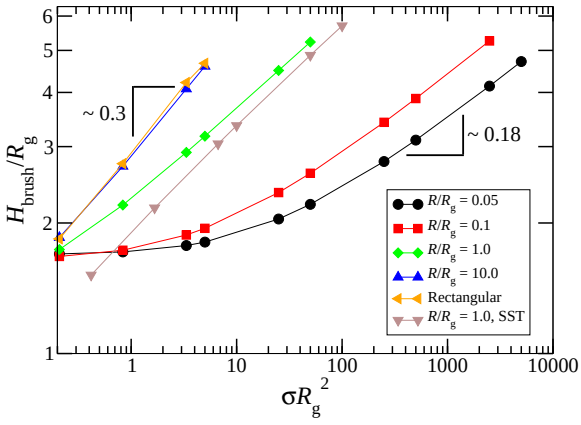

Figure 2.3: Average height of grafted polymer, $H_{\text{brush}}/R_{\text{g}}$ as a function of σR_{g}^2 for various sphere radii R/R_{g}; $B = 100$.

heights determined using the Neumann boundary condition exhibit the theoretical scaling laws predicted for the curvature dependence. Since the Neumann boundary condition also prevents numerical errors associated with the Dirichlet boundary condition in the bispherical coordinate system, we use the Neumann boundary condition throughout this paper.

We first present results for the brush height on an isolated sphere of radius R covered by a grafted polymer layer. The brush height is calculated using an expression from Dan and Tirrell:[31]

$$H_{\text{brush}} = \left(\frac{\int_R^\infty dr r^2 (r-R)^2 \phi(r-R)}{\int_R^\infty dr r^2 \phi(r-R)} \right)^{1/2}. \tag{2.19}$$

Though in general we use R/H_{brush} to quantify curvature, in order to compare our results for brush height with previous scaling results, we characterize the

curvature of the system by the nondimensional variable R/R_g, where R_g is the radius of gyration of the unperturbed polymer chain. When the radius is large compared to R_g, the system is expected to be minimally curved and behaves similarly to a polymer-grafted flat plate. On the other hand, when R is small compared to R_g, the system is very curved and should resemble a star polymer. Figure 2.3 displays the average polymer height as a function of the grafting density for increasing values of R/R_g. When R/R_g is very small, it is observed that the average height (nondimensionalized by R_g) changes minimally in the small σR_{g}^2 regimes, corresponding to the "mushroom" regime. [33] The formation of a "brush" can be seen in the increasing height with increasing σR_{g}^2, eventually leading to a regime where $H_{\mathrm{brush}}/R_g \sim \sigma^{0.18}$, which is close to the value of $\sigma^{0.2}$ predicted scaling arguments for a star polymer.[32, 227] As R/R_g is increased, the shape of the curves becomes invariant and, above about $R/R_{\mathrm{g}} = 10$, reaches a scaling approximately equivalent to that predicted by Alexander[4] and de Gennes[33] for a flat brush, $H_{\mathrm{brush}}/R_g \sim \sigma^{1/3}$. Figure 2.3 also displays the prediction of H_{brush} from strong-stretching theory (SST) presented in Kim and Matsen (also cited in eq. (2.15) in Section 2.2.1 of this paper) for $R/R_g = 1.0$. [99] We observe that the SST predicts the SCFT curves fairly well and improves at moderate surface coverage as should be the case for SST. [97]

2.3.2 Interactions between a polymer-grafted sphere and a bare sphere

2.3.2.1 Effect of varying $R_{\mathbf{grafted}}/H_{\mathbf{brush}}$

We present our results for the two-sphere system by considering the interaction between a polymer-grafted particle and a bare particle. In Figures 2.4 (a)-(b) we present 2-D segment volume fraction profiles for the polymer-grafted particle on approach of a bare particle. As the bare particle begins to approach the brush, we observe that the brush becomes compressed. Additionally, as illustrated especially in Figure 2.4 (a), due to the curvature of the grafted sphere, the brush is able to deform around the bare particle. In both Figures 2.4 (a)-(b) the grafted particle and the bare particle are of equal size, the dimensionless grafting density σR_{g}^2 equals 0.8335, and the bare particles are approximately equally deep into the polymer layer (as measured by D/H_{brush}). However, the polymer chains grafted to the larger sphere (Figure 2.4 (b)) are seen to be more perturbed from their equilibrium conformations than the chains grafted to the smaller sphere (Figure 2.4 (a)). This can be rationalized by noting that decreased curvature of the grafted particle (ie, larger $R_{\mathrm{grafted}}/H_{\mathrm{brush}}$) prevents the chains from splaying around the bare sphere.

The above curvature effect is quantitatively shown in Figure 2.4 (c), where the interaction energy of the system with varying interparticle distance D is compared for different curvatures of the grafted particle. Plotting the energy on a per chain basis quantifies the effects arising specifically from curvature (by normalizing the increase in the number of chains with increasing

radius of the brush-covered particle). As observed above, when the brush-covered particle becomes smaller, the system becomes more curved and the brush is able to deform around the particle. Correspondingly, the energy costs associated with bringing the two particles together is seen to become less repulsive as the particle size decreases.

2.3.2.2 Effect of varying $R_{\mathbf{bare}}/R_{\mathbf{grafted}}$

One motivation of this work is to explore drug-protein interactions when they are of comparable but *different* sizes. The relative sizes of the particles thus becomes an important design parameter. The results of exploring the parameter $R_{\text{bare}}/R_{\text{grafted}}$ are shown in Figure 2.5, where the size of the bare particle is varied while the size of the brush-covered particle is held constant at $R_{\text{grafted}}/H_{\text{brush}} = 0.455$ and dimensionless grafting density is fixed at 0.8335. As the bare particle becomes larger relative to the brush-covered particle, it is seen to increasingly compress the brush (Figure 2.5 (b)), resulting in a stronger repulsive potential (Figure 2.5 (c)). Conversely, as the bare particle gets smaller (Figure 2.5 (a)), it perturbs the brush much less significantly while approaching the grafted particle, leading to weaker interaction forces (Figure 2.5 (c)).

2.3.2.3 Effect of varying $\sigma R_{\mathbf{g}}^2$

Another important design parameter in systems studied in this article is the grafting density. In Figures 2.6 (a)-(b) we show density profiles

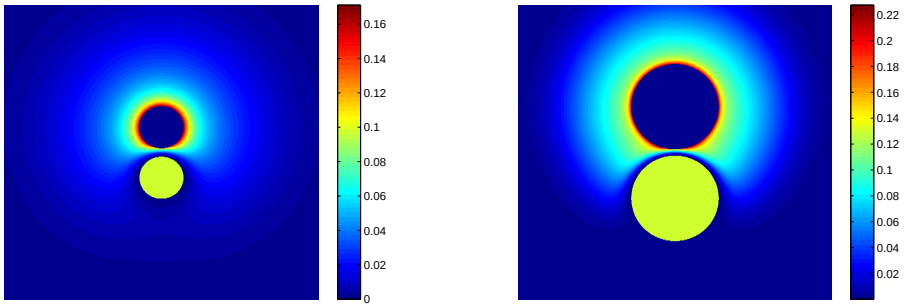

(a) (b)

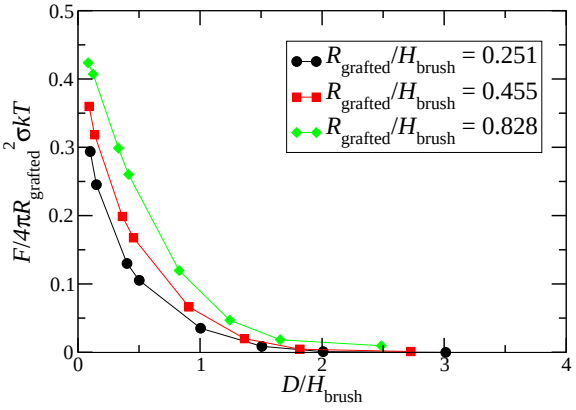

(c)

Figure 2.4: (a),(b) Contour plots of monomer volume fraction $\phi(\mathbf{r})$ for differing system curvatures. In (a) $R_{\text{grafted}}/H_{\text{brush}} = 0.251$; in (b) $R_{\text{grafted}}/H_{\text{brush}} = 0.828$. For each plot, the bare spheres are placed approximately equally deep into the brush, $D/H_{\text{brush}} \approx 0.1$. (c) Energy per chain for several values of $R_{\text{grafted}}/H_{\text{brush}}$ at varying depth of the bare sphere in the brush, D/H_{brush}. The two spheres are equal in size ($R_{\text{bare}}/R_{\text{grafted}} = 1$), $\sigma R_{\text{g}}^2 = 0.8335$, and $B = 100$.

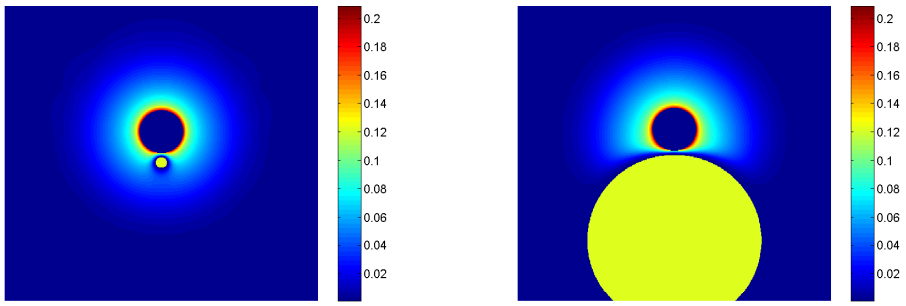

(a) (b)

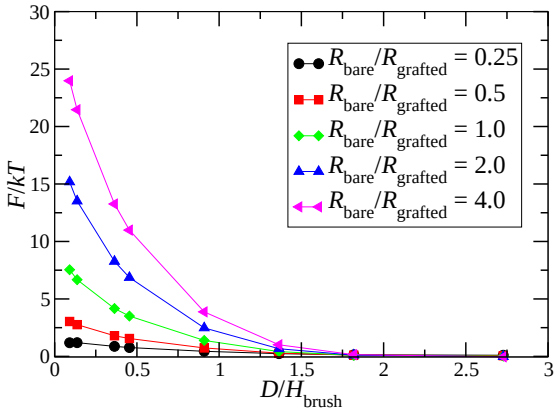

(c)

Figure 2.5: (a),(b) Contour plots of monomer volume fraction $\phi(\mathbf{r})$ for differing values of $R_{\text{bare}}/R_{\text{grafted}}$. In (a) $R_{\text{bare}}/R_{\text{grafted}} = 0.25$; in (b), $R_{\text{bare}}/R_{\text{grafted}} = 4$. The bare spheres are placed equally deep into the brush, $D/H_{\text{brush}} = 0.09$. (c) Energy plots for several values of $R_{\text{bare}}/R_{\text{grafted}}$. Grafted sphere size is held constant at $R_{\text{grafted}}/H_{\text{brush}} = 0.455$, $\sigma R_{\text{g}}^2 = 0.8335$, and $B = 100$.

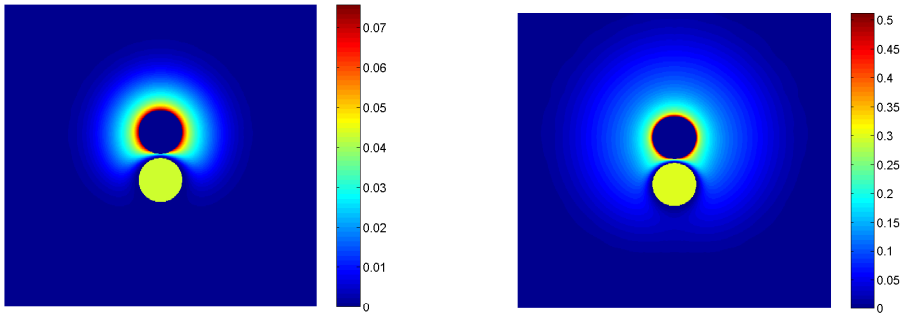

(a) (b)

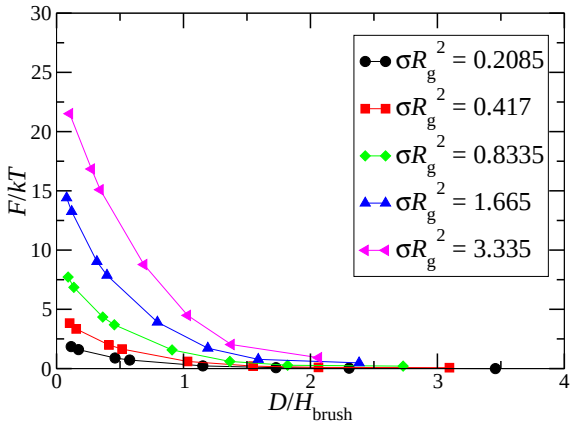

(c)

Figure 2.6: (a),(b) Contour plots of monomer volume fraction $\phi(\mathbf{r})$ for differing values of σR_{g}^2. In (a), $\sigma R_{\mathrm{g}}^2 = 0.2085$; in (b), $\sigma R_{\mathrm{g}}^2 = 3.335$. The bare spheres are placed equally deep into the brush, $D/H_{\mathrm{brush}} = 0.09$. (c) Energy plots for several values of σR_{g}^2. $R_{\mathrm{grafted}}/H_{\mathrm{brush}} = 0.455$, $R_{\mathrm{bare}}/R_{\mathrm{grafted}} = 1$, and $B = 100$.

and energy plots resulting from varying grafting density for conditions where $R_{\text{grafted}}/H_{\text{brush}} = 1$ and $R_{\text{bare}}/R_{\text{grafted}} = 1$. Increased crowding of the grafted layers resulting from increasing the grafting density (Figure 2.6 (b)) increases the excluded volume energy costs. Thus, compressing a denser brush costs more energy. This is reflected in Figure 2.6 (c), where the interparticle interactions display stronger repulsive interactions with increasing grafting density.

2.4 Discussion

While the numerical results presented in the preceding sections clarify the parametric underpinnings of the interactions between a grafted particle and a bare one, it is of interest to ask if we can justify the SCFT numerical results through analytical approximations or scaling theories. In this section we explore two such constructs, based on the Derjaguin approximation and scaling theories.

2.4.1 Derjaguin approximation

The Derjaguin approximation is a commonly-used technique to estimate the interactions in curved systems by making the assumption that locally the systems behave as if they were flat. [82, 238] In Section 2.2.1 we detail the adaptation of this approximation based on the work by Kim and Matsen[99] to derive an estimate of the free energy of the grafted sphere-bare sphere system. This approach requires prior knowledge, either through SCFT or strong-stretching theory (SST), of the free energy required to compress one

grafted chain in a direction perpendicular to the direction in which the surface is assumed to be flat. We choose to use the Derjaguin approximation using results from SST. We note that the Derjaguin approximation only considers the energy costs arising from the compression of the chains, and in effect neglects the costs arising from the splaying of the chains around the particle. The disparities between the Derjaguin approximation and SCFT are expected to arise from the latter contribution as well as the errors inherent in the use of SST results for curved brushes.

In order to assess the validity of the above approximation for our system, we compare interaction energy as a function of interparticle distance obtained from numerical solutions of SCFT with similar results obtained using both the standard version and a modification (based on the idea proposed by Kim and Matsen[99]) of the Derjaguin approximation. The standard approximation assumes that compression of the chains is in the direction of the axis connecting the spheres, while the modified approximation assumes that compression is in the radial direction. Figure 2.7 shows these results for the cases of $R_{\text{grafted}}/H_{\text{brush}} = 0.251$ and 0.828 and varying $R_{\text{bare}}/R_{\text{grafted}}$. Note that for $R_{\text{grafted}}/H_{\text{brush}} = 0.251$ and $R_{\text{bare}}/R_{\text{grafted}} = 0.5$, we are only able to obtain physical results by adjusting the SST expression for $H_{0,max}$ using eq. (2.19). We discuss this further in Section 2.2.1.

For the case of small, very curved polymer-coated particles ($R_{\text{grafted}}/H_{\text{brush}}$ = 0.251, Figures 2.7 (a) and (b)) we observe that the *modified* Derjaguin approximation predicts the behavior of the energy reasonably well, while the

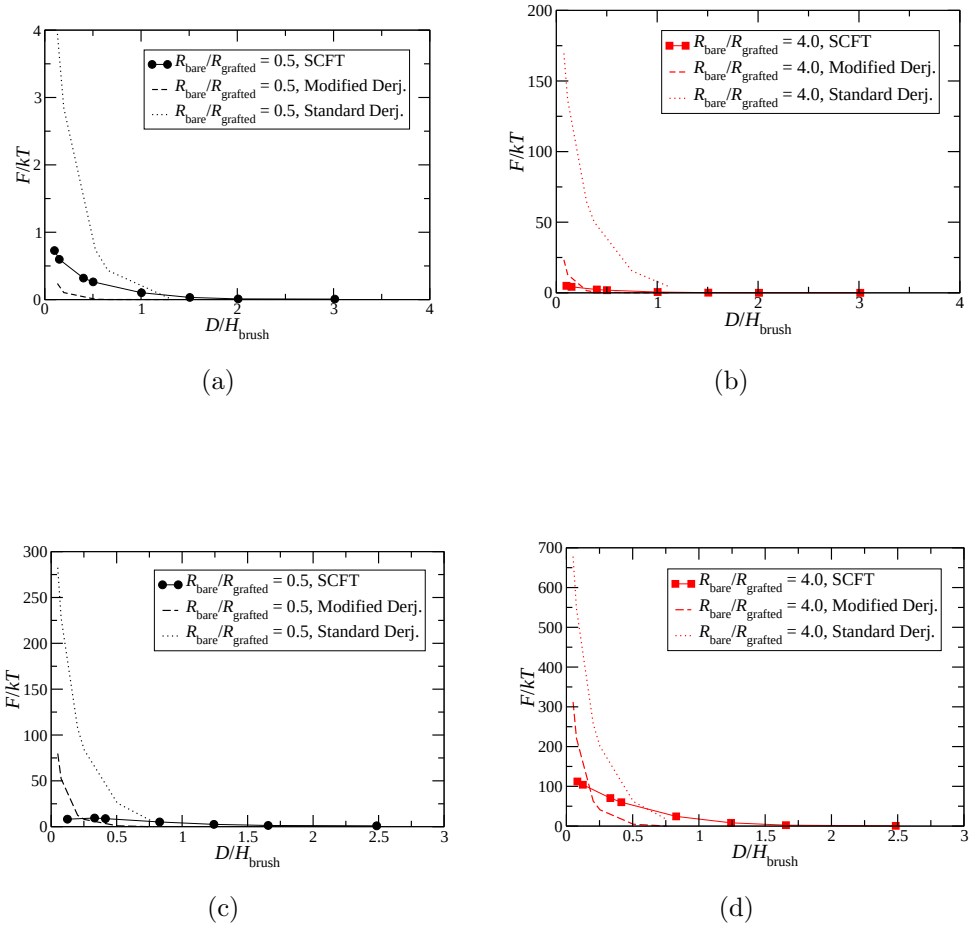

Figure 2.7: Energy plots comparing SCFT to the standard and modified Derjaguin approximations for several values of $R_{\text{bare}}/R_{\text{grafted}}$. In (a) and (b), $R_{\text{grafted}}/H_{\text{brush}}$ = 0.251 and in (c) and (d), 0.828. $\sigma R_{\text{g}}^2 = 0.8335$ and $B = 100$.

standard Derjaguin approximation substantially overestimates the energies. This is because the standard approximation assumes that all the compression of chains occurs in the direction of the interparticle axis (Section 2.2.1). However, due to the radial nature of the chains, the modified approximation allows for chains to escape the compression of the bare particle. Hence, the standard approximation overestimates the chain compression costs relative to the modified approximation (and reality).

For larger polymer-grafted particles ($R_{\text{grafted}}/H_{\text{brush}} = 0.828$, Figures 2.7 (c) and (d)), it is seen that for small bare particles the standard and modified approximations behave similarly to the case of small grafted particles. This is because (similar to the reasoning above) the modified approximation allows for the chains to be less compressed as a function of the curvature of the bare particle. When the polymer-grafted particles and bare particles are large, the accuracy of the standard approximation improves at predicting the SCFT values of interaction energies. As demonstrated in Figures 2.4 (a)-(b) of Section 2.3, the larger grafted particle is less able to splay around the bare particle and hence resembles a flat brush. Thus the standard approximation, which treats compression of the chains as along the axis connecting the particles, becomes increasingly accurate. For this situation, the modified Derjaguin approximation also provides a good estimate of the energies, which should be the case since as the grafted particles become large, the difference between the standard and modified approximations vanishes. We note that in Figure 2.7 (c) the slight decrease in interaction energy predicted by SCFT is due to

numerical inaccuracy.

Our results suggest that the *modified* Derjaguin approximation can be used to obtain a good estimate of interaction energy between the grafted and bare spheres when the grafted sphere is small and when the grafted sphere is large compared to the bare sphere. However, the standard and modified Derjaguin approximations both predict the interaction energies qualitatively when both spheres are large (still within the range $R_{\text{bare}}/R_{\text{grafted}} \simeq O(1)$ and $R_{\text{grafted}}/H_{\text{brush}} \simeq O(1)$).

2.4.2 Scaling

A useful result would be to show that there is some scaling relationship that could potentially collapse all energy curves for different values of design parameters. By an empirical shifting of the curves we find that the interaction energies exhibit a scaling of the form

$$\frac{F}{kT} \sim \sigma \left(\frac{R_{\text{bare}}}{R_{\text{grafted}}}\right)^{0.93} \left(\frac{R_{\text{grafted}}}{R_{\text{g}}}\right)^{2.25} \ln\left(\frac{D}{H_{\text{brush}}}\right). \tag{2.20}$$

The regime we explored in this work is $0.5 < R_{\text{grafted}}/R_{\text{g}} < 2$, $0.25 < R_{\text{bare}}/R_{\text{grafted}} < 4$, and $0.2085 < \sigma R_{\text{g}}^2 < 3.335$. The resulting universal curve is shown in Figure 2.8 and can potentially be used to obtain interaction profiles for other radii and grafting densities not explored in this article. Additionally, the above indicates that the range of the interaction scales as H_{brush} and the potentials exhibit a logarithmic dependence on the interparticle distance D.

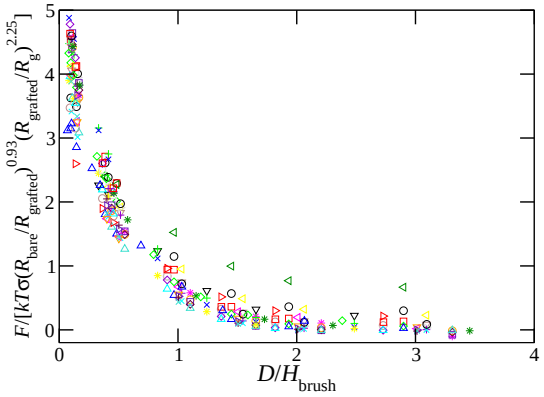

(a)

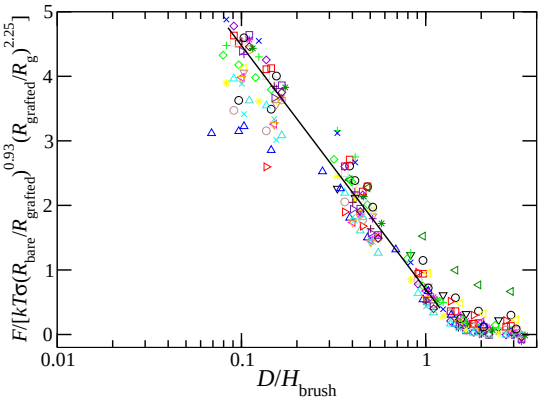

(b)

Figure 2.8: Energy plots adjusted by empirical scaling; in (a), plotted as a standard plot and in (b) as a semi-log plot. The regime covered is $0.5 < R_{\text{grafted}}/R_{\text{g}} < 2$, $0.25 < R_{\text{bare}}/R_{\text{grafted}} < 4$, and $0.2085 < \sigma R_{\text{g}}^2 < 3.335$.

In seeking to obtain some perspective for the above scaling, we note that earlier researches [100, 167, 226] have considered the energy of insertion into a dry polymer brush and predicted it (in the limit that the particle does not perturb the structure of the brush) to be proportional to the pressure field felt within the flat brush, $P(z)$, times the volume of the particle $V_{\text{bare}}(\sim R_{\text{bare}}^3)$. This result is expected to hold for large grafted particles, and also for the insertion of a small particle into spherical brushes and star polymers (except insofar as the osmotic pressure representing the appropriate expression for a curved brush). In such a case, the energy of interaction is expected to scale as the volume of the bare particle, R_{bare}^3. It is apparent, however, that our theoretical results do not display this scaling with R_{bare}, suggesting that the regime we have explored corresponds to a larger bare particle where the perturbation of the brush cannot be ignored.

For larger bare particles, direct scaling approaches are not possible due to the perturbation of the brush structure caused by the insertion of the particle. While the Derjaguin approximation incorporates the compression of the brush, it neglects effects arising from splaying of the chains around the particle (which, as discussed earlier, may prove important for some situations considered in the article). Indeed, a simple nondimensionalization of the Derjaguin approximation yields a scaling dependence of σ^2, indicative of the interaction between grafted chains. In contrast, it is seen that our results correspond to a linear scaling in σ, presumably representing the weak interchain interactions arising due to curvature and splaying effects. Consequently, we are unable to

provide a theoretical justification for the scaling collapse displayed by the interaction energies. However, despite this limitation we believe that the scaling law so discerned may be useful for estimating the free energy of interaction for other systems and parameters not explored in this work.

In terms of the range of the logarithmic functional form noted for the interaction potential, we observe that the latter agrees with the range and functional form for interaction between two star polymers obtained by Witten and Pincus from scaling arguments. [227] Moreover, within the Derjaguin approximation the free energy of compression for a given brush height l scales as $1/l$ for small l, leading to a free energy scaling (for small l) as $\ln(D)$. Together, these results suggest that the logarithmic scaling may be a generic feature expected for curved systems, which is consistent with our results.

2.5 Summary

By solving the SCFT equations in a bispherical coordinate system, we studied the interaction between a polymer-grafted sphere and a bare sphere, representative of a polymer-grafted drug and an MPS protein. The radii of the polymer-grafted sphere and the bare sphere as well as grafting density were varied. We found that the interaction energy increased upon increasing the grafting density and bare particle size, and upon decreasing grafted particle curvature. We compared our results to those obtained with a modified Derjaguin approximation for this system and found that it qualitatively predicts the behavior of the energies. We also found that our energy plots can be

collapsed onto a master curve, which allows a quantitative prediction of the interaction energies within the range of the parameters we studied.

Chapter 3

Curvature effects upon interactions of polymer-grafted nanoparticles in chemically identical polymer matrices

3.1 Introduction

Dispersing nanoparticles in polymer matrices is emerging as a common strategy to enhance the mechanical, electrical, or optical properties of the polymer material.[145] Numerous experimental studies have shown that properties of polymer-nanoparticle mixtures are vitally dependent on the extent to which the nanoparticles are dispersed in the bulk polymer.[108, 177] However, many combinations of polymers and nanofillers tend to be immiscible either due to strong Van der Waals interactions between the fillers or due to polymer-mediated interparticle attractions. Such filler aggregation and clustering usually has a detrimental impact upon the interfacial contact between the polymer and the filler and in turn upon the resulting properties. Not surprisingly, finding strategies for efficient dispersion of nanoparticles in polymer matrices remains an active area of research.

In the above context, functionalizing the fillers with a variety of anionic or cationic oligomeric surfactants and grafted polymers [50, 65, 69, 78, 150, 175]

has emerged as a popular approach to stabilize the nanoparticles. Such approaches strive to exploit favorable interactions between the functionalizing group and the polymer matrix, and thereby enhance the dispersability of the particles. Among these approaches, the model system which has attracted the most attention from both an experimental and theoretical perspective is one where the nanoparticle surfaces contain grafted polymers which are chemically identical to the matrix polymer. In such cases there are no competing enthalpic interactions and the interactions and dispersion characteristics arise primarily from the entropic effects pertaining to the grafted polymer and the matrix chains. Early research efforts to model such systems neglected the effects of curvature and approximated the system as a polymer-grafted flat plate in contact with a melt of free chains. [7, 10, 46, 48, 67, 75, 115, 127, 132, 136, 170, 187, 225, 234]. The results of these studies suggested that for the case when the matrix polymers are small, the free chains penetrate the grafted chains in order to maximize their translational entropy (termed the wetting regime). However, when the matrix chains become large enough, the translational entropy benefit decreases and the cost of brush swelling increases enough that the chains are expelled from the brush (the dewetting regime). The transition from wetting to dewetting is accelerated with increasing grafting density due to the accompanying increase in stretching cost of the grafted chains. By explicitly determining interparticle potentials, the dewetting situation was shown to be correlated with a net interparticle attraction and potential segregation of the nanoparticles from the matrix. In contrast, the wetting situation was

shown to be correlated to a net repulsive interaction and potentially a regime corresponding to the stable dispersion of nanoparticles.[136]

While the above studies provided valuable guidelines toward the design of polymeric functionalizers, notably missing in such studies was an explicit treatment of the particle curvature effects relevant for applications in the nanoparticle regime. We note that curvature can be quantified by the parameter R/H_b, where R denotes the radius of the particle and H_b the height of the brush. Approximating the system as a flat plate as discussed above corresponds to the regime $R/H_b \gg 1$. In contrast, recent experimental studies have focused on applications involving the regime $R/H_b \simeq 1$. Specifically, experiments of Meli and Green [145] used grafted nanoparticles in which R/H_b varied between about 0.17 and 0.57, where H_b here is approximated as the height of a melt brush. Another experimental study using grafted nanoparticles reported values of R/H_b ranging from 0.76 to 49.3, where the ratio is here calculated from experimental values of R and H_b reported in the paper.[144]

Initial efforts to model the effects of curvature in these systems approximated the grafted particles as star polymers, which corresponds to the other limiting case of $R/H_b \ll 1$.[60, 169, 188] More recently however, there have been several theoretical studies focusing on the regime of intermediate curvatures. Specifically, self-consistent field theory (SCFT),[16, 74, 230] Monte Carlo (MC) simulations,[106, 107, 196] molecular dynamics (MD) simulations,[191] density functional theory (DFT),[46, 196] and integral equation theories [84] have been used to study both the wetting behavior of a single grafted sphere as

well as the interactions between two grafted spheres in a chemically identical polymer matrix. These studies have demonstrated that increasing the curvature of the grafted particle reduces the crowding of the grafted chains and allows the free chains to more effectively wet the brush. In turn, such effects were shown to lead to a repulsive interparticle potential with increasing curvature of the grafted particles. A number of prior theoretical researches have addressed the effects of curvature in the regime where the brush is in contact with a solvent, which corresponds to the limit of a free polymer size equal to one monomer. [32, 99, 227] The key finding in the good solvent regime is that the small solvent molecule fully penetrates the brush due to translational entropy, resulting in a purely repulsive interparticle potentials. The main effects of curvature in such cases is to decrease chain stretching and the steepness of the repulsive potentials.

While the above-mentioned theoretical works have shed light on the effects of curvature, a comprehensive picture of the interplay of the different parameters such as the grafting density, curvature and matrix molecular weight (relative to the grafted chain length) is still lacking. In particular, we further the researches mentioned above in several ways: 1) Rather than using the Derjaguin approximation to quantify interparticle potentials or using energetic considerations from single particle results, we use a full numerical implementation of SCFT to quantify the parametric dependencies. As an aside, we note that we have found that results using the Derjaguin approximation (to maintain brevity, we do not present these in the article) compare very

poorly to the SCFT results; 2) We present a more complete treatment of the effect of changing the relative sizes of the free and grafted chains, which was not thoroughly explored by previous work that used SCFT to generate two-particle potentials; 3) We report details about the interfacial widths and how they correlate to with the interparticle potentials (discussed further below); 4) We seek to rationalize our results thoroughly using physical arguments and scaling theories, and qualitatively connect them to key experimental results.

Our line of research is motivated by the scaling ideas proposed [33, 59, 113, 114] for the situation of flat grafted surfaces, which indicates that for the situation of partial wetting and long melt chains, the width of interpenetration between the free and the grafted chains determine the interaction potentials between the grafted surfaces. Motivated by such considerations, we probe in this study whether a similar *quantitative correlation* can be established between the brush-melt interpenetration widths and the polymer-mediated interparticle potentials for curved systems. Establishing such a correlation can be valuable since modeling the interpenetration widths is typically much simpler even for curved systems and requires only consideration of single particle characteristics. Additionally, recent scattering experiments and viscometry measurements have demonstrated the ability to study the structure of the grafted layers in order to deduce the extent of wetting and dewetting with varying free chain length.[25, 144] A connection between such data and the interparticle potentials could provide an efficient way to explore the locus of parameters in which dispersion is likely to occur. Additionally, we expect

that a more accurate prediction of the interparticle potentials combined with knowledge of interparticle attractions such as Van der Waals forces will allow for a more accurate treatment of many-body problems such as the anisotropic self-assembly of polymer-grafted particles.[2, 168, 198]

To accomplish the above-mentioned goals, we model the free and grafted particle chains using self-consistent field theory (SCFT). The theoretical methodology we use is similar to that used in our previous work to address the interaction between polymer grafted particles and bare particles in a good solvent,[205] except that for our present system we eschew using the energetic contribution associated with excluded volume interactions and merely assume that the only relevant energetic contributions are a Gaussian stretching elastic energy of the polymer components. Moreover, we assume that the system of grafted chains together with the free melt chains is overall incompressible with a constant density. The resulting mean-field equations are very similar to those derived and elaborated in Ferreira and our previous work.[48, 205] To account for the curved geometry of the two-sphere system, we solve the appropriate SCFT equations in bispherical coordinates. We exploit the correspondence between the (symmetric) two-sphere system in a polymer melt and that of a single sphere system interacting with a reflecting surface through a polymer melt. To maintain brevity of this brief article, we forgo elaborating the governing equations and instead refer the interested reader to the original articles. In Appendix 3.2, we provide a brief compendium of the numerical details.

The parameters we study are the ratio of the lengths of the free chains (N_f) and the grafted chains (N_g), $\alpha = N_f/N_g$, and the curvature of the system, quantified by R/R_g, where R_g is the unperturbed radius of gyration of the brush polymer. We also study the effect of varying the grafted density $\bar{\sigma}/C$, where $\bar{\sigma}$ is number of chains per unit area, normalized by R_g^2; $C = \rho_0 R_g^2/N_g$ is a dimensionless monomer density, where $\rho_0 = 1/a^3$ and a is the length of a statistical segment.

This article is organized as follows: in the Section 3.3.1 we present results for the interpenetration of the matrix chains into the grafted polymer. In Section 3.3.2 we present results for two sphere matrix-mediated interparticle potentials. Lastly, in Section 3.4, we make qualitative comments on the relationship between our results and experimental considerations.

3.2 Numerical details

Here we comment on a few differences between our theoretical construction and that found in a closely related previous works.[205] We use a partition function very similar to that used in our previous work,[205] except that the excluded volume term is replaced with a delta function which enforces the incompressibility of the system, similar to that used by Ferreira, et al.[48] The diffusion equation and initial conditions on chain propagators are identical to our previous work, except that the diffusion equation is modified by a field enforcing the incompressibility constraint.

We solved the resulting self-consistent field equations with the appro-

priate boundary conditions. For reasons discussed by Matsen,[136] we used a reflecting wall as one of the boundaries of our system, which dictates that we impose Neumann boundary conditions at this surface. For numerical reasons discussed further in our previous work,[205] instead of using the common Dirichlet boundary conditions on the surface of the grafted sphere, we also used a Neumann boundary condition on this surface. In order to fully capture the unique geometry of a grafted particle and a reflecting wall, we solved the diffusion equation in a bispherical coordinate system using the alternating-direction implicit method described by Roan and Kawakatsu.[174] We used an η mesh size of 0.02 - 0.03, a θ mesh size of $\pi/100$, and an s mesh size of 0.0004. The mean-field equations were iterated 5000 times for $R/R_g = 2$ and 15000 times for $R/R_g = 1$. This resulted in a mean-squared error in potential of at most 0.004. For the isolated sphere, the corresponding equations were solved numerically using a Crank-Nicholson method.[1]

3.3 Results

3.3.1 Interpenetration Widths

We begin by presenting results for the interpenetration between the free polymers and the grafted chains for the case of a single grafted sphere immersed in a polymer melt chemically indistinguishable from the grafted chains. In Figure 3.1 we show density profiles of the grafted and free chains for $R/R_g = 1.0$ and $R/R_g = 50.0$, representing the limits of high and low curvature. As the system becomes more curved, the stretching cost of the

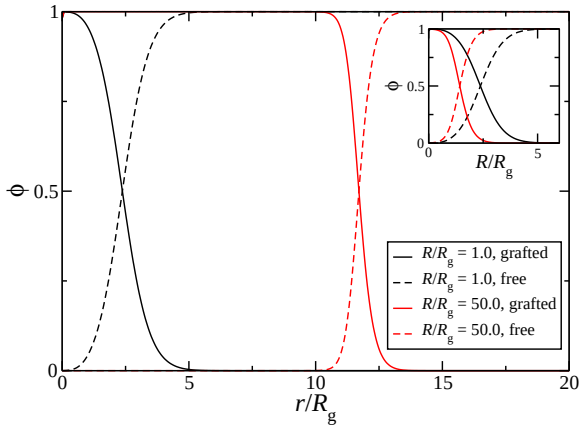

Figure 3.1: Density of grafted polymer-free polymer interface as a function of radial distance away from the sphere surface, r/R_g, for spheres of size $R/R_g = 1.0$ and $R/R_g = 50.0$. $\bar{\sigma}/C = 14.70$ and $\alpha = 1.0$. In the inset, the profile for $R/R_g = 50.0$ is shifted to allow for comparison of the interpenetration widths.

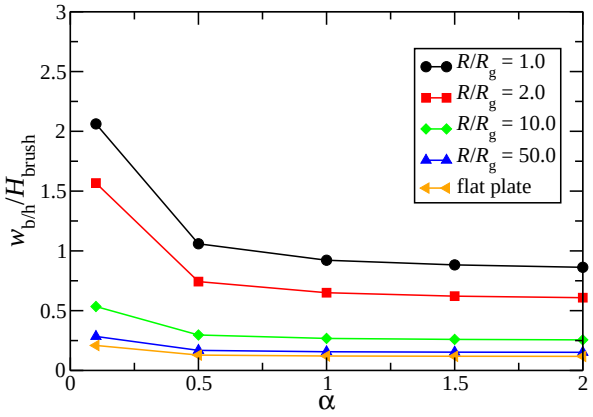

Figure 3.2: Width of the grafted polymer-free polymer interface as a function of α for various values of R/R_g; $\bar{\sigma}/C = 14.70$.

grafted chains associated with the penetration of the free chains is reduced and, as a consequence, it is seen that the free chains are more freely able to penetrate into the brush.

To quantify the degree of interpenetration between the brush and free chains, we determine an interpenetration width defined as:

$$w_{b/h} = \frac{\phi_g(0)}{\phi'_g(r_{1/2})} \tag{3.1}$$

where $\phi_g(r)$ is the volume fraction of the grafted segments and $\phi'_g(r)$ is the derivative of this volume fraction profile. Also, $r_{1/2}$ is the radius at which the density of the brush is half of its surface value. The above definition of $w_{b/h}$ embodies a similar physical significance as the "adsorption-length" used for modeling adsorption of polymers to surfaces.[33, 199–201] However, a small drawback of the above definition is the fact $w_{b/h}$ can in principle be greater than height of the brush itself. Since the latter is unphysical, in the discussion of the scaling results and in establishing the correspondence between $w_{b/h}$ and the interparticle potentials we omit such results corresponding to complete penetration. However, when we report raw values of $w_{b/h}$, we allow points in this regime to remain, since they still serve to quantify the degree of penetration of the free chains into the brush in the wetting regime.

In Figure 3.2 we display the quantity $w_{b/h}$ (normalized by the respective brush height) as a function of α for different R/R_g and fixed grafting density. We observe that the interpenetration width decreases with increasing α and plateaus at large α. These results may be rationalized by noting that the

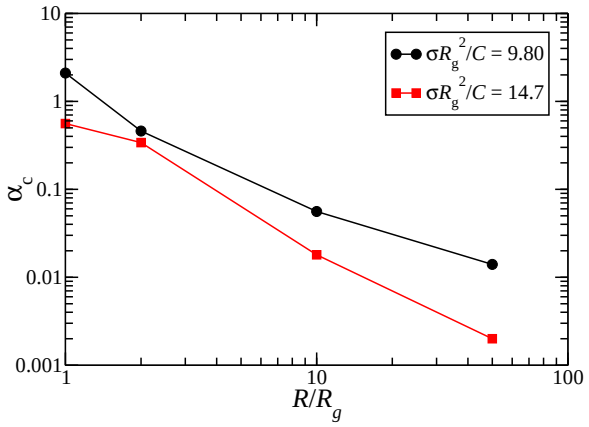

Figure 3.3: The critical $\alpha \equiv \alpha_c$ for the criterion $w_{b/h}/H_b = 1$ displayed as a function of R/R_g for $\bar{\sigma}/C = 9.8$ and 14.7.

interpenetration of free chains is facilitated by the gain in their translational entropy. Since this entropy gain scales as $N_f^{-1} \equiv \alpha^{-1}$, smaller free chains exhibit large interpenetration widths, whereas the interpenetration widths become insensitive to α at large α. More interesting are the effects of curvature which can be noted in the Figure 3.2. We observe that $w_{b/h}$ decreases with increasing particle size R/R_g, indicating that as the system becomes more curved, the degree of interpenetration between the melt and the brush chains becomes enhanced for a given α. These results are in accord with the prevailing notion that curvature effects tend to enhance the propensity for wetting (i.e. increase the interpenetration between the free and the grafted chains).

In many experimental applications,[144, 145] it is common to design systems based on a critical molecular weight which delineates the transition between "complete wetting" and "partial wetting." While demarcating a tran-

sition between such states involves a degree of arbitrariness in assigning the state of wetting and dewetting,[136] based on the results like those of Figure 3.2 one may crudely assign a critical α for this transition as the one where $w_{b/h}/H_b = 1$. Shown in Fig. 3.3 are the results for the curvature dependence of the critical molecular weights for two different grafting densities σ (in some cases, we had to extrapolate the $w_{b/h}$ to determine α_c). The scaling of these curves for these intermediate range of curvatures is $R^{1.25}$ for $\bar{\sigma}/C = 9.8$ and $R^{1.5}$ for $\bar{\sigma}/C = 14.7$. We see that as the curvature decreases, α_c decreases, which supports earlier results which indicate that the wetting-dewetting transition occurs at smaller α as the chains are increasingly expelled from the brush with decreasing curvature. Additionally, the fact that the exponent is larger for larger grafting density is due to the fact that for larger grafting density the chains are more likely to be expelled from the brush, in effect compounding the effect of decreasing curvature.

While the above results pertain to the effects of varying α, results presented in Figure 3.4 depict the interplay of grafting densities and curvature upon $w_{b/h}/H_b$. We note that for flat surfaces, scaling laws predict that $w_{b/h} \sim \sigma^{-1/3}$,[16] and since H_b scales as σ for the melt brush case (representative of the situation when the interpenetration width is small compared to the height of the brush),[16] the ratio $w_{b/h}/H_b$ is expected to scale as $\sigma^{-4/3}$. From the results displayed in Figure 3.4, it is indeed seen that $w_{b/h}/H_b$ depends explicitly on the grafting density for large particles and scales with an exponent of 1.35 which is very close to the expected value for flat surfaces. In contrast, for smaller

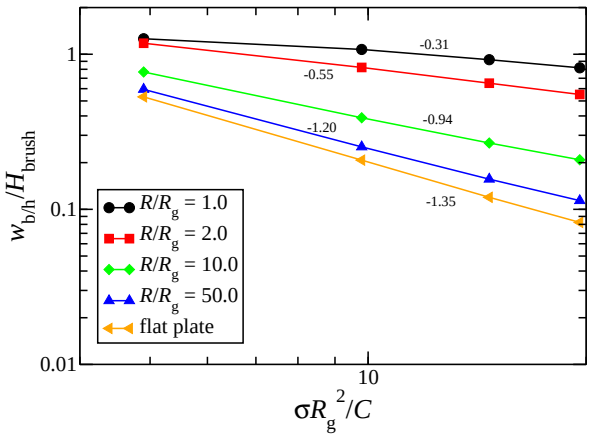

Figure 3.4: Width of the grafted polymer-free polymer interface as a function of $\bar{\sigma}/C$ for various values of R/R_g; $\alpha = 1.0$. Scaling exponents are given adjacent to each curve.

particles it is seen that $w_{b/h}/H_b$ becomes relatively insensitive to the grafting density, an effect which manifests in the much smaller scaling exponents for $w_{b/h}$ as a function of σ at different curvatures.

We observe that the above grafting density dependencies bear significant ramifications for the design of functionalizers for nanoparticles. Indeed, it is generally believed that the grafting density of the functionalizers will play a critical role in the transition to the dewetting regime (due to the scaling of $w_{b/h}$ verses σ for flat plates) and the resulting interparticle attraction and stability of the particle suspension.[145] In contrast, the above results suggest that for curved systems this dependency is much less sensitive, and may therefore experimentally facilitate a much wider range of grafting densities (than that expected from considerations of grafted surfaces) before the dewetting

and aggregation effects become manifest.

While the above results were obtained based on numerical SCFT calculations, it would be of interest to probe if the behavior in Figs. 3.2 - 3.4 can be rationalized based on some simple scaling ideas. Toward this objective, we propose a simple scaling argument which validates our results obtained for the case of *partial interpenetration* (i.e. $w_{b/h}/H_b < 1$), and for the regime of larger α values in which the $w_{b/h}$ becomes independent of α. This argument draws upon the original scaling proposal for the interpenetration widths for flat surfaces in the limit of long free melt chains.[113] In such contexts, the interpenetration widths can be estimated based on the energy cost $\sigma w_{b/h}^2$ for stretching the end of the brush by an amount $w_{b/h}$ and the entropic gain $w_{b/h}^{-1}$ arising from the variations in the density of the melt chains. Balancing these terms yields a scaling of $w_{b/h} \sim \sigma^{-1/3}$ for the flat plate situation. To modify this idea for curved systems, one may crudely renormalize the grafting density present in the elastic energy cost by an "effective" grafting density at the *surface* of the brush:

$$\sigma_{\text{eff}} = \frac{\sigma R^2}{(R + H_b)^2}. \tag{3.2}$$

Using the above grafting density, one would expect the width of the interface $w_{b/h} \sim \sigma_{\text{eff}}^{-1/3}$, or effectively,

$$w_{b/h} \sim \sigma^{-1/3} \left(1 + \frac{H_b}{R}\right)^{2/3}. \tag{3.3}$$

In other words, we expect that

$$\frac{w_{b/h}}{w_{b/h}^{\text{flat}}} \sim \left(1 + \frac{H_b}{R}\right)^{2/3}. \tag{3.4}$$

The above scaling behavior is expected to hold for the regime when the width of the interface is smaller than the height of the brush (partial interpenetration). Equation (3.4) is validated in Fig 3.5 in which it is seen that the results for $w_{b/h}/w_{b/h}^{\text{flat}}$ does indeed collapse into a universal curve with an exponent close to the prediction.

The above arguments now provide a physical understanding of the curvature effects upon the interpenetration widths. Specifically, for $H_b/R \ll 1$, we enter the flat plate regime, wherein $w_{b/h}/H_b$ scales as $\sigma^{-2/3}$. In contrast, for the other extreme, $H_b/R \gg 1$, the above arguments suggest a scaling of the form

$$w_{b/h} \sim \sigma^{-1/3}(H_b/R)^{2/3}. \tag{3.5}$$

Using the result for the brush $H_b \sim \sigma^{1/3}R^{2/3}$ derived for star polymers (appropriate for the limit $H_b/R \gg 1$ and when the brush height is not perturbed significantly due to the interpenetration),[7] we obtain

$$w_{b/h}/H_b \sim \sigma^{-4/9}. \tag{3.6}$$

which is close to the exponents deduced for the case of small particles in Figure 3.4.

In summary, we used our numerical results for interpenetration widths to show the onset of dewetting with increasing α, $\bar{\sigma}/C$, and R/R_g. Using scaling arguments, we justified these trends as well as the curvature dependence of the $w_{b/h}$ - $\bar{\sigma}/C$ plots. These arguments allowed us to collapse our data onto a single curve that showed scaling approximately the same as that predicted by

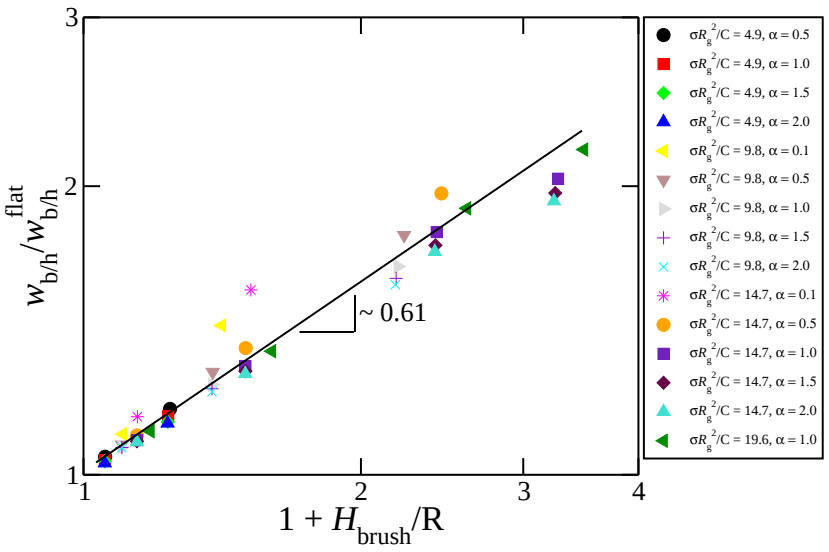

Figure 3.5: Width of the grafted polymer-free polymer interface divided by width of the flat plate interface as a function of $1 + H_b/R$ for various values of $\bar{\sigma}/C$ and α.

our scaling theory. The main outcome of this section is the emergence of the concept of an "effective grafting density" as a means to quantify the curvature effects upon the interpenetration widths.

3.3.2 Interparticle Potentials

In this section, we present the interparticle potentials to examine their correspondence to the curvature, α and σ dependencies of the interpenetration widths $w_{b/h}$. We first show in Figure 3.6 the interaction potentials for the case when α is varied. We see explicitly here that as α increases, an attraction emerges in the interparticle potential. We also note that for larger α values, the potential appears to be less sensitive to α, a result consistent with the behavior

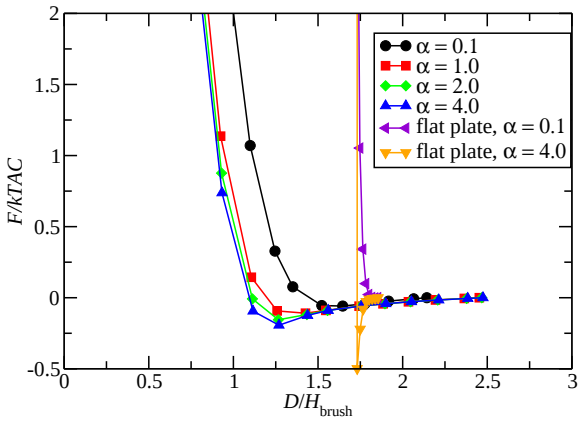

Figure 3.6: Interaction potential between polymer-grafted spheres (per unit area) as a function of the interparticle distance D (normalized by brush height). The parameters $R/R_g = 2$ and $\bar{\sigma}/C = 19.60$.

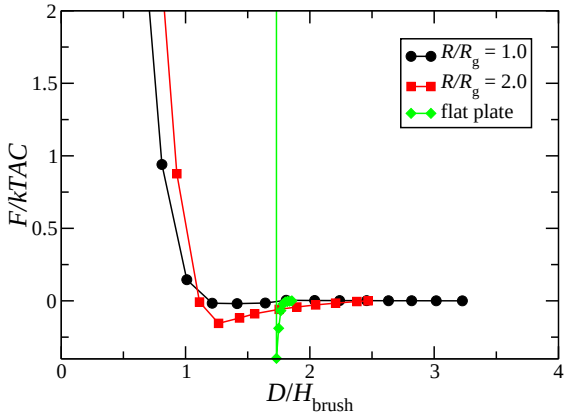

Figure 3.7: Interaction potential between polymer-grafted spheres (per unit area) as a function of the interparticle distance D (normalized by brush height). The parameters $\alpha = 2.0$ and $\bar{\sigma}/C = 19.60$.

exhibited by the interpenetration widths $w_{b/h}$ (cf. Fig. 3.2). These results render explicit the connection between the partial interpenetration observed for a grafted sphere with increasing α and the occurrence of attraction in the interparticle interactions.

The results for the limiting case of flat grafted surfaces is also presented in Figure 3.6 for two values of α. It is seen that the location of the repulsion is smaller for the curved geometries, while the width of the attractive well is larger. This behavior results from the fact that the chains can splay laterally in a curved system whereas in a flat system they cannot; this results in a greater degree of "softness" in the curved particles. We show explicitly the effect of changing the curvature in Figure 3.7. As the particle size increases, the interparticle potential becomes increasingly attractive. This is seen to correlate with the decrease in interpenetration width (increased dewetting) with decreasing curvature shown in Figures 3.2 and 3.4.

We present the interparticle potentials for varying $\bar{\sigma}/C$ in Figure 3.8. For the (reasonably large) values of $\bar{\sigma}/C$ that we chose to explore, the potentials in the limiting case of a flat plate are composed of an attractive well combined with a strongly repulsive potential, whereas for the curved system we again see that the potential has an attractive well and a soft repulsion. However, for both the flat plate and the curved system, it is seen that the attractive well gets deeper with increasing $\bar{\sigma}/C$, albeit this depth being much larger for the flat plate compared to the curved system at constant $\bar{\sigma}/C$. In Figure 3.4 we demonstrated that the interpenetration width decreases with

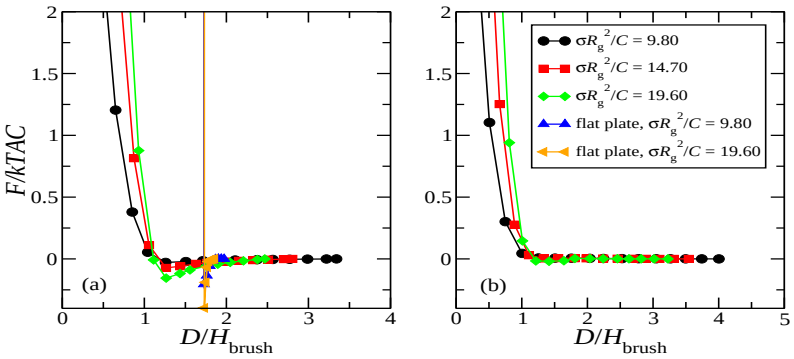

Figure 3.8: Interaction potential between polymer-grafted spheres (per unit area) as a function of the interparticle distance D (normalized by brush height). The parameters $\alpha = 2.0$, and in (a), $R/R_g = 2.0$ and in (b), $R/R_g = 1.0$.

grafting density, consistent with the free chains being expelled from the brush. Here we show explicitly the correspondence of this behavior and an increasingly attractive interparticle potential. Moreover, in Figure 3.8 (b) we also see that for smaller R/R_g, the potentials are less dependent on grafting density. This again is consistent with trends exhibited by the interpenetration widths.

Our interparticle potentials show a decrease in attraction with decreasing α, $\bar{\sigma}/C$, and R/R_g. Since these trends *qualitatively* correspond to the ones noted in the context of the interpenetration width $w_{b/h}$, it is of interest to probe if the interaction potentials are *quantitatively* correlated to the widths $w_{b/h}/R_g$. In Figure 3.9(a) we examine the validity of this hypothesis by displaying the potentials (normalized by σ to account for the different numbers of chains on the particles) for the different $w_{b/h}/R_g$. It is indeed seen that the potentials generally become more attractive for decreasing $w_{b/h}/R_g$,

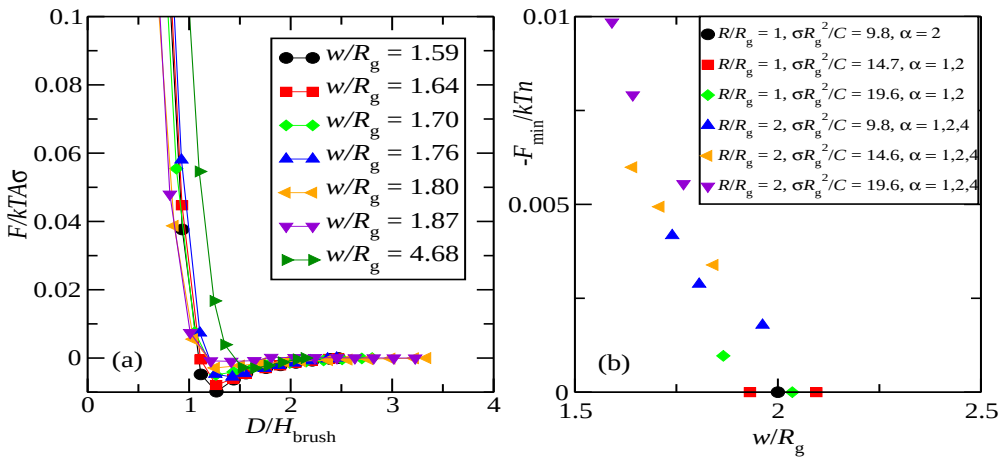

Figure 3.9: (a) Potentials from the previous plots (for $R/R_g = 2.0$) as a function of $w_{b/h}/R_g$; (b) Well depth per chain as a function of interpenetration width in the dewetting regime. In the legend, we use w to represent $w_{b/h}$ due to space considerations.

which points to a strong quantitative correlation between the interpenetration between the brush and the free chains from the melt, and the increased attraction between the two particles. A more stringent verification of this correlation is displayed in Figure 3.9(b), where we plot well depth per unit chain against interpenetration width for the regime of partial interpenetration. We see that the well depth and interpenetration width show a correlation that appeals to the relationship between wetting and dewetting of the melt and interparticle attraction or repulsion.

3.4 Experimental Implications and Outlook

In summary, we have explored the wetting and dewetting of a single sphere immersed in a chemically identical homopolymer melt as well as the interparticle potential of two spheres immersed in a melt. Our results suggest a quantitative correlation between the depth of attraction in the polymer-mediated interactions and the interpenetration width between the melt and the brush chains. Moreover, in the nanoparticle regime our results suggest that for a reasonably wide choice of parameters, the effective grafting density defined in Eq. (3.2) serves to quantify the interpenetration widths. Using these insights, we can identify some general design considerations for the effective use of polymeric functionalizers in dispersing nanoparticle systems. We summarize these below:

1. Explicitly, it is seen that grafting density is much less of a significant parameter in causing attractive interactions in nanoparticle systems (relative to the flat plate case). Indeed, by the scaling arguments proposed (and confirmed by numerical results), the interpenetration widths vary as $\sigma^{-1.33}$ in the large particle case, whereas, they vary only $\sim \sigma^{-0.4}$ for the nanoparticle regimes.

2. Since the effective grafting density scales as $(R + H_b)^{-2}$, a possible strategy to compatibilize nanoparticles (i.e. increase the interpenetration widths) is to functionalize them with long tethers and increase H_b instead. This result accords with the conclusions of a recent simulation study by Smith and Bedrov[191] and provides a physical basis for their results.

3. Finally, we also saw that the "wetting-dewetting" transitions arising with increasing α (or the melt molecular weights) is shifted to much larger α for nanoparticle systems (cf. Fig. 3.3). This suggests that wetting-dewetting transitions arising from the disparities in the molecular weights of the grafted and free chains are much less of a concern in nanoparticle systems.

We also note that our results for the wetting and dewetting of the free chains on the brush are also consistent with the experimental results discussed in the introduction. For instance, the results from Bansal *et al.*[12] use microscopy to show a tendency for dewetting to occur with increasing free chain length (increasing α), which is consistent with the results for the interpenetration widths. The results from Meli *et al.*[145] show a tendency toward dispersion with decreasing free chain length (decreasing α), increasing brush chain length (decreasing α), and decreasing R/R_g, which is reflected in our results which show a tendency toward dewetting with similar parameter changes. Also, our interparticle potentials show that curved grafted particles are able to be compressed more deeply than flat grafted particles. This is related to results reported by McEwan *et al.*[144] which show that for a purely repulsive interparticle potential, the more curved particles behave as "softer" particles compared to larger, less curved particles. We also note that the grafting densities we have used are on the same order of magnitude as those used by key experiments. For example, Meli et al report grafting densities (adjusted to our dimensionless parameters) ranging from about 4 to about 28, values which compare reasonably with the those we use, which range from about 5

to about 20.

Possible extensions to the results discussed in this paper include the study of a brush-coated particle interacting with a chemically different melt. While the interaction between chemically different polymers is usually unfavorable, one could envision a case in which a negative Flory χ parameter exists between the polymers, resulting in a more favorable net particle-polymer interaction.[16, 96] Additionally, the tools we have developed could be extended to model the case of a random copolymer brush, which would allow for the tuning of the interfacial energy between the brush and the melt.[129]

Chapter 4

Glass Transition Behavior of PS Films on Grafted PS Substrates

4.1 Introduction

The glass transition temperature is one of the key parameters determining the mechanical properties of polymers for different applications. Indeed, at the glass transition (with increasing temperature), the storage modulus (or melt viscosity) drops remarkably by a factor of thousands, while the volume and enthalpy begin to discernibly increase. [192] Not surprisingly, many prior studies have investigated a variety of phenomena and properties near the glass transition temperature of different polymeric materials.

More recently, research efforts have directed their efforts toward the impact of confinement, and specifically, the role of interfacial interactions upon the glass transition behavior of polymer materials.[52, 93, 94, 142, 204, 209, 211] Several experimental techniques have been used to probe this transition due to the changes in the volume and physical properties, including ellipsometry,[14, 35, 68, 87, 92, 102–104, 189] X-ray and neutron reflectometry,[15, 56, 91, 149, 156, 163, 213, 228] atomic force microscopy,[88, 89, 179] Brillouin light scattering,[51, 52] positron annihilation lifetime spectroscopy,[6, 35, 229] and fluo-

rescence spectroscopy.[47, 105, 165]

Keddie et al. pioneered these researches where they observed a film thickness dependence of glass transition temperature (T_g) for polystyrene (PS) films on hydrogen-passivated Si wafers.3 Compared to the T_g ($\sim 100°C$) of the bulk material, a noticeable decrease in T_g was found as the film thickness ($\leq 100nm$) was reduced. A similar but more significant decrease in T_g for freestanding PS films was observed by Forrest et al,[52, 142] and Torkelson et al.[47, 105, 165] They suggested potentially two different mechanisms, arising from either the polymer chain confinement or a finite size effect depending on the characteristic molecular length scale. More insights into the influence of interfacial interactions were provided by the experiments of van Zanten et al., who observed an increase in T_g for poly(2-vinylpyridine) (P2VP) films on native oxide substrate of Si wafer with decreasing film thickness.[211] They attributed these trends to the fact that the substrate interactions are favorable with the polar P2VP. Furthermore, Keddie et al. demonstrated both an increase and decrease in T_g (with changing film thicknesses) can result for the same material by controlling the substrate interactions.[94] Explicitly, thin films of poly(methyl methacrylate) (PMMA) on a gold substrate that is unfavorable with PMMA displayed a decrease in T_g with decreasing film thickness, whereas for the films on native oxide substrate of Si wafer that is favorable with PMMA, they showed an increase in T_g with decreasing film thickness.

Many theoretical studies and computer simulations have also addressed the role of interfacial interactions upon the glass transition temperatures of

polymer films [56, 204, 207] and have been discussed in a number of review articles.[3, 13] Pertinent to the present study are the results by Torres et al. which indicated an increase or decrease in T_g (compared to the glass transition of the bulk) in ultrathin films strongly dependent on the strength of the interfacial interactions between the substrates and the polymer chains. [204, 207] With decreasing film thickness, their results showed an increase in T_g for polymer films with the stronger surface energies, while a decrease in T_g was seen for polymer films with the weaker surface energy and for freestanding films. These results yet again have confirmed the importance of the interfacial interactions between the polymer chains and the substrate in influencing the confinement-induced glass transition behavior.

Grafting polymers to surfaces is commonly used as a means to tune the surface interactions with surrounding polymer matrices. Free polymer chains in contact with the grafted (or brush) polymer layer can show either wetting or dewetting (or segregation) behavior depending on the ratio of molecular weights of the matrix component to grafted polymer chains and the grafting densities of the brush component. [49, 61, 77, 95, 119–122, 125, 126, 135, 136, 170–172, 187, 212, 233] For polymer chains on the brushes of the same chemical identity, this behavior (termed autophobic dewetting) can be attributed to the entropic effects of the matrix polymer and the grafted polymer chains.[61, 77, 95, 119, 120, 125, 126, 135, 136, 170–172, 187, 212, 233] More recently, other researchers from our group have investigated the dewetting behavior of a polymer matrix of different chemical identity on the brush sub-

strates. Specifically, we studied the dewetting behavior of PMMA melts on grafted PS layers as a function of brush thickness (or grafting density),[96] and found, in agreement with theoretical calculations, that the behavior of this pair of chemically distinct melts was qualitatively similar to that expected for autophobic dewetting behavior.

In this study, we probe the inter-relationship between the interfacial interactions arising from grafted polymer layers and the T_g behavior of thin polymer films. This effort is motivated by two objectives: because grafting polymers is a common approach for dispersing particulate fillers in polymer matrices, it is of interest to know the manner in which the interfacial T_g properties of the polymer melt (i.e., the properties of the polymers matrix near grafted surface) differ from the bulk regions of the matrix. A second objective of this study is to probe whether interfacial energy considerations that have been used to explain the T_g behavior of thin polymer films near substrates can equally well be extended to rationalize the T_g behavior of thin polymer films on brush substrates.

We note that, in an earlier work by Tsui et al., a grafted random copolymer approach to surface modification was used to study the T_g behavior of PS films. In their study, the interfacial interactions on the substrate were controlled by the composition of random copolymers of styrene (S) and methyl methacrylate (MMA).[209] They presented intriguing results which are yet to be satisfactorily rationalized in terms of the interfacial energies. As another study pertinent to our work, Tate et al. considered the T_g of grafted PS

polymers and noted a significant elevation in the T_g of brushes (relative to the bulk polymers) whose magnitude increased with increasing confinement.[202]

Our work presented in this article deals with conceptually more straightforward case of a polymer melt of the same chemical identity as that of the brush. With this model system, we investigate the glass transition behavior of PS films on a brush layer of the same chemical identity as a function of film thickness, where the brush thickness and grafting density of underlying PS layers are adjusted by the molecular weight of hydroxyl-terminated polystyrene (PSOH) that anchored onto the native oxide substrate of Si wafer. It was found that for the PS films the T_g decreases with decreasing film thickness of the polymer melt. Interestingly, the decrease in T_g turns out to be more significant for the films on the shorter brushes with higher grafting density. We provide a rationalization of the results by using mean-field theory to compute the melt-brush interfacial energy for the experimental parameters probed. Such considerations are also used in a percolation model for the glass transition to explain the observed thickness dependence.

4.2 Experimental Results

Figure 4.1 shows the characteristic brush thickness and grafting density (σ) for grafted PS layers as a function of the number-average molecular weight (M_n) of PSOH, as presented in Table 4.2. Grafting density of underlying PS layers was evaluated by $\sigma(chains/nm^2) = \rho d_0 N_A/M_n$, where F and N_A denote the mass density of PS (1.05 g/mol) and Avogadros number, and the

Table 1. Characteristics of PSOHs for the Surface Modification and PS in This Study

sample code	M_n	M_w/M_n	R_g[a] (nm)	grafting density[b] (σ; chains/nm^2)	brush thickness (d_0; nm)
PSOH-04	3700	1.08	1.666	0.688	4.0
PSOH-10	10000	1.05	2.739	0.554	8.8
PSOH-20	19500	1.05	3.824	0.379	11.7
PSOH-38	38000	1.09	5.339	0.210	12.6
PS (100K)	100000	1.02	8.660		

[a] Radius of gyration calculated by assuming linear PS chains. [b] Grafting density of underlying PS layers was evaluated by $\sigma = \rho d_0 N_A / M_n$, where ρ and N_A denote the mass density of PS (1.05 g/mol) and the Avogadro's number, and two variable parameters such as d_0 and M_n indicate brush thickness and the number-average molecular weight of PSOH, respectively.

parameters d_0 and M_n represent the brush thickness and the number-average molecular weight of PSOH, respectively. It can be seen that the low molecular weight PSOH-04 (3700 g/mol) has a brush thickness of 4.0 nm, at which PS chains are grafted densely at the substrate ($0.688 chains/nm^2$). With increasing molecular weight of PSOH, the brush thickness is measured to increase to 12.6 nm for PSOH-38 (38000 g/mol), while the grafting density decreases to $0.210 chains/nm^2$, the latter decrease is likely due to the low concentrations of the end-hydroxyl group and the slow diffusion of high molecular weight PSOH-38.

Figure 4.2 summarizes the experimental results for T_g of the PS films on the various grafted PS layers as a function of film thickness. For a fixed grafted PS layer (or PSOH), a decrease in T_g of PS films is seen with decreasing film thickness. However, the variations with thickness are seen to be more significant for films on the shorter brushes with the higher grafting densities. Indeed, the confinement effects upon the T_g are seen to follow the sequence in

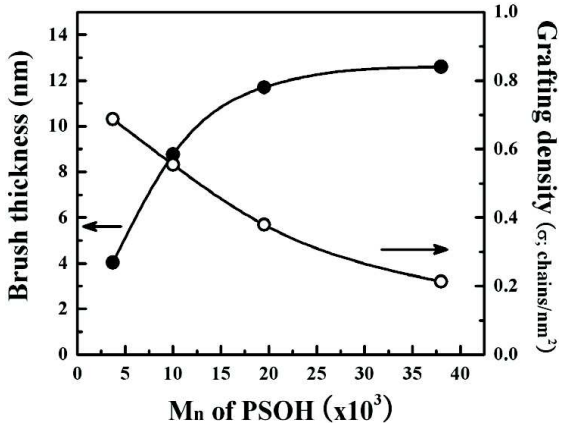

Figure 4.1: Brush thickness and the (calculated grafting density (σ for grafted PS layers as a function of the number-average molecular weight of PSOH.

this experiment: $PSOH-04 > PSOH-10 > PSOH-20 > PSOH-38$. The T_gs of thick PS films like 140 nm are constant ($103°C$) and close to that ($102°C$) of the bulk regardless of the brush thickness (or grafting density of underlying PS layers). In the next section, we provide a qualitative rationalization of the experimental observations.

4.3 Summary of Modeling Methods.

In this section, we discuss the methods we used to model the glass transition and interfacial properties in the context of a homopolymer melt in contact with a homopolymer brush. Our values of $w_{b/m}$ and $\gamma_{b/m}$ were obtained using the same tools as those reported for homopolymer melts on homopolymer brushes in the previous chapter.

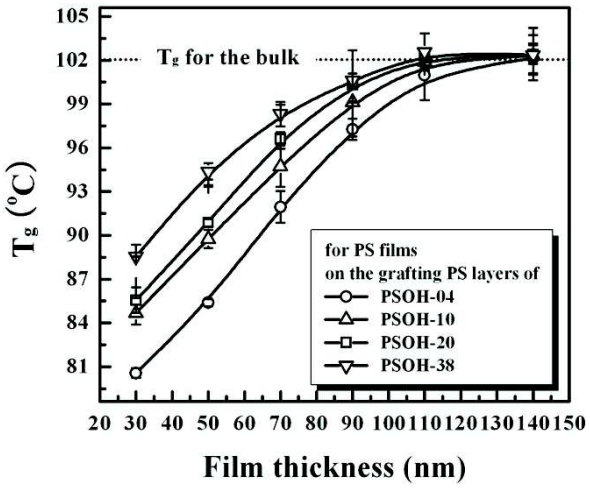

Figure 4.2: T_g as a function of film thickness for PS films on the various grafted PS layers (or PSOHs).

We discuss in more detail the implementation of the percolation model used to generate the results of Figure 4.4(b). Because much of the details are identical to those expounded in earlier publications,[109, 123, 166] we eschew repeating them here and instead refer the interested reader to the original references. Briefly, the percolation approach ascribes glass transition to a percolation of slow, immobile domains in the system. In a computational framework, this is accomplished by considering the site percolation transition on a lattice of the slow domains. The probability for occurrence of a slow domain is representative of the material characteristics and the temperature. The probability (temperature) at which there is a site percolation transition is ascribed as the glass transition temperature. Confined freely suspended films (repelling surfaces) are represented in this framework by considering the influence of

bounding surfaces that possess lower probabilities for forming slow domains (representing the surface induced enhancement in polymer mobilities). In such cases, the percolation of slow domains (in the direction parallel to the film) is expected to occur at a higher probability, representing a confinement-induced lowering of the T_g. Such a model was used by Long and Lequex [123] to explain the long-range nature of confinement-induced T_g effects (albeit, see Lipson and Milner [118] for some caveats regarding the quantitative nature of such effects).

In this work, we adapted the above model while incorporating interfacial zones near one of the confining surfaces (modeling the brush substrate). The other substrate was modeled similar to the case of freely suspended film. These interfacial zones were to be characterized by a length scale parameter Δ representing the thickness (in lattice units) of the interfacial zone. In addition, the skin zone was characterized by a parameter δ representing the (dynamical) strength of the interfacial interactions. Explicitly, the probability of forming a slow domain in the interfacial zones was assumed to be enhanced (relative to the bulk) by a factor $1+\delta$. When this framework was used, the site percolation probability $p_c(h)$ for a two-dimensional lattice was determined as a function of the confinement thickness (in lattice units) h and the interfacial zone thickness Δ (as mentioned in the text, we chose to retain δ fixed at $\delta = 0.1$ in all the results). While the so-determined $p_c(h)$ can be related to the actual T_g pending knowledge of some phenomenological material parameters, [123] such an effort is unnecessary for the purely illustrative spirit in which we have used the per-

colation model. Whence, we ascribe $p_c(h = \infty) - p_c(h) = T_g(h) - T_g(h = \infty)$ up to an arbitrary prefactor. These results are displayed in Figure 4.4b.

4.4 Discussion

We note that there is still a lack of complete understanding of the origins of the T_g behavior of thin polymer films. A number of (not necessarily mutually exclusive) candidate explanations have been proposed, including effects such as density and/or free volume perturbations[56, 143] arising from interfacial interactions, polymer mobility perturbations resulting from confinement and/or interfacial interactions,[13, 34] confinement-induced changes in the energy landscape, and so on.[207] Below, we draw upon these earlier advances and propose two speculative hypotheses for rationalizing the experimental observations.

Our first hypothesis relies on considerations of interfacial energies. Despite the lack of consensus on the mechanistic underpinnings of T_g of thin films, it is generally accepted that on surfaces with which the polymer exhibits favorable interactions, the T_g of thin films tends to be enhanced with respect to bulk and increases further with confinement.[3, 13, 56, 204] In contrast, for situations where the polymer is repelled by the substrate, the T_g of thin films tends to be lowered with respect to the bulk and decreases upon confinement. Keeping in mind that in the present study grafted PS layers screen the interactions from the native oxide layer of Si substrate, the mechanism responsible for the decrease in T_g with decreasing film thickness for the PS films is likely

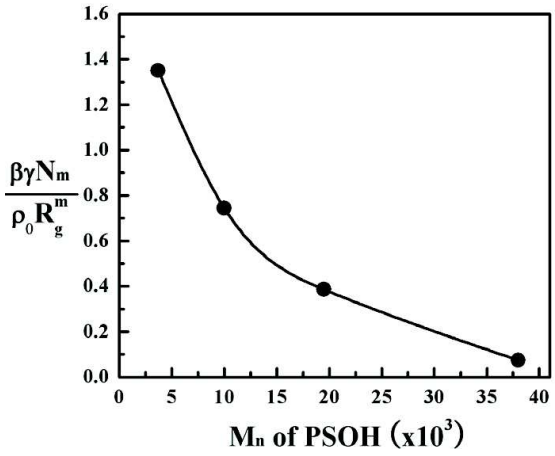

Figure 4.3: Brush-melt interfacial tension γ (normalized by $\beta = (k_B T)^{-1}$, number of segments in the polymer melt Nm, the molecular volume of segments ρ_0, and the radius of gyration of the melt polymers R_g^m as a function of molecular weight of grafted PS brushes (or PSOHs) considered in this study.

distinct from that arising due to the unfavorable interactions between the polymer and the bare substrate. Instead, the interfacial interactions between the polymer matrix and the brush is likely responsible for the experimental results in this study.

To verify the above hypothesis, we characterize the polymer brush-matrix (or melt) interfacial interactions by an effective interfacial tension parameter γ_{b-m} (the term effective is used to emphasize that the interfacial tension is not between two bulk phases). Prior researchers have used scaling theories,[48] strong segregation approximation,[96, 181] and polymer self-consistent field theories[125, 136] (SCFT) to quantify γ_{b-m} between a polymer brush and melt of the same chemical identity. Explicitly, γ_{b-m} has been computed as a

function of the ratios of the molecular weights of the brush to matrix polymers and grafting densities of the brush. Such calculations have been used to shed light on the wetting-dewetting transitions of the matrix polymer. In the present work, we adapted the SCFT calculation methodology proposed by Matsen and Gardiner [136] to calculate the interfacial tension γ_{b-m} for the experimental parameters. Because the accompanying theory and calculation procedures are very similar to that detailed in the article by Matsen and Gardiner, we eschew repeating the details here. Shown in Figure 4.3 are the so-calculated γ_{b-m} for the four different polymer brushes considered in this study. The cases PSOH-04, PSOH-10, and PSOH-20 correspond to the dewetting situation, while PSOH-38 corresponds to a partially wetting situation (in this case the interfacial tension was obtained based on the free energy per unit area difference between an infinitely thick film and the coexisting polymer film of finite thickness).[136] It is evident that the interfacial tensions follow the sequence $\gamma_{b-m}(PSOH-04) > \gamma_{b-m}(PSOH-10) > \gamma_{b-m}(PSOH-20) > \gamma_{b-m}(PSOH-38)$. This result can be explained physically in terms of the lower stretching free energy incurred by longer brush chains to accommodate the interpenetration with the matrix chains. Because a larger interfacial tension correlates to stronger unfavorable interaction, the preceding results qualitatively rationalize the trends seen in the experimental observations in Figure 4.2.

An alternative, albeit more tentative, quantitative explanation for the shape of the curves in the experimental observations can be proposed based

on dynamical considerations relating to the interpenetration between the polymer melt and the brush. To provide a physical picture of this hypothesis, we note that in the extreme situation of very high grafting densities and small molecular weights of the brush polymers, the melt chains have very little interpenetration with the brush chains. In such a case, the brush surface may be viewed as a hard repelling surface, and the matrix polymer mobilities near the brush surface may be expected to be enhanced relative to the bulk unperturbed state. Upon increasing molecular weights of the brush polymer, there is a thickening of the interpenetration zone between the matrix and the brush polymer. This result is quantitatively demonstrated in Figure 4.4(a), which displays the interpenetration widths deduced from the SCFT volume fraction profiles for the melt and brush chains for the experimental parameters. The enhanced penetration between the matrix polymer and the brush is expected to increase the friction on the matrix chains and lead to a retardation of the dynamics of the matrix chains near the brush-melt interface relative to the case of no or little interpenetration. In an earlier work, a quantitative demonstration of such retardation effects was provided in the context of melt dynamics of block copolymer compatibilizers at polymer blend interfaces. [154, 155, 159] The results of the preceding work suggested that the length scale over which the retardation of dynamics persists correlates with the extent of brush-melt interpenetration, whereas the strength of such retardation effects were shown to correlate with the grafting density of the brush (expressed in units of squared radius of gyration of the brush chains, also shown in Figure

4.2(a)). An alternative physical picture that leads to a similar hypothesis is suggested by the experimental results of Tate et al.[202] in which the authors demonstrate a significantly elevated T_g for a film of grafted polymers. The latter results also indicate that the melt polymers in the interpenetration zone are in an environment of significantly reduced mobilities. Below, we adapt a simple phenomenological model for glass transition to demonstrate the manner in which such dynamical retardation effects can rationalize the experimental results.

To provide a schematic illustration of the impact of the above effects on the T_g of thin polymer films, a static percolation model of glass transition was adapted,[123] which was previously used to model phenomena in thin films and polymer nanocomposites. [123, 159] Such percolation models are based on the hypothesis that glass transition in materials occur as a result of the percolation of slow, immobile domains through the system. In a recent work,[123] Long and Lequex used such an idea in conjunction with bounding surfaces that accelerate and decelerate the dynamics to successfully explain the thickness dependence and the long-range nature of T_g changes in thin polymer films. While more recent work has cast doubts on whether such percolation models can suffice quantitatively to explain the phenomena,[118] nevertheless, we use it here for an illustration of the manner in which the above discussed effects can lead to trends which qualitatively mirror the experiments. For this purpose,we follow our recent work [123, 159] and incorporate the above surface interaction effects in such percolation models by including a skin of influence

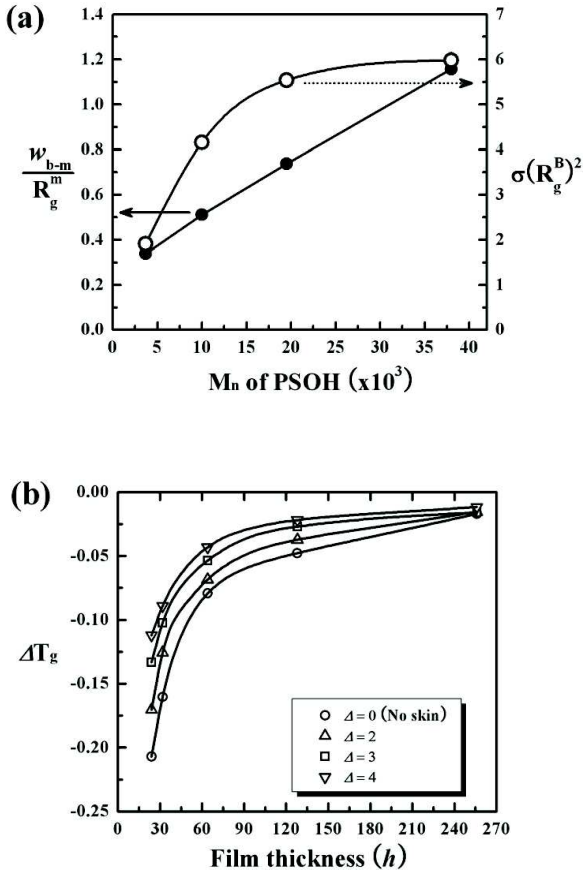

Figure 4.4: (a) Brush-melt interpenetration thickness w_{b-m} (normalized by R_g^m) and the grafting densities (expressed in units $(R_g^B)^2$) as a function of molecular weight of grafted PS brushes (or PSOHs) considered in this study, and (b) Percolation model results for ΔT_g (defined as $T_g(h) - T_g(h = \infty)$, expressed in arbitrary units) as a function of film thickness (expressed in lattice units) for different skin thicknesses denoted by Δ.

around the surface in consideration. Physically, such a skin represents the zone over which the polymer (matrix) dynamics is affected by the surface. Such a skin is characterized by two parameters, namely, the strength of influence and its thicknesses. Based on our discussion in the preceding paragraph, it is evident that in transitioning from shorter brushes to longer brushes, both these parameters are enhanced. However, in the purely schematic spirit of this discussion, we just consider the influence of increasing the zone of influence of the substrate while keeping its strength a constant (allowing the strength of interaction to vary would only serve to enhance the effects reported below). Section 4.3 presents more details on the manner in which the percolation model is implemented, while the outcome of such analysis is depicted in the results displayed in Figure 4.4(b). It is seen that the dynamical retardation effects tend to enhance the T_g relative to the unperturbed case. Such effects are seen to become more pronounced as the thickness (of the polymer film) is reduced and approach the bulk T_g for large thicknesses. More importantly, larger skin zones of influence are seen to lead to more significant effects. Taken in conjunction with the results presented in Figure 4.4(a) (which quantifies the skin thickness as a function of the brush molecular weights), the result of Figure 4.4(b) rationalizes the experimental result of Figure 4.2 and provides a qualitative picture which is strikingly similar to the trends noted therein.

4.5 Summary

In summary, in this work we presented experimental results of the T_g of polymer films on grafted substrates of the same chemical identity. Our objective was to shed light on the influence of the different physical parameters upon the overall confinement-dependent T_g of polymer films. These results indicated that the T_g of the polymer films on such substrates were lowered relative to the bulk.More interestingly, the confinement effects were seen to become diminished with increasing molecular weight (and brush thickness) of grafted PS layers. These trends were rationalized by invoking two possible explanations. The first explanation relied on the interfacial free energies at the interface of brush and melt and its variations with increasing brush thickness of grafted PS layers. The second explanation relied on the dynamical effects which may arise in the overlap zone between the brush and melt polymers. It is likely that the experimental trends are a result of a combination of the preceding effects. Our results suggest that brush substrates may serve as a facile means to tune the confinement effects upon T_g (and aging) of polymer films. Indeed, a variety of physicochemical interactions can be achieved by changing the grafting densities, molecular weights and the chemical identities of the brush polymers. [170] In addition to the practical importance, such studies may provide valuable insights which may allow one to sort through the different mechanisms speculated to be responsible for the confinement effects on the glass transition of polymer films.

Chapter 5

Interfacial properties of statistical copolymer brushes in contact with homopolymer melts

5.1 Introduction

An ability to tune the interfacial energies between incompatible polymers and between polymers and surfaces is extremely important in applications which strive to enhance the properties of polymer materials. For example, in the context of polymer blends, reducing the interfacial energy between the two components is crucial for achieving mixing and better adhesion between immiscible components. [112] As another example, design of polymer nanocomposite materials is often confronted with tuning the interfacial energies between particle fillers and the matrices to facilitate the dispersion of the particles. [65, 145, 150, 198, 201] Also, grafted polymers are used to introduce a repulsion between nanoparticles in drug delivery and nanocomposite applications. [193] In other contexts, diblock copolymer lithography applications commonly require surfaces that have comparable energy of interaction with the two blocks. Such "neutral" surfaces have been shown to give rise to perpendicularly oriented patterns of block copolymers which are especially useful for electronic materials applications. [79, 80, 130, 164, 190, 197]

A popular means of modification of interfacial properties involves grafting polymers on surfaces or using compatibilizers for polymer-polymer interfaces to mediate the interfacial energies. In particular, the use of copolymers is a widely used method for tuning the interfacial energy between two surfaces. A key variable in such approaches is the chemical sequence in the copolymer. The simplest of such polymers is a diblock copolymer, whereas polymers with other sequence distributions, such as random copolymers and gradient copolymers, have also been extensively explored. More recently, researches have also synthesized protein-like chains with tunable sequence distributions for applications as compatibilizers.[124, 182, 195]

Experimental researches have extensively studied the effect of sequence distribution on the efficacies of statistical copolymers as compatibilizers between incompatible solvents and blends, and in applications as interfacial modifiers for surfaces and particles. Results from experiments in the context of incompatible homopolymers have shown that long random copolymers have superior capability to strengthen interfaces compared to their diblock copolymer counterparts. [21, 24, 30, 185] Such experiments have also shown the critical role of the loops formed by the compatibilizers to achieve effective compatibilization.[30] There have also been experiments exploring the use of random copolymers to aid the design of neutral surfaces. Such an approach was demonstrated by Mansky and coworkers, who used contact angle measurements to show that the interfacial energies between melt and grafted surfaces become favorable to the melt when the composition of the grafted

random copolymer layer on the substrate becomes chemically more similar to that of the melt. [129] Later studies also showed the successful achievement of perpendicular morphologies of block copolymers by using such approaches. [70, 72, 80, 130, 197] Recent studies have also shown promising results using diblock cooligomers as surface modifiers to achieve perpendicular morphologies.[85]

The above experimental studies have also motivated a number of theoretical studies, especially in the context of the use of random copolymers as compatibilizers. To study such systems, researchers employed methods such as scaling and analytical theories, [58, 148, 232] Flory theory, [8, 9, 148] molecular dynamics (MD) simulations, [232] Monte Carlo (MC) simulations, [29, 64, 90] and numerical solutions of mean-field equations. [62, 112] These studies focused on characteristic loop lengths, interfacial widths, excess adsorption of interfacial chains, and interfacial energies to quantify the compatibilizing effectiveness of the copolymers. Some of the above studies have also considered the effect of the compatibilizers as a function of the "blockiness" of the chains, where the limits are such that the least blocky chains are alternating copolymers, while the most blocky are diblock copolymers. The results of such theoretical studies have shown that the behavior of the copolymer compatibilizers is driven by an interplay between the stretching entropy cost of the chains being confined at the interface and the energetic cost of chains being exposed to a chemically different milieu. [232] This results in an optimum blockiness that achieves maximum contact between the favorable components while opti-

mizing the entropy to form loops. A recent study also examined the efficacy of protein-like copolymers as compatibilizers and suggest that protein-like chains outperform random copolymers and alternating copolymers as interfacial compatibilizers, especially at lower temperatures. [128]

Theories have also been developed for grafted polymer systems such as grafted diblock copolymers, Y-shaped copolymers, spheres grafted with copolymers, and brushes comprised of two species of homopolymer chains. Methods used to study these systems have included self-consistent field theory, [49, 139] analytical theories, [40, 131, 237] and Monte Carlo simulations. [19, 110, 180] Grafted statistical copolymers have also been studied, albeit not as extensively compared to the studies on their compatibilization efficiency. Pickett used scaling theories and SCFT to study the chain-end exclusion zone in a gradient copolymer melt brush [160] and Gersappe and coworkers studied a random copolymer brush in a solvent selective for one block using MC and SCFT. [63] The latter authors demonstrated a tendency for incompatible segments to segregate away from the solvent due to the distribution in sequence composition, an effect that was more pronounced for increasing blockiness.

In this article, we present results from a theoretical study of the interfacial properties of grafted statistical copolymers. Specifically, we propose to quantify the interfacial energies between grafted surfaces in contact with a homopolymer melt and explore the sensitivity of such interfacial properties upon various physicochemical parameters of the system. This work is motivated by the following objectives: (i) Recent work [96] has demonstrated that the in-

terfacial energies between a grafted surface and an *incompatible* homopolymer melt can, in some instances, be comparable or even less than the energies between a grafted surface and a chemically identical homopolymer. Since such interfacial energies and the resulting polymer-mediated interactions are key to the use of grafted polymers as compatibilizers for surfaces and particulate fillers,[57, 198, 201] the preceding finding may open up the possibility of a wider range of chemistries for grafted polymers. In this study, we wish to explore this topic further by studying the interfacial properties of alternate chemistries of grafted polymers; (ii) A second motivation for the following study arises from the use of grafted statistical copolymers to design neutral surfaces capable of inducing perpendicular alignment of block copolymer lamellae and cylinders. In this regard, a pertinent question is the relationship between the chemical sequence of the grafted copolymer and its ability to achieve interfacial properties in the "neutral" window where such block copolymer morphologies can be achieved; (iii) In a previous work of ours,[96] we developed a simple strong stretching theory model for predicting the interfacial energies in chemically distinct brush-melt interfaces. We wish to extend and explore the accuracy of such a model for prediction of the interfacial energies between a melt and a statistical copolymer brush.

In pursuit of the above objectives, we use self-consistent field theory (SCFT) and a strong stretching theory-based model to explore the manner in which the interfacial widths and interfacial energies between a homopolymer melt and the grafted layer of statistical copolymer changes as a function of

the volume fraction of one of the species in the grafted chains (f), the interaction between the two blocks (quantified in this work by the Flory-Huggins interaction parameter χ), the ratio of the number of segments in the free (N_f) and grafted (N_g) chains, denoted $\alpha = N_f/N_g$, and the grafting density σ for different sequence distributions. The rest of the paper is organized as follows: In Section 5.2 we present key details of our theoretical model and numerical methods; in Section 5.3 we show the results of varying different system parameters; lastly, in Section 5.4 we discuss selected ramifications of our results for experimental considerations. In Appendix 5.2.2 we provide a brief discussion of the computational procedure used to generate the protein-like chains is also provided.

5.2 Theory and Numerical Methods

5.2.1 Self-consistent field theory

We use self consistent field theory for tethered polymer chains [53] to determine the structure of a grafted layer of statistical copolymers composed of segments denoted A and B which interacts with a melt of A homopolymers. While previous articles have already detailed the theoretical framework appropriate for similar situations,[136, 137] for the sake of completeness we present the pertinent equations and details of the accompanying numerical method. The polymers are modeled as Gaussian chains whose conformations are described by continuous functions $\mathbf{R}_i(s)$ and $\mathbf{R}_j(s)$, where i denotes the free chains and takes on values from 1 to n_f (the number of free chains), and

j denotes the grafted chains and runs from 1 to n_g (the number of grafted chains). The variable s is a continuous chain index coordinate running from 0 to N_f for the free chains, where N_f denotes the chain length of free chains, and running from 0 to N_g for the grafted chains, where N_g denotes the number of segments in the grafted chains. For simplicity, we assume that the segmental densities of all the segments are identical and denote it as ρ_0. Using this notation, the partition function of the system in the canonical ensemble can be expressed as

$$\begin{aligned} Z &= \int \prod_{i=1}^{n_f} D\mathbf{R}_i(s) \int \prod_{j=1}^{n_g} D\mathbf{R}_j(s) \exp(-\beta U_0[\mathbf{R}_i(s)] - \beta U_0[\mathbf{R}_j(s)] \\ &\quad -\beta U_1[\mathbf{R}_i(s), \mathbf{R}_j(s)]) \delta(\hat{\rho}_A + \hat{\rho}_B - \rho_0), \end{aligned} \tag{5.1}$$

where $\hat{\rho}_A$ and $\hat{\rho}_B$ denote the microscopic densities of A and B chains, respectively. Also, $\hat{\rho}_A = \hat{\rho}_{A,g} + \hat{\rho}_{A,f}$, where $\hat{\rho}_{A,g}$ and $\hat{\rho}_{A,f}$ are the microscopic densities of component A arising from the grafted and free chains, respectively. On the other hand, all the B segments are on grafted chains, hence $\hat{\rho}_B = \hat{\rho}_{B,g}$. The delta function in eq. (5.1) enforces the incompressibility of the overall system by requiring that the sum of the A and B species densities, $\hat{\rho}_A$ and $\hat{\rho}_B$, equals the average melt system density ρ_0. In eq. (5.1), U_0 corresponds to the bonded elastic interactions and, in the Gaussian chain model we adopt, is modeled by a form:[45]

$$\beta U_0[\mathbf{R}_i(s)] = \frac{3}{2b^2} \sum_{i=1}^{n_g} \int_0^{N_f} ds \left| \frac{\partial \mathbf{R}_i(s)}{\partial s} \right|^2, \tag{5.2}$$

where b denotes the statistical segment length. U_1 describes the non-bonded interactions, in particular the energetic repulsion between chemically dissimilar

chains. We adopt a simple Flory model where

$$\beta U_1[\mathbf{R}_i(s)] = \upsilon_0 \chi \int d\mathbf{r} \hat{\rho}_A \hat{\rho}_B. \tag{5.3}$$

with the Flory parameter χ quantifying the energetic penalty associated with the contact of chemically dissimilar segments.

The functional eq. ((5.1)) can be transformed by using functional integral methods into a field theory in which the fundamental degrees of freedom are potential fields $w_+(\mathbf{r})$and $w_-(\mathbf{r})$, [54] such that

$$Z = \int Dw_+ \int Dw_- \exp(-\beta H[w_+(\mathbf{r}), w_-(\mathbf{r})]). \tag{5.4}$$

where H is an "effective" Hamiltonian given by

$$\begin{aligned} \frac{H[w_+(\mathbf{r}), w_-(\mathbf{r})]}{k_{\mathrm{B}}TCA} &= \int dz[\frac{1}{\chi N_g} w_-^2 + iw_+ + \frac{\chi N_g}{4}] - \frac{V_h}{\alpha A} \ln Q_f[-iw_+ - w_-] \\ &\quad - \frac{\bar{\sigma}}{C} \ln Q_g[-iw_+ - w_-, -iw_+ + w_-]. \end{aligned} \tag{5.5}$$

In eq. ((5.5)), length scales have been nondimensionalized by the unperturbed radius of gyration, $R_{\mathrm{g}} = N_g^{1/2} b/6^{1/2}$, of the grafted chains. This results in a nondimensionalization of the grafting density σ (defined as chains per area) to $\bar{\sigma} = \sigma R_g^2$. The potentials w_+ and w_- and the continuous chain index s have been rescaled by N_g. With this nondimensionalization, the constant $C = \rho_0 R_{\mathrm{g}}^{\mathrm{d}}/N_g$ and $\alpha = N_f/N_g$ emerge as dimensionless parameters. Also, the equation is expressed on a per unit area basis, reflecting the assumption that the key behavior of the system can be captured by modeling it in one dimension. However, we do note that this does not take into account the

possibility that the segments of the random copolymer may segregate laterally, a phenomenon that could potentially be captured by modeling the system in two or more dimensions. Given the total system volume V and the cross sectional area A of the film (all dimensionless), we define the volume of the homopolymer melt V_h by the relationship $V/A = V_h/A + \bar{\sigma}/C$.

In ((5.5)) Q_g is the partition function of a single grafted chain in the fields $w_+(\mathbf{r})$ and $w_-(\mathbf{r})$, and is defined as

$$Q_g(\mathbf{r}_\perp; [\psi]) = \int d\mathbf{r} q_{\mathbf{r}_\perp}(\mathbf{r}, s; [\psi]). \tag{5.6}$$

In the above equation, the field $q_{\mathbf{r}_\perp}(\mathbf{r}, s; [\psi])$, referred to as the chain propagator, provides a statistical description of grafted chain conformations and satisfies a diffusion-like equation[54]

$$\frac{\partial q_{\mathbf{r}_\perp}}{\partial s} = \nabla^2 q_{\mathbf{r}_\perp} - \psi(\mathbf{r}, s; \theta(s)) q_{\mathbf{r}_\perp}; \quad q_{\mathbf{r}_\perp}(\mathbf{r}, s = 0) = \delta(\mathbf{r} - \mathbf{r}_\perp). \tag{5.7}$$

The initial condition in eq (5.7) is the result of the fact that one end of the chain is grafted to the surface, denoted by $\mathbf{r}_\perp$. In the above equation, the potential $\psi(\mathbf{r}, s)$ is the potential field acting on the different monomers and is based on the statistical distribution of the monomers. In this work, we use a "quenched" representation of the randomness in the chains. Explicitly, this invokes the modeling of a collection of chains whose sequences match the statistics of the prescribed random copolymer. Subequently, the conformational weights of the polymers are calculated for *each* of such chains (which have different sequences) and then averaged over the different chains to obtain the segmental volume

fractions fields at a given location. If we use the a random variable $\theta(s)$ that takes on a value of 1 for an A monomer and 0 for a B monomer to quantify the sequence distribution within a specified polymer, then the potential field acting on the segments of that polymer is given by

$$\psi(\mathbf{r}, s; \theta(s)) = \begin{cases} -iw_+(\mathbf{r}) - w_-(\mathbf{r}), & \text{if } \theta(s) = 1 \\ -iw_+(\mathbf{r}) + w_-(\mathbf{r}), & \text{if } \theta(s) = 0 \end{cases}. \tag{5.8}$$

In eq. (5.5) Q_f is the partition function of a single free chain in the field $w(\mathbf{r})$ and is defined as

$$Q_f = \int d\mathbf{r} q_f(\mathbf{r}, s = \alpha). \tag{5.9}$$

The field $q_f(\mathbf{r}, s)$ also satisfies a diffusion equation,

$$\frac{\partial q_f(\mathbf{r}, s)}{\partial s} = \nabla^2 q_f(\mathbf{r}, s) - [-iw_+(\mathbf{r}) - w_-(\mathbf{r})] q_f(\mathbf{r}, s); q_f(\mathbf{r}, s = 0) = 1. \tag{5.10}$$

The potential field in the above equation arises as a consequence of the fact that the free chains are assumed to be A chains. The volume fraction profile of the melt chains, composed of species A only, is defined as $\phi_{A,f} = \rho_{A,f}/\rho_0$, and is obtained as

$$\phi_{A,f}(\mathbf{r}) = \frac{V_h}{V Q_f \alpha} \int_0^\alpha ds q_f(\mathbf{r}, s) q_f(\mathbf{r}, 1 - s). \tag{5.11}$$

The single chain partition function of the grafted chains, Q_g, can be rewritten using a factorization property as [53]

$$Q_g(\mathbf{r}_\perp) = \int d\mathbf{r} q_{\mathbf{r}_\perp}(\mathbf{r}, s) q_g(\mathbf{r}, 1 - s), \tag{5.12}$$

where $q_g(\mathbf{r}, s)$ is a complementary chain propagator that satisfies eq. (5.7) with an initial condition of $q_g(\mathbf{r}, s = 0) = 1$. A further complementary propagator

can be defined as

$$q_{gc}(\mathbf{r}, s) = \int d\mathbf{r}_\perp \frac{\bar{\sigma} q_{\mathbf{r}_\perp}(\mathbf{r}, s)}{Q_g(\mathbf{r}_\perp, s)}. \tag{5.13}$$

which can be shown to satisfy eq. (5.7) with, however, an initial condition

$$q_{gc}(\mathbf{r}, s = 0) = \frac{\bar{\sigma}\delta(\mathbf{r} - \mathbf{r}_\perp)}{q_g(\mathbf{r} = \mathbf{r}_\perp, s = 1)}. \tag{5.14}$$

The volume fraction profiles of species A and B in the brush, $\phi_{A,g}(\mathbf{r})$ and $\phi_B(\mathbf{r})$ (also normalized by ρ_0), are then found as

$$\phi_{A,g}(\mathbf{r}) = \sum_{\{\theta(s)\}} \int_0^1 ds\theta(s) q_{gc}(\mathbf{r}, s) q_g(\mathbf{r}, 1 - s),, \tag{5.15}$$

and

$$\phi_B(\mathbf{r}) = \sum_{\{\theta(s)\}} \int_0^1 ds(1 - \theta(s)) q_{gc}(\mathbf{r}, s) q_g(\mathbf{r}, 1 - s)., \tag{5.16}$$

where the summation indicates the quenched averaging over the sequence distribution of monomers.

Replacing eq. (5.4) with the value of the exponent at its saddle point constitutes the approximation termed as self-consistent field theory (SCFT). The saddle point fields, w_+^* and w_-^*, found by setting the functional derivative of eq. (5.5) with respect to $w_+(\mathbf{r})$ and $w_-(\mathbf{r})$ to be zero, correspond to the solutions of the equations

$$1 - \phi_A(\mathbf{r}) - \phi_B(\mathbf{r}) = 0 \tag{5.17}$$

and

$$\phi_A - \phi_B - (2/\chi N) w_-^* = 0. \tag{5.18}$$

The free energy of the system can then be approximated using the value of $H[w_+^*(\mathbf{r}), w_-^*(\mathbf{r})]$ at the saddle point as

$$\frac{F[w(\mathbf{r})]}{k_{\mathrm{B}}TAC} = \frac{-\ln Z}{AC} = \int d\mathbf{r}[\frac{1}{\chi N} w_-^{*2} + i w_+^* + \frac{\chi N}{4}] - \frac{V_h}{\alpha A}\ln Q_f - \frac{\bar{\sigma}}{C}\ln Q_g. \quad (5.19)$$

Computation of F requires the solution of equations (5.7) - (5.12) and (5.14) - (5.18) with the appropriate boundary conditions. As discussed in previous theoretical studies in the context of thin films, [136] we use a reflecting wall boundary condition at the top of the film, which describes the assumed neutral interaction between the melt and air at this interface and enforces that the melt takes on its bulk density value up to the surface. This dictates that we impose Neumann boundary conditions, $\mathbf{n} \cdot \nabla q_f = \mathbf{n} \cdot \nabla q_g = \mathbf{n} \cdot \nabla q_{gc} = 0$ at this surface. For numerical reasons discussed in our previous work, [205] instead of using the Dirichlet boundary conditions on the grafted surface, we use a Neumann boundary condition on this surface.

The saddle point fields $w_+(\mathbf{r})$ and $w_-(\mathbf{r})$ are determined using a Picard iterative scheme of the form

$$w_+^*(\mathbf{r})_{new} = w_+^*(\mathbf{r})_{old} + \epsilon_+[1 - \phi_f(\mathbf{r}) - \phi_g(\mathbf{r})]. \quad (5.20)$$

and

$$w_-^*(\mathbf{r})_{new} = w_-^*(\mathbf{r})_{old} + \epsilon_-[\phi_A - \phi_B - (2/\chi N) w_-]. \quad (5.21)$$

where ϵ_+ and ϵ_- are relaxation parameters whose values were chosen to be between 0 and 1. Additionally, the average value of w_+ is enforced to be zero at every iteration. Because we assumed invariance along the surface of

the substrate, we numerically solved the diffusion equation in the dimension perpendicular to the wall using the Crank-Nicholson method. [1] We used a constant spatial mesh size of 0.04 and a discretization of the contour size of 0.0004. The mean field equations were iterated to a mean-squared error in w_+ of less than 3.5×10^{-4} and an error in w_- of less than 1.5×10^{-6}.

Mimicking the experimental conditions involving statistical copolymers requires us to generate an ensemble of chains whose overall composition of species A is represented by the parameter f but with a distribution of sequences reflecting the statistical nature of their sequences. For this purpose, we use the construction of Fredrickson *et al.* [55] to generate our copolymers. A parameter P_{jk} is defined as the conditional probability that a segment of type j at an arbitrary location in the chain is immediately followed by a segment of type k, where j, k = A or B. Because the only options that exist are A or B segments, by construction $P_{AB} = 1 - P_{AA}$ and $P_{BA} = 1 - P_{BB}$. Also, to ensure that the average volume fraction of the segments is f, we have $f = P_{AA}f + P_{BA}(1 - f)$. Given these equalities, it can be shown that the resulting statistical distribution of sequences on the chains can be described by the parameter $\lambda = P_{AA} + P_{BB} - 1$ and that $P_{AA} = f(1 - \lambda) + \lambda$ and $P_{BB} = f(\lambda - 1) + 1$. The parameter λ quantifies the tendency of a new segment to remain chemically equivalent to the previous one. Specifically, $\lambda = 0$ corresponds to the purely random case, $\lambda = -1$ corresponds to an alternating copolymer, and $\lambda = 1$ corresponds to a homopolymer with chemical identity determined by the probability associated with the first segment in the chain.

To implement this strategy, we generate an ensemble of chains based on the above procedure and average the results over them to account for the statistical nature of sequences in the polymers.

Since the numerical discretization "Δs" is distinct from the physical size of a segment in the chain, we also specify the number of segments in the chain and generate "segments" composed of the appropriate number of s points. In Appendix 5.2.2 an explanation of the explicit procedure used to generate the protein-like chains is also provided. The SCFT calculations are then performed on all n_g of these chains and the results averaged at each iteration. For each parameter set, we did two runs on 500 chains composed of 100 segments and averaged the results. Given that $\Delta s = 0.0004$ and $0 < s < 1$, this means that each segment is composed of 25 s points.

To quantify the interfacial energy between the bulk film and the brush, we use an approach similar to that expounded in Matsen. [136] Explicitly, the free energy of the system $F(d)$ is calculated as a function of the total film thickness d (which includes both free and grafted chains). Subsequently, the interfacial energy between the bulk film and the brush is obtained as [136]

$$\gamma_{b/h} = \frac{F(\infty) - F(d_{min})}{A} \tag{5.22}$$

where d_{min} is the thickness for which $F(d)$ is a minimum and A is the area of the substrate.

5.2.2 Generating Protein-like Chains

To generate protein-like chains, we used the bond fluctuation model proposed by Carmesin and Kremer.[22, 38] We use this construction under the assumption that the 27 sites near each site are excluded as neighbors, while all the 54 next nearest neighbors interact with an attraction of $-1kT$ regardless of the exact site to site distance. We initiate our simulations with an unperturbed Gaussian chain configuration (with no attraction) and turn on the above attractive interactions to allow the coil to reach a collapsed globular state. Once this is done, the monomers are sorted in order of increasing distance from the center of mass and the closest monomers are "colored" as dissimilar from the homopolymer melt until the appropriate value of f is achieved in the chain. This procedure is repeated for each new chain to ensure statistical independence of the chains. We do note that the sequence generated by the procedure and the quantitative values of the resulting interfacial energies depend on the strengths of the monomer-monomer attractive interactions. This is similar to the temperature dependence of the sequences synthesized in experiments.

5.2.3 Strong-stretching theory

In the following sections we present the SCFT results for the interfacial widths between the brush and the homopolymer melt and the interfacial energy, $\gamma_{b/h}$. In rationalizing the trends seen, it is also of interest to explore whether the results for interfacial width and interfacial energy can be explained using scaling ideas or simpler theories. Towards this objective we develop such

a theory based on ideas from strong-stretching theory (SST) models used for polymer brushes. [96, 137, 181] Such theories have played an important role in the development of a fundamental understanding of interfacial properties of polymer brushes. The key assumption of such theories is that the chains are strongly stretched and therefore the partition function can be estimated by the statistics of the single polymer path that minimizes the energy. [133] In the situation where the brush and melt are chemically identical (termed "autophobic dewetting" due to the expulsion of free chains from the brush by purely entropic forces), several numerical studies have indicated that the qualitative behavior of density profiles, free energies, and other key quantities predicted by SCFT are in most cases well-captured by strong segregation theory. [133, 134, 136, 137] A shortcoming of SST is that its assumptions are valid only at grafting densities typically larger than those found in experiments. In a recent study, Matsen has pointed out that such limitations lead to significant quantitative discrepancies between the predictions of SCFT and SST in the case of autophobic dewetting ($f = 1$). [133]

We use an extension of the SST from the autophobic case [136, 181] developed in our earlier work. We first recall the main elements of this model for the case of a melt-brush interface between chemically distinct homopolymers whose enthalpic interactions are denoted as χ. In this model, the free energy per unit area of a film of total thickness d (including brush and melt)

was approximated as

$$\frac{FN_g}{\rho_0 R_g} = \int_0^d dz \left[\frac{\pi^2}{16} z^2 \phi_b(z) + \frac{1}{4} \frac{(d\phi_b/dz)^2}{\phi_b(1-\phi_b)} + \frac{(1-\phi_b)\ln(1-\phi_b)}{\alpha} + \chi N_g \phi_b (1-\phi_b) \right] \tag{5.23}$$

where $\phi_b(z)$ is used to denote the volume fraction profile of the brush monomer species. Here all variables are nondimensionalized in the same manner as detailed in the preceding section. In eq. (5.23), the first term corresponds to the stretching energy of the grafted chains, whereas the second term represents the configurational entropy costs due to the interface between the grafted and free polymers. The third term above quantifies the translational entropy of the homopolymer chains and the fourth term corresponds to the enthalpic interactions between unlike segments. We note that the quantitative discrepancies between SST and SCFT have been shown to be associated with the inability of the second term to accurately represent the actual configurational entropy as calculated from SCFT. [134]

For partial interpenetrations between the brush and melt, $\phi_b(z)$ was assumed to be of the form

$$\phi_b(z) = \frac{1}{2} \left[1 - \tanh \left(\frac{2(z - \bar{\sigma}/C)}{w} \right) \right]. \tag{5.24}$$

where, as in the case of the SCFT, $\bar{\sigma}/C$ represents the volume per unit area of the brush, which is equivalent to the unperturbed brush height. Using this assumption, the interfacial energy between A and B was then estimated as

$$\frac{\gamma_{A-B} N}{\rho_0 R_g} = \left[\frac{\pi^4}{36} \frac{\bar{\sigma}}{C} w_{b/h}^2 + \frac{1}{w_{b/h}} - \frac{0.41123}{\alpha} w_{b/h} + \chi N \frac{w_{b/h}}{4} \right]_{min} \tag{5.25}$$

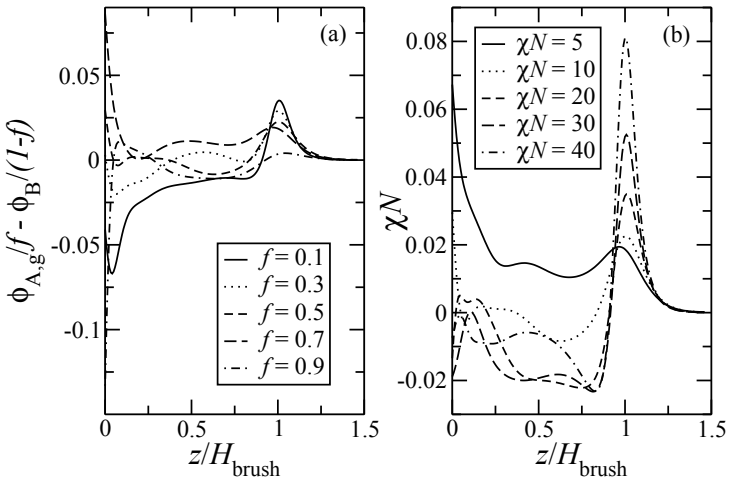

Figure 5.1: Enrichment of segments in the brush for different f ($\sigma R_g^2/C = 4.9, \alpha = 1$, and $\chi N = 10$); b) different χN ($f = 0.5$, $\sigma R_g^2/C = 4.9$, and $\alpha = 1$).

where the subscript min indicates that the right-hand side was evaluated at the value of $w_{b/h}$ which minimizes $\gamma_{b/h}$.

To extend the above theory to describe the interface between a statistical copolymer brush and melt, we postulate that the grafted chains rearrange their ends to allow for the ends of the chains which are enriched in A to be in contact with the melt chains. We hypothesize that such rearrangements would take advantage of the favorable interaction between similar segments while resulting in little entropic cost. This hypothesis is corroborated by a plot of $\phi_{A,g}(z)/(1-f) - \phi_B(z)/f$ as a function of the distance from the grafting surface obtained using the exact results of SCFT. This quantity tracks the enrichment (relative to the average composition), if any, existing in the A and B segments. Explicitly, a positive value would correspond to enrichment of

A chains and a negative value to the enrichment of B chains. In Figure 5.1, we show such plots for different f and χN. We note the increasingly large positive peak near $z/H_{brush} = 1$ in the structure as the grafted and free chains become more dissimilar (decreasing f) and as the interaction between different segments increases (increasing χN). This points to a rearrangement of the grafted chain ends in order to ensure that the ends with the most A segments are in contact with the melt.

Our modification to the SST theory of equations of (5.23) and (5.25) involves replacing the Flory parameter χ in eq. (5.23) by a parameter χ_{eff} which captures the fact that the segments in the interfacial region are enriched in the A component. To maintain simplicity, we approximate the brush as a melt brush with a step-function density profile and a free end distribution [137]

$$g(z_0) = \begin{cases} z_0/(L\sqrt{L^2 - z_0^2}), & \text{if } 0 < z_0 < \frac{\bar{\sigma}}{C} \\ 0, & \text{if } z_0 > \frac{\bar{\sigma}}{C} \end{cases} . \tag{5.26}$$

The above corresponds to the free end distribution of a homopolymer melt brush and we use it under the assumption that the free end distributions are unchanged due to i) interpenetration and ii) enthalpic interactions with the melt chains. We then estimate the fraction of chains whose ends are within the interfacial width w_b as

$$\mu(w_{b/h}) = \int_{\bar{\sigma}/C - w_{b/h}}^{\bar{\sigma}/C} g(z_0) dz_0. \tag{5.27}$$

We also estimate the fraction of segments κ that reach the interface as the ratio of the interfacial width to the dry brush height

$$\kappa(w_{b/h}) = \frac{w_{b/h}}{\bar{\sigma}/C}. \tag{5.28}$$

Given a set of n_g randomly generated chains with size N_g segments each, the number of segments of the brush that reside in the interfacial region $w_{b/h}$ is assumed to be $\kappa(w_{b/h})N_g$. Using this value, we find the fraction of A segments in the part of each chain that resides in the interface. We then select the $n_{max}(w_{b/h}) = \mu(w_{b/h})n_g$ chain ends that are richest in A segments and assume that they will be the chains whose ends reside in the interface. We average the composition f_i of these n_{max} chain ends to find their average composition, $f_{eff}(w_{b/h})$. Assuming these chains are the ones that exist in the interface, we then define $\chi_{eff} = (1 - f_{eff})\chi$ to be used in equation (5.25). Because the method is fast, we obtain better statistics by using duplicate trials with $n = 10000$ chains generated by the scheme described above. Subsequently, a Newton method is used to obtain the value of $w_{b/h}$ which a minimizes eq. (5.25). We note that equation (5.25) is only valid for the case when the minimum energy occurs at the dry brush height d_0 as a function of film thickness. Because of this, when f is varied we do not report results for $f > 0.7$ and when α is varied we do not report results for $\alpha < 1$ since in these cases the minimum energy occurs at a thickness d_0.

In Figure 5.2 we compare the SCFT and SST predictions for the effective volume fraction of A segments in the interface, f_{eff}, as a function of interfacial width for varying grafting densities. While the enrichment is predicted in both cases, we note that the SST captures this effect only qualitatively and that it substantially overestimates this f_{eff}. Since overestimating f_{eff} corresponds to underestimating χ_{eff}, this has the possibility of causing

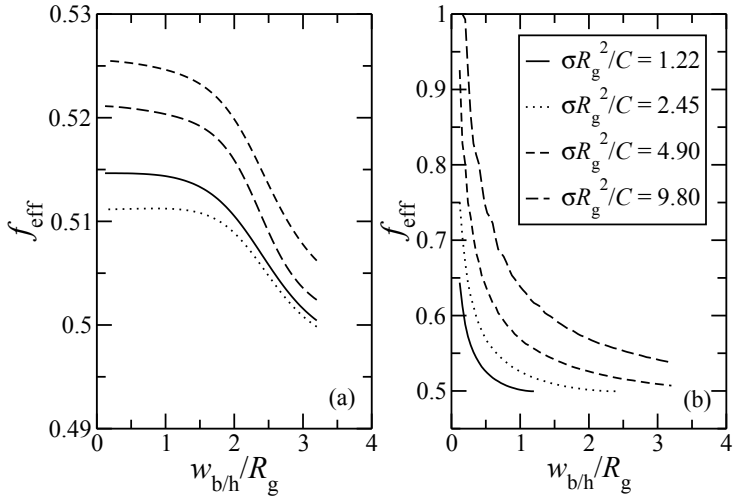

Figure 5.2: Effective volume fraction of A segments in the interface f_{eff} as a function of $w_{b/h}$ calculated from SCFT (left) and SST (right) for different values of $\sigma R_g^2/C$. Overall volume fraction of A segments in the brush is $f = 0.5$. Parameters $\alpha = 1$, and $\chi N = 10$.

the magnitude of the energetic term in eq. (5.25) to be underestimated, especially with increasing grafting density. However, considering the qualitative match in the trends noted, we still use the proposed extension of the SST to test its ability to predict the interfacial widths and energies.

5.3 Results

5.3.1 Brush-Melt Interfacial Width

We first present results which explore the effect of different parameters in the system upon the interfacial width between the melt and brush. The latter is a measure of the interpenetration of the free chains into the brush and is expected to be inversely correlated to the interfacial energy between

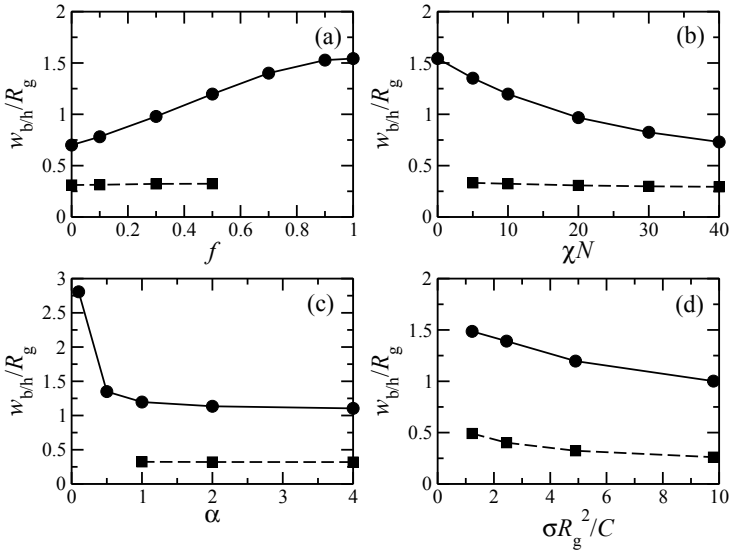

Figure 5.3: Interfacial widths from SCFT (solid) and SST (dashed) as a function of the key parameters. Unless otherwise stated, chains are purely random ($\lambda = 0$); a) Varying f, $\chi N = 10.0$, $\alpha = 1.0$, and $\sigma R_g^2/C = 4.90$; b) Varying χN, $f = 10.0$, $\alpha = 1.0$, and $\sigma R_g^2/C = 4.90$; c) Varying α, $f = 10.0$, $\chi N = 10.0$, and $\sigma R_g^2/C = 4.90$; d) Varying $\sigma R_g^2/C$, $f = 10.0$, $\chi N = 10.0$, and $\alpha = 1.0$.

the melt and brush. We define the interfacial width as [136]

$$w_{b/h} = \frac{\phi_g(0)}{\phi_g'(z_{1/2})} \tag{5.29}$$

where $\phi_g(z)$ is the volume fraction of the grafted segments as a function of the distance z from the substrate and $\phi_g'(z_{1/2})$ is the derivative of this volume fraction profile evaluated at the location $z_{1/2}$, corresponding to the distance at which the volume fraction of the brush is half its value at the surface. The interfacial width and its trends allow us to glean physical insights into the results for interfacial energies presented subsequently. Additionally, the interfacial width is often used as a measure of the quality of the interface in the context of interfacial compatibilization applications of random copolymers and thus this quantity serves as a useful starting point for a discussion of our results. We note that unless otherwise stated, the following discussions pertain to purely random chains ($\lambda = 0$).

Figure 5.3(a) shows the effects of varying the overall volume fraction of A segments in the grafted chains (denoted f) upon the interfacial widths, $w_{b/h}$. At small f, the grafted chains are predominantly composed of B monomers which are chemically incompatible with the melt, resulting in small interfacial widths. However, with increasing f, the grafted and melt chains become increasingly similar and the chains are more able to penetrate into the brush. The limiting case of $f = 1$ corresponds to the *autophobic* situation where all species in the system are chemically similar and the melt chains have no energetic driving force to be expelled from the melt and thus the free chains maximally penetrate into the brush.

In Figure 5.3(b), we present results depicting the effects of changing χN on the interfacial widths. As χN increases, the unlike monomers have an increasingly repulsive interaction. Therefore the free chains are expected to be increasingly expelled from the brush, which rationalizes the decrease in the interfacial width. In Figure 5.3(c) we show the effect of varying α, which denotes the relative sizes of the free and grafted chains. As the free chain size increases relative to the grafted chain length, the free chains accrue less translational entropy benefit from penetrating the grafted chains when compared to the stretching cost incurred by the grafted chains for this penetration. This is expected to lead to a reduced interpenetration between the melt and brush, a trend consistent with the results. The preceding effects are expected to be compounded by increasing the grafting density due to a concomitant increase in the cost of brush stretching associated with interpenetration. This manifests in the results shown in Figure 5.3(d), where increased grafting density is seen to lead to a smaller interfacial width. Overall, the above results show that the trends in the interfacial width as a function of chains lengths and grafting densities reflect trends qualitatively similar to those in the autophobic ($f = 1$) case.

In Figure 5.3 we also compare our results for interfacial widths from strong stretching theory to those from SCFT. We observe that while the predictions of SST qualitatively agree with the SCFT, the SST is seen to underpredict the value of the interpenetration width and to be generally less sensitive to variation of many of the parameters. Comparisons between SST

and SCFT in the autophobic case show a similar underprediction. [136] In a subsequent section, we discuss the origins of the discrepancies between SCFT and SST.

Figure 5.4(a) shows the effects of varying the type of randomness on $w_{b/h}$. It is seen that at smaller levels of blockiness (λ), this parameter has only little effect on the interfacial width. However, when the chains become very blocky the interfacial widths are seen to become substantially larger (compared to the less blocky counterparts). To explain these trends, in Figure 5.4(b) we display an increasing enrichment of A segments (quantified by $\phi_{A,g}(z)/(1-f) - \phi_B(z)/f$) near the interface with increasing blockiness. Thus, increased interpenetration of the free A chains can be understood as a consequence of the presence of larger A blocks near the interface and the accompanying reduction in the enthalpic costs. This effect is similar to trends noted in the context of statistical copolymers in compatibilizers, where large values of blockiness allow larger regions of chemical species in the chains to segregate to the chemically similar side of the interface. [232]

5.3.2 Brush-Melt Interfacial Energies

In Figure 5.5 we first display the effect of varying the composition of A segments in the grafted chains upon the free energies $F(d)$, which represent the free energy of a film of thickness d (including the free and grafted chains). We have shifted the resulting potentials such that they take a value of zero at the distance d_∞ where the energies cease changing. In the light of equation (5.22),

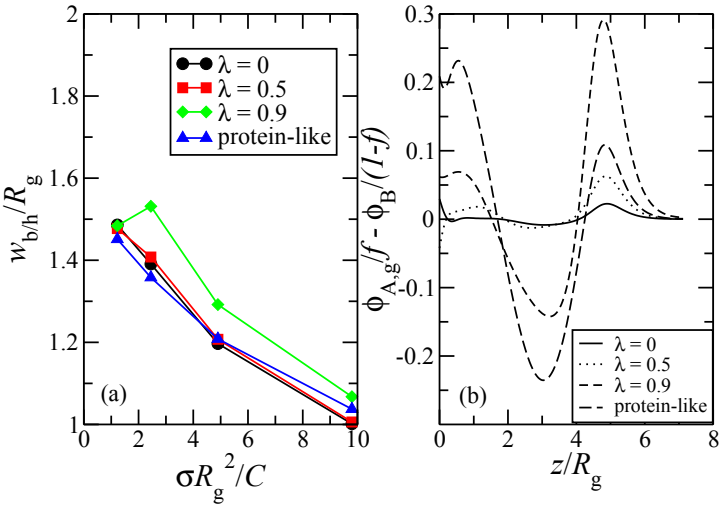

Figure 5.4: a) Interfacial widths between the brush and the melt as a function of $\sigma R_g^2/C$, with $f = 1.0$, $\chi N = 10.0$, and $\alpha = 1.0$ for different blockiness of sequences; b) Enrichment of segments in the brush structure for different blockiness of sequences. Parameters $f = 1.0$, $\sigma R_g^2/C = 4.9, \alpha = 1$, and $\chi N = 10$.

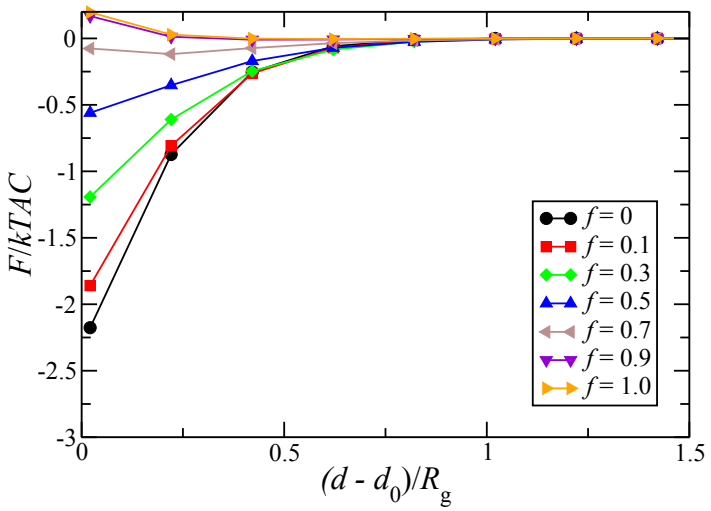

Figure 5.5: Interaction potentials for different values of f. $\chi N = 10.0$, $\alpha = 1.0$, and $\sigma R_g^2/C = 4.90$.

the case of $F_g(d_{min}) \approx F_g(\infty)$ is indicative of stability of the free chains on the grafted chains, whereas $F_g(d_{min}) \ll F_g(\infty)$ corresponds to a tendency for the free chains to dewet from the film due to a large interfacial energy. To quantify the thickness of the melt overlayer, the total film thickness is shifted by the one-dimensional box size $d_0/R_g = \sigma R_g^2/C$, which is the value (normalized by R_g) at which a dry brush is achieved.

From the results presented in Figure 5.5, it can be seen that at small f (corresponding to a larger fraction of B segments) a large attractive well in $F(d)$ occurs at $d = d_0$. The latter corresponds to the situation where the free chains are completely expelled from the brush, due to the fact that at small f the grafted polymers are chemically incompatible with the melt.

With increasing f, the grafted and melt chains become increasingly similar and the *energetic* driving force for the free chains to be expelled from the grafted chains is reduced and eventually the minimum occurs at a location $d > d_0$. The latter reflects an increasing tendency for the chains to wet the brush, corresponding to the situation of coexistence of a macroscopic droplet with a film of finite thickness $d - d_0$. [18, 82] These results are also consistent with the larger interfacial widths noted in Figure 5.3(a). The limiting case of $f = 1$ corresponds to the autophobic situation where all species in the system are chemically similar. In this situation, the attractive well becomes relatively small since the melt chains have no enthalpic driving force to be expelled from the brush.

As has been noted by earlier authors in the autophobic scenario [136], there is a mathematical equivalence between the models of a plate grafted with a polymer brush immersed in a melt where a reflecting boundary condition is imposed at the free surface, and the symmetric case of two plates grafted with polymers interacting in a polymer melt. As a result, the potentials shown in Figure 5.5 also address the interaction between two surfaces containing random copolymers in a polymer matrix. The use of brushes that are chemically different from the melt has been suggested as a potential means of achieving this goal and previous theoretical results suggest that the use of high molecular weight grafts or polymers whose Flory interaction parameter χ is negative may be a viable strategies for achieving dispersion, especially if synthesis or grafting methods are limiting factors. [17, 75, 96] The potentials shown in Figure 5.5

indicate that the limiting case of $f = 1$ has the greatest potential for achieving particle dispersion due to the small potential well. However, according to our results larger values of f may also be used if a random copolymer brush is preferred during synthesis. In particular, when $f \geq 0.7$, the existence of a minimum at $d_{min} > d_0$ corresponds to small values of interfacial energy that have the potential to be used as grafts to help achieve dispersion of particles.

Figures 5.6(a)-(c) display the interfacial energies (derived from eq. (5.22)) as a function of different parameters. Figure 5.6(a) displays the interfacial energies as a function of f. These exhibit trends consistent with the free energies discussed in Figure 4. We note that while the concept of simple mixing of unlike chains would dictate that the interfacial energy would decrease linearly with f, in contrast the results for interfacial energy shows a negative deviation from this expectation. The fact that at larger values of f the interfacial energy is smaller than that expected from simple mixing rule considerations is consistent with a rearrangement of those chain ends that are richer in A segments toward the interface. In particular, our interfacial energies suggest that this effect is more pronounced as the brush and melt become more chemically similar.

In Figure 5.6(b) we explore the effect of varying χN at fixed $f = 0.5$. As χN increases, unlike monomers have an increasingly repulsive interaction. As a result, the interfacial energy between the grafted and melt chains increases, representing an increased tendency for a film of A chains to dewet the grafted chains. These trends are observed to be consistent with the results for the

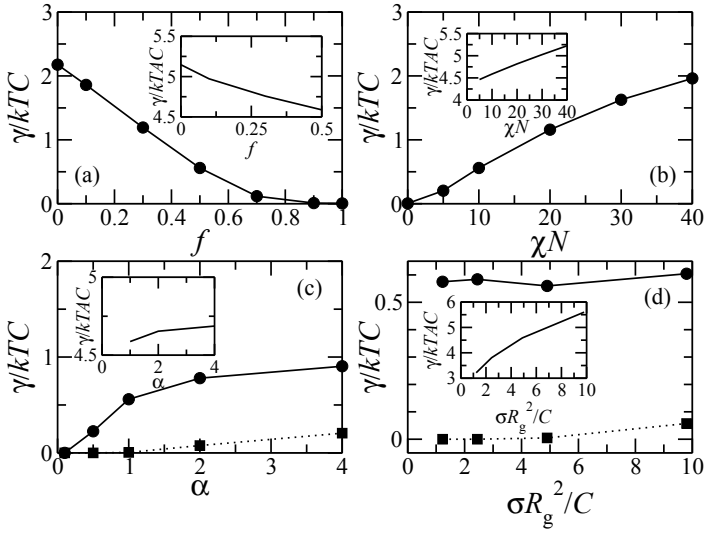

Figure 5.6: Interfacial energy of the brush-melt interface for purely random chains ($\lambda = 0$) a) for different values of f ($\chi N = 10.0$, $\alpha = 1.0$, and $\sigma R_g^2/C = 4.90$); b) for different values of χN ($f = 0.5$, $\alpha = 1.0$, and $\sigma R_g^2/C = 4.90$); c) for different values of α ($f = 0.5$, $\chi N = 10.0$, and $\sigma R_g^2/C = 4.90$); d) for different values of $\sigma R_g^2/C$ ($f = 0.5$, $\chi N = 10.0$, and $\alpha = 1.0$). The dotted lines in (c) and (d) show predictions for the autophobic scenario. The insets show corresponding predictions from SST.

interfacial widths presented in Figure 5.3(b).

In Figure 5.6(c) we show the effect of varying α, the relative size of the grafted and free chains. Even for $f = 0.5$, the trends in interfacial energy are seen to qualitatively display trends similar to those displayed by the autophobic ($f = 1$) case. Explicitly, as α increases, the relatively larger free chains are less able to penetrate into the grafted chains (as was seen in the results for the interfacial widths in Figure 5.3(b)), resulting in less favorable interfacial interactions between the grafted and free chains.

We also display the results for the behavior of the interfacial energies

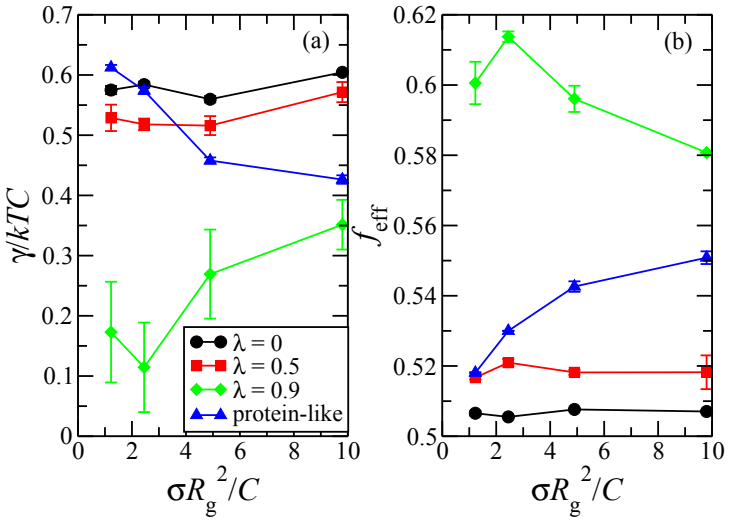

Figure 5.7: a) Interfacial energy and b) Effective concentration of A segments in the interfacial region displayed as a function of $\sigma R_g^2/C$ for different kinds of randomness. $f = 0.5$, $\chi N = 10.0$, and $\alpha = 1.0$.

as a function of grafting density in Figure 5.6(d). The slight increase in the interfacial energies as a function of grafting density is seen to be very similar (within numerical inaccuracy) to the predictions for the autophobic case. [136] These results also agree with the predictions from Kim, et al which indicate that, in the case of a homopolymer melt interacting with a chemically different brush, the interfacial energies increase as a function of grafting density. [96]

In Figure 5.7(a) we explore the effect of changing the sequence distribution by showing the effect of varying grafting densities for different kinds of sequence distributions. In the range $\lambda = 0 - 0.5$, it can be seen that the variations in blockiness have only a minimal effect upon the interfacial ener-

gies. However, it is seen that only the chains which are very blocky ($\lambda = 0.9$) manifest a significant difference. We hypothesize that the decrease in the interfacial energy with increasing blockiness is due to the fact that the increased blockiness allows for larger regions of A segments to populate the interpenetration zone and interact favorably with the melt polymer, which results in larger interpenetration of the brush and melt chains and an energetically more favorable interface. In Figure 5.7(b) we corroborate this hypothesis by displaying the effective concentration of A segments in the interpenetration zone, f_{eff}. For this calculation, we find f_{eff} to be best defined as the region in which the value of $\phi_{A,g} - \phi_B$ is enriched in A segments, in other words the location where curves such as those found in Figure 5.1 cross the x-axis from the positive side for the first time. For the different levels of blockiness, it is seen that the effective concentration of A segments in the end chains shows similar (but inverse) trends (and within the error associated with the random chains) as those shown by the interfacial energies. Specifically, we note the dramatic enrichment of species A in the distribution of end segments as a function of blockiness.

In Figure 5.7(a) we also show the effect of varying $\sigma R_g^2/C$ for grafted protein-like chains. While for larger grafting densities the protein-like chains have surface energies comparable to those associated with random chains with $\lambda > 0.5$, at smaller grafting densities the interfacial energy takes on values that are comparable to lower values of λ. Based on Figure 5.7(b), it is seen that these trends result from the tendency for the chain ends of protein-like chains

to rearrange themselves near the interface with increasing grafting density (compared to blocky chains).

We also comment on the implications of the results in Figures 5.6 and 5.7 for dispersion of particles. Given the assumption that particle dispersability usually correlates to melt-brush interfacial energies, [96] the limiting cases shown in Figures 5.6(a) - (b) reinforce the fact that the autophobic case is best for achieving particle dispersion. However, Figure 5.6(c) also suggests that small values of α, which (when the melt chain length is fixed) correspond to larger grafted chain length, also have the potential to achieve small values of interfacial energies and thus improved dispersion even in the presence of chemically different segments in the grafted layers. Also, Figure 5.7(a) indicates that the use of very blocky chains (in which the chains more closely resemble homopolymers) could also be used to reduce the interfacial tension and achieve dispersion. Densely grafted layers of protein-like chains also show potential for reducing the surface energy and possibly achieving particle dispersion, while for smaller grafting densities the protein-like chains are predicted to perform poorly for achieving dispersion.

In Figure 5.6 we also show a comparison of the SST predictions for the interfacial energies to the predictions from SCFT. As mentioned earlier, equation (5.25) is only valid for the case when the minimum energy occurs at the dry brush height d_0 as a function of film thickness. Because of this, we do not report SST values for $f > 0.7$ and $\alpha < 1$, where this condition is not satisfied. From Figure 5.6, it can be seen that trends displayed by

the SST and SCFT show qualitative agreement as a function of f, χN, and α. However, grafting densities are seen to influence the SST results in a much more pronounced manner than SCFT. This disagreement is also consistent with comparisons between SCFT and SST presented by Matsen for the autophobic case which show that the SST substantially overpredicts the interfacial energies compared to SCFT. The latter was shown to be a consequence of inaccuracies in the second term in equation (5.23), which represents the conformational entropy associated with forming an interface in the grafted and free chains. An additional source of error in the SST was also pointed out in our earlier discussion, viz., the underestimation of the enthalpic effect in the SST. This may rationalize the fact that the SST results qualitatively mirror more closely the trends noted for the autophobic situation rather than the situation of incompatible polymers.

5.4 Discussion

In this section, we comment on the significance of our results specifically in the context of 1) the ramifications of the trends noted in interfacial energies for the design of neutral surfaces and dispersion of particles; and 2) for characterization of blockiness of polymers using interfacial energy measurements.

5.4.1 Implications For Particle Dispersion and Neutral Surfaces

As discussed in the introduction, grafted polymers are often used to facilitate efficient dispersion of particles. The results presented in the preceding section demonstrates that grafted random copolymers may also be a viable way to achieve dispersion of particles in nanocomposite systems. In particular, this approach is viable if reaction conditions are designed such that f is reasonably large or the Flory interaction parameter χ between the polymers is small. Also, the use of long grafted chains and blocky chains has great potential to achieve the small interfacial energies that are generally associated with particle dispersion.

An important consideration for patterning applications is the design of neutral surfaces, that is, surfaces which exhibit comparable interfacial energies when in contact with either the A or B blocks. These surfaces have the tendency to promote the formation of perpendicularly aligned lamellae or cylinders when in contact with AB diblock copolymers which are attractive for electronic materials applications. While in our model, neutral surfaces always occur at $f = 0.5$ (due to the absence of substrate-polymer interactions), the range over which a surface can be *approximately* neutral is expected to vary for different parameter values. It is also expected that a surface in which a broader range of parameters will result in an *approximately* neutral surface will be more forgiving to imperfections in actual synthesis. We assess the size of this range by plotting $\gamma(f) - \gamma(1-f)$ vs f for varying grafting density and α. For comparison, we draw upon a phase diagram recently reported by

Meng, et al for a diblock copolymer thin film confined by two smooth surfaces. [146] When the preference for the top surface is set to zero (appropriate for the no flux boundary condition we impose on the free surface of the film), a symmetric block copolymer is used, and $\chi N = 15$, they report a neutral window (adjusted to the units we use) of $-0.15 < \gamma/kTC < 0.15$. This window is shown in Figure 5.8. The width of this distribution indicates the range over which a surface can behave as approximately neutral and induces the formation of perpendicular lamellae.

In Figure 5.8(a) we plot $\gamma(f) - \gamma(1-f)$ vs f for varying grafting density. Our results show that the range over which a neutral surface occurs (as defined by the width of the distribution) increases with increasing grafting density, a trend consistent with the fact that at large grafting densities the surface becomes effectively an impermeable rigid surface. In Figure 5.8(b) we explore the effect of different kinds of randomness on the neutral window. Changing the type of randomness is seen to have little effect on the size of the neutral window, although the protein-like chains appear to show the greatest promise for the achievement of a larger range of neutrality.

Our results in Figure 5.6(a) are partially consistent with experimental trends shown by Mansky et al. for a methyl methacrylate (MMA) and styrene (S) random copolymer brush in contact with a film of polystyrene (PS). [129] Specifically they show that as f increases (the brush and the melt become similar), the interfacial energy decreases. However, for grafting densities comparable to what we use, and for $\alpha \simeq 3$, these authors show that a neutral

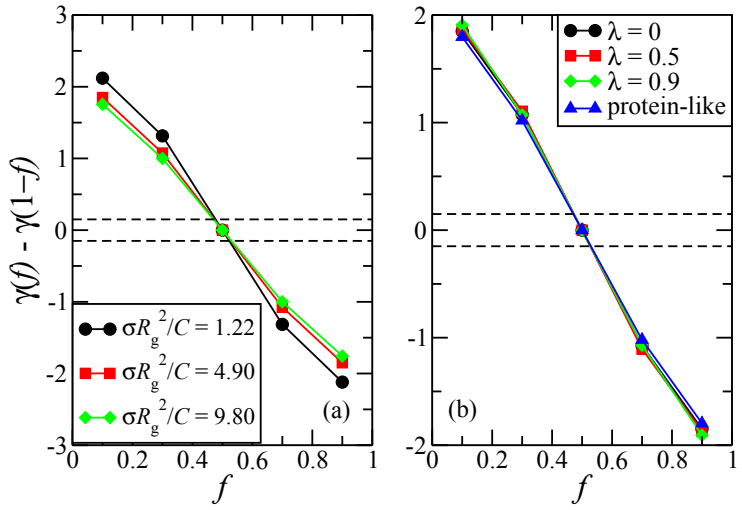

Figure 5.8: a) Plot of $\gamma(f) - \gamma(1-f)$ vs f as a function of $\sigma R_g^2/C$. $\chi N = 10.0$, and $\alpha = 1.0$. b) Plot of $\gamma(f) - \gamma(1-f)$ vs f as a function of type of randomness. $\alpha = 1.0$, $\chi N = 10.0$, and $\sigma R_g^2/C = 4.90$. In both plots, the dotted lines correspond to the theoretically reported limits of the neutral window from Meng, et al. [146]

surface occurs at $f = 0.57$. This shift away from $f = 0.5$ is due to the fact that one of the blocks has a preference for the substrate over the other. [209] Thus, while our results are useful for providing insight into the size of the neutral window as a function of system parameters, we expect that they will be shifted based on the relative affinity of the blocks for the substrate.

5.4.2 Characterization of blockiness using interfacial properties

An interesting question is whether contact angle measurements between the brush and homopolymer can be used to quantify the degree of blockiness of the polymer. In order to assess the viability of this strategy, one may extract an approximate measure of the contact angle using the equation[136] $\theta_c = (2 * \gamma_{b/h}/\gamma_{p/a})^{1/2}$, where $\gamma_{p/a}$ is the interfacial energy between the polymer and air (We note that the preceding equation is only accurate in assumption that air-homopolymer interfacial tensionis identical or comparable to the air-grafted layer interfacial tension). To assess this, we use the experimental parameters in Mansky et al for polystyrene, which yields $C = 0.238$, their experimental temperature of 170 C, and $\gamma_{p/a} = 29.9$, which is the value for styrene given in the paper and differs minimally from the value for MMA of 30.02 calculated in their paper. [129] We find that the contact angles vary by less than a degree between $\lambda = 0$, $\lambda = 0.5$ and the protein-like chains, but that the case of $\lambda = 0.9$ varies from the previous situations by about 3 degrees. We conclude that only very blocky random copolymers may exhibit a measurably different contact angle than less blocky ones. This conclusion is consistent

with recent findings by experimentalists.[1]

5.5 Summary

We studied a random copolymer brush of composed of segments A and B in contact with a thin film composed of homopolymer A. We reported interaction potentials which reflect the stability of the film on the brush and calculated interfacial widths and interfacial energies as a function of key system parameters. We find that interfacial characteristics reflect trends which can be surmised from the autophobic case. We also compared the interfacial qualities for different types of randomness and find that increasing blockiness has the effect of reducing the interfacial energy. While the homopolymer case is a helpful model system to begin to study the phase behavior of diblock copolymers on a random copolymer brush, in a future study we propose to study the more realistic case of phase behavior of diblock copolymers on random copolymer brushes in order to more accurately capture the system.

[1] A. Crosby, Private Communication (2011)

Chapter 6

Self-Assembly of Diblock Copolymer on Substrates Modified by Random Copolymer Brushes

6.1 Introduction

The self-assembly behavior of di- and multiblock copolymers has attracted significant attention in both fundamental and technological contexts. Among the many different morphologies exhibited by block copolymers, perpendicularly aligned lamellar and cylindrical phases of diblock (AB) copolymers have constituted a focus of attention in the design of semiconductor materials. The underlying idea involves modification of one of the blocks is modified with an etch-resistant material. If the structures are aligned perpendicularly, the self-assembly of the diblock then allows for the creation of alternating patterns in the polymer film which, when etched, leads to a high density array of patterns which can be transferred to the substrate. Because such patterns are small and tunable through the diblock chain lengths, they have attracted attention as a potential successor to traditional photolithographic methods. This method has been successfully used to create a variety of vertically aligned polymer patterns and that subsequent etching to transfer the pattern is feasible. [70–72, 176, 194]

A key challenge in the success of the above efforts is to be able to obtain perpendicularly aligned self-assembled structures that are free from defects. This in turn requires substrates which are energetically "neutral," i.e., that do not exhibit a preference for either of the components. Indeed, if the substrate exhibits a preference for one of the components, then it is more likely that this component will wet the substrate, resulting in the formation of parallel aligned phases. Unfortunately, however, many of the commonly employed substrates do exhibit an energetic preference for one of the blocks, necessitating additional strategies to render them neutral to the different components.

In relation to the above, experimentalists have pursued a variety of methods to induce the formation of perpendicularly aligned phases. One common approach involves modifying the substrate with a striped pattern that has an energetic preference for one of the blocks. While this might seem to require a method to chemically pattern the surface on the scale of the desired feature size, it has been shown that patterns whose features are coarser than the size of the desired lamella may even suffice to induce the formation of perpendicularly aligned phases. [176] Another method that has proved effective in inducing perpendicular patterning is the use of electric field-induced alignment.[151, 203]

Another common method of achieving perpendicular lamellae is to modify the interactions between the polymers and the substrate by using a grafted polymer. While modifying polymer-substrate interactions by grafted polymers has long been used in applications such as dispersing particles and

for preventing flocculation, Mansky, *et al.* first demonstrated the viability of this approach for controlling the alignment and self-assembly of diblock copolymers. [129] Explicitly, they used a styrene (S) and methylmethacrylate (MMA) random copolymer (P(S-r-MMA)) brush with varying compositions of S and MMA as the substrate for alignment of the block copolymer. By measuring the surface energy of homopolymers polystyrene (PS) and polymethylmethacrylate (PMMA) on the brush as a function of the composition of S and MMA in the brush, these authors showed that the surface energies of the brush (with the different components) could be tuned by modulating the compositions of the brush copolymer. [129] More pertinently, they identified a regime called the "neutral window," for which the grafted substrate exhibited approximately equal preference for S and MMA blocks, and showed that in such a regime the substrate was effective in creating perpendicular aligned phases. [129, 130] However, since the free surface had an affinity for the PS, parallel morphologies still tended to be formed near the free surface. [130] The same authors later used an end-functionalized random copolymer segregated to the polymer-air interface to induce perpendicular lamellar structures throughout the film. [80]

Complementing the above experimental efforts, there has also been extensive modeling and simulation work focusing on the self-assembly behavior of di- and multiblock copolymer films. While early work of Turner, Mayes, and others used simple scaling-type theories, [162, 210, 214] later research by Shull, Matsen, Balazs, and coworkers pioneered a more direct numerical approach

based on polymer self-consistent field theory which helped to shed light on the different parameters underlying the self-assembly behavior of block copolymers. [138, 161, 186] These researchers modeled a diblock copolymer thin film bounded by homogeneous substrates with energetic preference for one of the blocks. Using such a model, it was confirmed that substrates displaying an energetic preference for one of the components tended to induce the formation of parallel aligned lamellar phases. In contrast, for a neutral substrate, a perpendicular arrangement was always preferred or degenerate with parallel arrangements. More interestingly, such studies demonstrated the critical role played by the film thickness in modulating these trends for confined polymer films. Explicitly, in parallel aligned phases confined to thicknesses which are noncommensurate with the equilibrium lamellar thickness, they showed that there is a competition between the energetic gain arising from the interactions with the substrate and the entropic costs that may be incurred in deforming the lamellae to fit them within the confined space. This competition was shown to result in the formation of perpendicularly aligned phases for certain ranges of thickness even for preferential substrates. Similar behavior for diblock copolymers between homogeneous surfaces was also shown using Monte Carlo simulations. [219] Additionally, more recent studies of diblock copolymer thin films bounded by homogeneous surfaces has elucidated the plethora of mixed morphologies that may occur as a function of the complex system parameter space.[146] Subsequent work has extended the above developments by focusing on the cases of asymmetric diblock copolymers,[217] multiblock

copolymers,[41, 86, 140, 141, 184, 236] and the impact of patterned hard surfaces [36, 37, 215, 216, 220] including the effects of roughness.[37, 208]

At the other end of the spectrum, much modeling work has also been accomplished in the context of the interfacial properties of grafted chemically heterogeneous polymers. This has included studies of grafted diblock copolymers,[20, 40, 49, 139, 180] Y-shaped copolymers,[237] and systems with two species of homopolymer.[19, 110, 131] Grafted statistical copolymer systems such as grafted gradient copolymer melts[160] and random copolymers in a selective solvent[63] have also been studied. In order to further modeling effects on grafted statistical copolymers and by analogy to the early work of Mansky *et al.*, we recently completed a study of a random copolymer brush in contact with a homopolymer melt. Our results qualitatively agreed with their experimental results. Moreover, we also showed that an important phenomena that manifest in such random copolymers is the possibility of the chains to rearrange their ends to expose a more "enriched" fraction of the favorable phase to the melt in contact. In our earlier work, we showed that the surface energies between the hompolymer melt and the brush is crucially dependent upon this rearrangement effect.[206]

Both the experimental work of Mansky *et al.*[129] as well as our previous work on the interfacial properties of random copolymer brushes have used the surface energies of A and B homopolymers on random copolymer brushes to draw conclusions about the expected behavior for diblock copolymer alignment on such substrates. While this is a reasonable strategy, such an approach

however leaves unaddressed many interesting issues relating to the synergistic aspects between the self-assembly of the block copolymer and grafted copolymer. Explicitly, grafted copolymers differ from the hard walls modeled previously in that they represent a soft substrate which can potentially modulate their thicknesses to accommodate the self-assembly of the block copolymers. A more interesting possibility in the case of random copolymers brushes is that they can create lateral and/or normal chemical inhomogeneities, and thereby modulate the surface energies to either template or accommodate the self-assembled structures of the block copolymer film. These considerations prompt the question of whether there indeed is a "strict" correspondence between the surface energies and the actual alignment of the diblock copolymer, and whether this alignment matches the behavior predicted for self-assembly of diblock copolymers on smooth, hard walls.

Only very few articles have modeled the self-assembly characteristics of block copolymers on grafted surfaces. Ren and coworkers considered the self-assembly of asymmetric block copolymer melts on homopolymer brushes using polymer self-consistent field theory (SCFT). [173] They found that, as a function of grafting density, the system alternated between lamellar and spherical morphologies and that templating of the grafted homopolymer occurred in response to the spherical phases. However, these studies did not address the issues regarding the connection between surface energies and the self-assembly morphologies. Moreover, the possibility of self-assembly driven chemical inhomogeneities in the grafted layers is a feature unique to the con-

text of random copolymer and multicomponent polymer brushes which does not have an analogue in the homopolymer context. To address the above-raised issues, in this work we go beyond our previous work on the interfacial properties of random copolymers by modeling directly the self-assembly of block copolymers on grafted copolymer brushes. We quantitatively explore the influence of various parameters, which include grafting densities, chain lengths, film thicknesses, composition of the random copolymer and the blockiness of its chemical sequences. To minimize the number of parameters to be studied, we hold constant the interaction between dissimilar segments (quantified by the Flory parameter χ) and also focus only on the case of a "symmetric" diblock copolymer, which forms lamellar phases. Moreover, we also assume that the film is "symmetric" and has identical grafted layers on both surfaces. In order to isolate the specific effect of the random copolymers, we assume that the substrate on which the polymers are grafted is a "neutral" surface for the two components of the diblock copolymer.

Using the above model and assumptions, we study the self-assembly of the block copolymers upon random copolymer brushes. Our results indicate novel synergy between the block copolymer self-assembly and the inhomogeneities induced in the brush. This feature renders the self-assembly in our system to be much more complex than the behavior observed for block copolymers confined by smooth, hard walls. The latter is also reflected in the quantitative comparisons we present between the surface energies and the stabilities of perpendicularly and parallel aligned phases.

The rest of the article is arranged as follows: In section 6.2 we explain key details of our theoretical and numerical methods. In Section 6.3 we discuss some key relevant morphological features arising in the parallel and perpendicular self-assembly of block copolymers on the grafted layers. In Section 6.3 we present results pertaining to the "neutral window," that is, the parametric regime which leads to perpendicular alignment of the block copolymer. We present an explicit comparison of this regime to the surface energies of the homopolymers on random copolymer brushes and comment on the correspondences and discrepancies.

6.2 Theory and Numerical Methods

To model the self-assembly of block copolymers on grafted random copolymer surfaces, we use a numerical implementation of polymer self-consistent field theory (SCFT). The details of the formalism for the system under consideration is almost identical to that used in our previous work which modeled the behavior of (A) hompolymer films on random copolymer (AB) brushes. To model the behavior of diblock copolymer films, the modifications arise only in the manner in which the densities and volume fraction profiles of different components are computed. Specifically, the presence of the B component in the film adds to the total volume fraction of the B component.

In the previous work, since we were only interested in the density profiles and free energies of homopolymers, we could restrict our consideration to one-dimensional variations in the density profiles of the different components.

However, in the present context, since we are explicitly concerned with the formation of parallel and perpendicular lamellae, we now solve the resulting self-consistent field theory equations while allowing for inhomogeneities in two spatial dimensions: one normal to the substrate, denoted z, and one tangential to the substrate, denoted x. We solved the diffusion equation resulting in the SCFT in two dimensions using an alternating-direction implicit method. To calculate the surface energies (to compare with the neutral window regimes), we revert back to an one-dimensional formalism where the diffusion equation is solved using a Crank-Nicolson method in only the z dimension. For our two-dimensional calculations, the spatial dimensions are resolved on a mesh size of $\Delta x = \Delta z = 0.1$ and the contour length coordinate s is resolved on a mesh size of $\Delta s = 0.005$. For our one-dimensional calculations, the need for free energy results very close to the surface dictates that we solve the equations on a smaller mesh size of $\Delta z = 0.04$ and $\Delta s = 0.0004$. The self-consistent field equations are solved until the maximum change in the self-consistent fields (see below for details and notation) was 10^{-2} for w_+ and 5×10^{-3} for w_-. The random copolymer chains grafted to the surface were generated by using a method identical to that employed in our previous work. In the present study, we use an ensemble of 500 chains in our self-consistent field theory. As in the last study, we create chains that have 100 segments, which when $\Delta s = 0.005$ dictates that each segment has two contour mesh (s) points.

From this point in the paper, we choose to denote the volume fraction of species A in the brush chain by f, the grafting density by σ, the blockiness

parameter as λ (see below for details), and the ratio between the chain lengths of the free and grafted chains as α.

6.2.1 Details of Theoretical and Numerical Methods

We use self consistent field theory for tethered polymer chains [53] to determine the structure of a grafted layer of statistical copolymers composed of segments denoted A and B which interacts with an AB diblock copolymer. While previous articles have already detailed the theoretical framework appropriate for similar situations,[136, 137] for the sake of completeness we present the pertinent equations and details of the accompanying numerical method. The polymers are modeled as Gaussian chains whose conformations are described by continuous functions $\mathbf{R}_i(s)$ and $\mathbf{R}_j(s)$, where i denotes the free chains and takes on values from 1 to n_f (the number of free chains), and j denotes the grafted chains and runs from 1 to n_g (the number of grafted chains). The variable s is a continuous chain index coordinate running from 0 to N_f for the free chains, where N_f denotes the chain length of free chains, and running from 0 to N_g for the grafted chains, where N_g denotes the number of segments in the grafted chains. For simplicity, we assume that the segmental densities of all the segments are identical and denote it as ρ_0. Using this notation, the partition function of the system in the canonical ensemble can be expressed as

$$\begin{aligned} Z &= \int \prod_{i=1}^{n_f} D\mathbf{R}_i(s) \int \prod_{j=1}^{n_g} D\mathbf{R}_j(s) \exp(-\beta U_0[\mathbf{R}_i(s)] - \beta U_0[\mathbf{R}_j(s)] \\ &\quad -\beta U_1[\mathbf{R}_i(s), \mathbf{R}_j(s)])\delta(\hat{\rho}_A + \hat{\rho}_B - \rho_0), \end{aligned} \tag{6.1}$$

where $\hat{\rho}_A$ and $\hat{\rho}_B$ denote the microscopic densities of A and B chains, respectively. Also, $\hat{\rho}_A = \hat{\rho}_{A,g} + \hat{\rho}_{A,f}$, where $\hat{\rho}_{A,g}$ and $\hat{\rho}_{A,f}$ are the microscopic densities of component A arising from the grafted and free chains, respectively. The density of B segments is calculated similarly as $\hat{\rho}_B = \hat{\rho}_{B,g} + \hat{\rho}_{B,f}$. The delta function in eq. (6.1) enforces the incompressibility of the overall system by requiring that the sum of the A and B species densities, $\hat{\rho}_A$ and $\hat{\rho}_B$, equals the average melt system density ρ_0. In eq. (6.1), U_0 corresponds to the bonded elastic interactions and, in the Gaussian chain model we adopt, is modeled by a form:[45]

$$\beta U_0[\mathbf{R}_i(s)] = \frac{3}{2b^2} \sum_{i=1}^{n_g} \int_0^{N_f} ds \left| \frac{\partial \mathbf{R}_i(s)}{\partial s} \right|^2, \tag{6.2}$$

where b denotes the statistical segment length. U_1 describes the non-bonded interactions, in particular the energetic repulsion between chemically dissimilar chains. We adopt a simple Flory model where

$$\beta U_1[\mathbf{R}_i(s)] = \upsilon_0 \chi \int d\mathbf{r} \hat{\rho}_A \hat{\rho}_B. \tag{6.3}$$

with the Flory parameter χ quantifying the energetic penalty associated with the contact of chemically dissimilar segments.

The functional eq. (6.1) can be transformed by using functional integral methods into a field theory in which the fundamental degrees of freedom are potential fields $w_+(\mathbf{r})$and $w_-(\mathbf{r})$, [54] such that

$$Z = \int Dw_+ \int Dw_- \exp(-\beta H[w_+(\mathbf{r}), w_-(\mathbf{r})]). \tag{6.4}$$

where H is an "effective" Hamiltonian given by

$$\frac{H[w_+(\mathbf{r}), w_-(\mathbf{r})]}{k_{\mathrm{B}}TCA} = \int dz[\frac{1}{\chi N_g}w_-^2 + iw_+ + \frac{\chi N_g}{4}] - \frac{V_h}{\alpha A}\ln Q_f[-iw_+ - w_-, -iw_+ + w_-] - \frac{\bar{\sigma}}{C}\ln Q_g[-iw_+ - w_-, -iw_+ + w_-]. \quad (6.5)$$

In eq. (6.5), length scales have been nondimensionalized by the unperturbed radius of gyration, $R_{\mathrm{g}} = N_g^{1/2}b/6^{1/2}$, of the grafted chains. This results in a nondimensionalization of the grafting density σ (defined as chains per area) to $\bar{\sigma} = \sigma R_g^2$. The potentials w_+ and w_- and the continuous chain index s have been rescaled by N_g. With this nondimensionalization, the constant $C = \rho_0 R_{\mathrm{g}}^{\mathrm{d}}/N_g$ and $\alpha = N_f/N_g$ emerge as dimensionless parameters. Given the total system volume V and the cross sectional area A of the film (all dimensionless), we define the volume of the homopolymer melt V_h by the relationship $V/A = V_h/A + \bar{\sigma}/C$. Q_g is the partition function of a single grafted chain in the fields $w_+(\mathbf{r})$ and $w_-(\mathbf{r})$, and is defined as

$$Q_g(\mathbf{r}_\perp; [\psi]) = \int d\mathbf{r} q_{\mathbf{r}_\perp}(\mathbf{r}, s; [\psi]). \quad (6.6)$$

In the above equation, the field $q_{\mathbf{r}_\perp}(\mathbf{r}, s; [\psi])$, referred to as the chain propagator, provides a statistical description of grafted chain conformations and satisfies a diffusion-like equation[54]

$$\frac{\partial q_{\mathbf{r}_\perp}}{\partial s} = \nabla^2 q_{\mathbf{r}_\perp} - \psi(\mathbf{r}, s; \theta(s)) q_{\mathbf{r}_\perp}; \quad q_{\mathbf{r}_\perp}(\mathbf{r}, s = 0) = \delta(\mathbf{r} - \mathbf{r}_\perp). \quad (6.7)$$

The initial condition in eq (6.7) is the result of the fact that one end of the chain is grafted to the surface, denoted by $\mathbf{r}_\perp$. The potential $\psi(\mathbf{r}, s)$ is the

potential field acting on the different monomers and is based on the statistical distribution of the monomers. If we use the definition of a random variable $\theta(s)$ that takes on a value of 1 for an A monomer and 0 for a B monomer, then

$$\psi(\mathbf{r}, s; \theta(s)) = \begin{cases} -iw_+(\mathbf{r}) - w_-(\mathbf{r}), & \text{if } \theta(s) = 1 \\ -iw_+(\mathbf{r}) + w_-(\mathbf{r}), & \text{if } \theta(s) = 0 \end{cases}. \tag{6.8}$$

We note that, as discussed further below, experimental conditions dictate that $\theta(s)$ is different for each chain in the system. The equations presented here reflect our implementation of the SCFT for one realization of $\theta(s)$, and we discuss below how this construction is used to model the presence of many chemically distinct chains in the system. Q_f is the partition function of a single free chain in the field $w(\mathbf{r})$ and is defined as

$$Q_f = \int d\mathbf{r} q_f(\mathbf{r}, s = \alpha). \tag{6.9}$$

The field $q_f(\mathbf{r}, s)$ also satisfies a diffusion equation,

$$\frac{\partial q_f(\mathbf{r}, s)}{\partial s} = \nabla^2 q_f(\mathbf{r}, s) - \xi(\mathbf{r}, s) q_f(\mathbf{r}, s); q_f(\mathbf{r}, s = 0) = 1. \tag{6.10}$$

where

$$\xi(\mathbf{r}, s) = \begin{cases} -iw_+(\mathbf{r}) - w_-(\mathbf{r}), & 0 \leq s \leq f_{diblock}\alpha \\ -iw_+(\mathbf{r}) + w_-(\mathbf{r}), & f_{diblock}\alpha < s \leq \alpha \end{cases}. \tag{6.11}$$

The potential field in the above equation arises as a consequence of the fact that the free chains are assumed to be AB diblock copolymer chains with volume fraction $f_{diblock}$. The volume fraction profiles of the melt chains, composed of species A and B segments, are defined as $\phi_{A,f} = \rho_{A,f}/\rho_0$ and $\phi_{B,f} = \rho_{B,f}/\rho_0$, respectively. They are obtained as

$$\phi_{A,f}(\mathbf{r}) = \frac{V_h}{V Q_f \alpha} \int_0^{f_{diblock}\alpha} ds q_f(\mathbf{r}, s) q_f(\mathbf{r}, 1 - s) \tag{6.12}$$

and

$$\phi_{B,f}(\mathbf{r}) = \frac{V_h}{VQ_f\alpha}\int_{f_{diblock}\alpha}^{\alpha} ds q_f(\mathbf{r},s)q_f(\mathbf{r},1-s). \tag{6.13}$$

The single chain partition function of the grafted chains, Q_g, can be rewritten using a factorization property as [53]

$$Q_g(\mathbf{r}_\perp) = \int d\mathbf{r} q_{\mathbf{r}_\perp}(\mathbf{r},s)q_g(\mathbf{r},1-s), \tag{6.14}$$

where $q_g(\mathbf{r},s)$ is a complementary chain propagator that satisfies eq. (6.7) with an initial condition of $q_g(\mathbf{r},s=0)=1$. A further complementary propagator can be defined as

$$q_{gc}(\mathbf{r},s) = \int d\mathbf{r}_\perp \frac{\bar{\sigma} q_{\mathbf{r}_\perp}(\mathbf{r},s)}{Q_g(\mathbf{r}_\perp,s)}. \tag{6.15}$$

which can be shown to satisfy eq. (6.7) with, however, an initial condition

$$q_{gc}(\mathbf{r},s=0) = \frac{\bar{\sigma}\delta(\mathbf{r}-\mathbf{r}_\perp)}{q_g(\mathbf{r}=\mathbf{r}_\perp,s=1)}. \tag{6.16}$$

The volume fraction profiles of species A and B in the brush, $\phi_{A,g}(\mathbf{r})$ and $\phi_B(\mathbf{r})$ (also normalized by ρ_0), are then found as

$$\phi_{A,g}(\mathbf{r}) = \int_0^1 ds\theta(s)q_{gc}(\mathbf{r},s)q_g(\mathbf{r},1-s), \tag{6.17}$$

and

$$\phi_{B,g}(\mathbf{r}) = \int_0^1 ds(1-\theta(s))q_{gc}(\mathbf{r},s)q_g(\mathbf{r},1-s). \tag{6.18}$$

Replacing eq. (6.4) with the value of the exponent at its saddle point constitutes the approximation termed as self-consistent field theory (SCFT). The saddle point fields, w_+^* and w_-^*, found by setting the functional derivative

of eq. (6.5) with respect to $w_+(\mathbf{r})$ and $w_-(\mathbf{r})$ to be zero, correspond to the solutions of the equations

$$1 - \phi_A(\mathbf{r}) - \phi_B(\mathbf{r}) = 0 \tag{6.19}$$

and

$$\phi_A - \phi_B - (2/\chi N)w_-^* = 0. \tag{6.20}$$

The free energy of the system can then be approximated using the value of $H[w_+^*(\mathbf{r}), w_-^*(\mathbf{r})]$ at the saddle point as

$$\frac{F[w(\mathbf{r})]}{k_{\mathrm{B}}TAC} = \frac{-\ln Z}{AC} = \int d\mathbf{r}[\frac{1}{\chi N}w_-^{*2} + iw_+^* + \frac{\chi N}{4}] - \frac{V_h}{\alpha A}\ln Q_f - \frac{\bar{\sigma}}{C}\ln Q_g. \tag{6.21}$$

Computation of F requires the solution of equations (6.7) - (6.14) and (6.16) - (6.20) with the appropriate boundary conditions. As discussed in previous theoretical studies in the context of thin films, [136] we use a reflecting wall boundary condition at the top of the film, which describes the symmetry condition at half the confinement thickness. This dictates that we impose Neumann boundary conditions, $\mathbf{n}\cdot\nabla q_f = \mathbf{n}\cdot\nabla q_g = \mathbf{n}\cdot\nabla q_{gc} = 0$ at this surface. For numerical reasons discussed in our previous work, [205] instead of using the Dirichlet boundary conditions on the grafted surface, we use a Neumann boundary condition on this surface.

The saddle point fields $w_+(\mathbf{r})$ and $w_-(\mathbf{r})$ are determined using a Picard iterative scheme of the form

$$w_+^*(\mathbf{r})_{new} = w_+^*(\mathbf{r})_{old} + \epsilon_+[1 - \phi_f(\mathbf{r}) - \phi_g(\mathbf{r})]. \tag{6.22}$$

and

$$w_-^*(\mathbf{r})_{new} = w_-^*(\mathbf{r})_{old} + \epsilon_-[\phi_A - \phi_B - (2/\chi N)w_-]. \tag{6.23}$$

where ϵ_+ and ϵ_- are relaxation parameters whose values were chosen to be between 0 and 1. Additionally, the average value of w_+ is enforced to be zero at every iteration.

Mimicking the experimental conditions involving statistical copolymers requires us to generate an ensemble of chains whose overall composition of species A is represented by the parameter f but with a distribution of sequences reflecting the statistical nature of their sequences. For this purpose, we use the construction of Fredrickson *et al.* [55] to generate our copolymers. A parameter P_{jk} is defined as the conditional probability that a segment of type j at an arbitrary location in the chain is immediately followed by a segment of type k, where j, k = A or B. Because the only options that exist are A or B segments, by construction $P_{AB} = 1 - P_{AA}$ and $P_{BA} = 1 - P_{BB}$. Also, to ensure that the average volume fraction of the segments is f, we have $f = P_{AA}f + P_{BA}(1 - f)$. Given these equalities, it can be shown that the resulting statistical distribution of sequences on the chains can be described by the parameter $\lambda = P_{AA} + P_{BB} - 1$ and that $P_{AA} = f(1 - \lambda) + \lambda$ and $P_{BB} = f(\lambda - 1) + 1$. The parameter λ quantifies the tendency of a new segment to remain chemically equivalent to the previous one. Specifically, $\lambda = 0$ corresponds to the purely random case, $\lambda = -1$ corresponds to an alternating copolymer, and $\lambda = 1$ corresponds to a homopolymer with chemical identity determined by the probability associated with the first segment in the chain.

To implement this strategy, we generate an ensemble of chains based on the above procedure and average the results over them to account for the statistical nature of sequences in the polymers.

Since the numerical discretization "Δs" is distinct from the physical size of a segment in the chain, we also specify the number of segments in the chain and generate "segments" composed of the appropriate number of s points. The SCFT calculations are then performed on all n_g of these chains and the results averaged at each iteration. For each parameter set, we did a run on 500 chains composed of 100 segments and averaged the results. Given that $\Delta s = 0.005$ and $0 < s < 1$, this means that each segment is composed of 2 s points.

To quantify the interfacial energy between the bulk film and the brush, we use an approach similar to that expounded in Matsen. [136] Explicitly, the free energy of the system $F(d)$ is calculated as a function of the total film thickness d (which includes both free and grafted chains). Subsequently, the interfacial energy between the bulk diblock copolymer film and the brush is obtained as [136]

$$\gamma_{b/d} = \frac{F(\infty) - F(d_{min})}{A} \tag{6.24}$$

where d_{min} is the thickness for which $F(d)$ is a minimum and A is the area of the substrate. Using equation (6.24), we obtain values of $\gamma_{b/d}$ at different values of f, denoted $\gamma(f)$. We then assume that, since the substrate interacts neutrally with both chemical components in the system, $\gamma(f) = \gamma_A$ and $\gamma(1-f) = \gamma_B$.

We calculate $\Delta\gamma = \gamma(f) - \gamma(1-f)$ as a way of quantifying the relative preference for the brush of components A and B in the melt.

6.3 Morphological Features of Self-Assembly

We begin the discussion of our results by presenting key features of the parallel and perpendicular morphologies that we observe from our SCFT calculations. In particular, we focus on two key aspects by which the grafted copolymer layers differ from hard surfaces and single component grafted layers, viz., (i) The ability of the surface to tune the *distribution of the different species* to accommodate the self-assembly of the diblock copolymer. This feature arises from the multicomponent nature of the copolymer and we term this as "chemical templating"; and (ii) The ability of the grafted surface to tune its heights to respond to the self-assembly. This feature arises due to the inherent "softness" of the grafted surface and we term this as "physical templating."

6.3.1 Templating of Parallel Lamella

In Figures 6.1(a) and (b) we display representative volume fraction profiles of the species A within the random copolymer brush and the diblock copolymer for the case when the diblock copolymer exhibits a lamellar phase with parallel alignment. While the displayed profiles correspond to the situation where the A component is in contact with the brush, since the random copolymer brush shown in Fig. 6.1 corresponds to a case of $f = 0.5$, we expect the case with the B component in contact with the brush to exhibit a

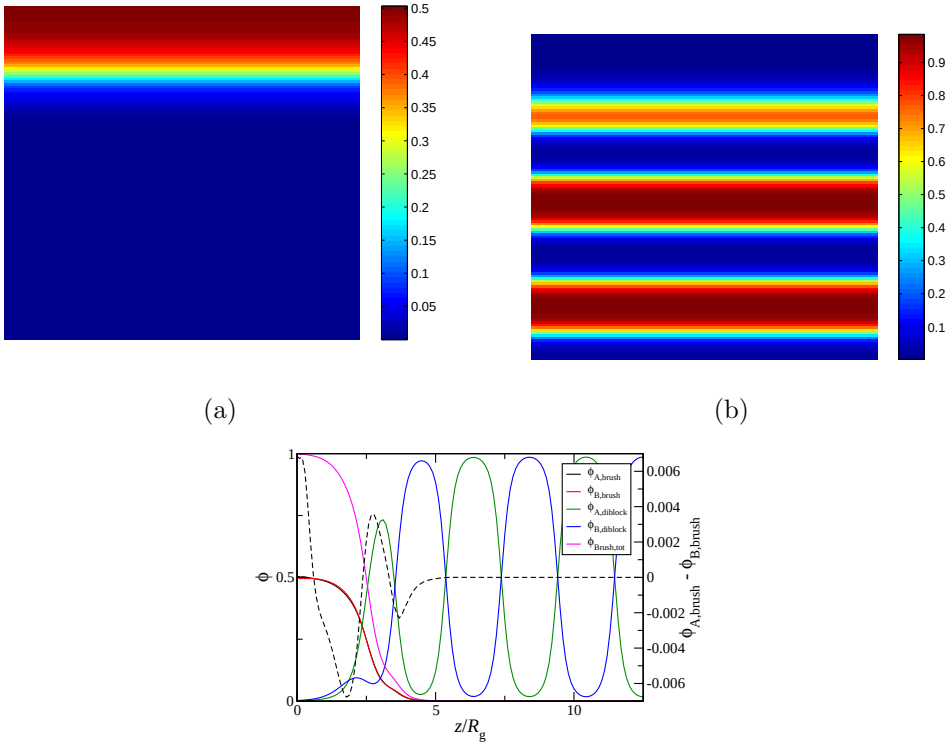

Figure 6.1: Pictures of parallel lamellar morphology; (a) Intensity plot of volume fraction of species A of the grafted polymer; b) Intensity plot of volume fraction of species A of the diblock copolymer; c) Averaged cross sections of volume fraction of all species, along with total brush density and $\phi_{\mathrm{A,brush}} - \phi_{\mathrm{B,brush}}$ (dotted). The parameters for these results are: $\sigma R_g^2/C = 2.45$, $f = 0.5$, and $\lambda = 0$. Diblock composition $f_{\mathrm{diblock}} = 0.5$ Chain lengths and segment interactions are defined by $\alpha = 1$ and $\chi N = 20$. Film thickness is $12.5R_{\mathrm{g}}$, which is the location of the minimum in energy of three parallel lamellae.

degeneracy in the free energies. Figure 6.1(c) displays the x-averaged volume fraction profile for the brush component (i.e. the sums of the volume fractions of the A and B components of the brush). We observe from Figures 6.1(a) and (c) that there are no perceptible *lateral* inhomogeneities in the brush profiles, confirming the absence of any "physical templating."

Since the brush conditions shown in Fig. 6.1 correspond to $f = 0.5$, in the absence of any chemical templating of the lamellar phase we would expect the volume fraction profiles of A and B components in the brush to be identical to each other. Hence, whether there is chemical templating of the self-assembly is most easily probed by considering the presence of compositional inhomogeneities within the grafted layer. In Figure 6.1(c) we display the x-averaged volume fraction profiles of the different components as a function of z, the dimension normal to the substrate. While superficially it appears as if the volume fraction profiles of A and B copolymers in the brush match each other, a subtle inhomogeneity in the profiles is indeed seen to develop and manifest in the behavior of $\phi_{A,brush} - \phi_{B,brush}$, shown in Fig. 6.1(c). Explicitly, it is seen that $\phi_{A,brush} - \phi_{B,brush}$ becomes positive in the region occupied by the A component of the diblock, which is indicative of an enrichment of the A component of the brush in contact with the A component of the diblock copolymer. To compensate for this enrichment, $\phi_{A,brush} - \phi_{B,brush}$ becomes negative in the interior regions of the brush, indicative of the depletion of A component in such regions.

The enrichment of the A component discussed above is equivalent to

a chemical templating of the diblock self-assembly morphology by the grafted layer. Such a phenomenon is also consistent with the results of our previous work which examined the behavior of random copolymers in contact with homopolymer melts. In that case, we showed that, even for $f = 0.5$, the chain ends of the random copolymer can rearrange themselves to present an enriched amount of the enthalpically similar component in the interfacial region where the brush overlaps with the free polymer. Such a rearrangement was argued to reduce the enthalpic component of the interfacial energies while costing little to nothing in the entropic component. Moreover, we showed that this rearrangement effect can in general (for $f \neq 0.5$) be quantified through the quantity $\phi_{A,brush}(z)/f - \phi_{B,brush}(z)/(1-f)$, which corresponds to the amount of enrichment in species A that occurs in the brush, normalized by the average volume fraction of each species.

In Figure 6.2 we present results which quantify the manner in which the above-discussed chemical templating varies with different parameters of the grafted layer. Figure 6.2(a) displays the variation of the rearrangement effect with increasing f, for which the brush and the melt become more chemically similar. As was observed in our previous work with random copolymer brushes and homopolymer melts, the enrichment of species A (i.e. the chemical templating effect) becomes less pronounced as f increases, evidenced by the decreasing magnitude of the positive peaks toward the right of the plots. This trend is easily understood by noting that with increasing f, there is a corresponding decrease in the amount of enrichment achievable in the interfa-

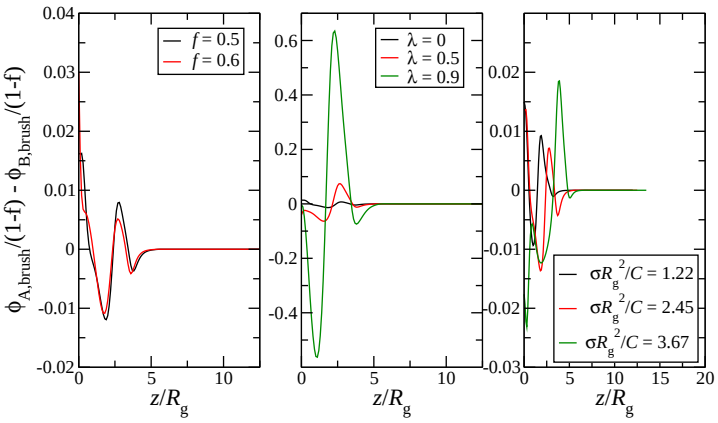

Figure 6.2: Segment rearrangement effect of a cross section at the film thickness corresponding the location of the minimum in energy of parallel morphology for 3 lamellae.(a) Varying f; (b) Varying λ; (c) Varying $\sigma R_g^2/C$; (d) Varying α. Unless otherwise stated,$\sigma R_g^2/C = 2.45$, $f_{brush} = 0.5$, and $\lambda = 0$. Diblock composition $f_{diblock} = 0.5$ Chain lengths and segment interactions are defined by $\alpha = 1$ and $\chi N = 20$. Film thickness is $12.5R_g$, which is the location of the minimum in energy of parallel morphology for 3 lamellaes.

cial region by rearranging the chains ends. Moreover, in such conditions the brush copolymer itself becomes more similar to the polymer in contact with it and hence there is inherently a favorable enthalpic interaction between them. While chain rearrangements do contribute to these favorable interactions, they are expected to do so only at a secondary level and therefore there is a reduced propensity for such behavior.

In Figure 6.2(b) we display the effect of increased blockiness (with f fixed at 0.5) on the rearrangement within the random copolymer brush. Similar to the results presented in our previous article for the case of a random copolymer brush in contact with a homopolymer, the rearrangement effect is seen to increases with increasing blockiness. This behavior, which also parallels results shown in other contexts, can be explained by noting that blockier polymers allow for a more substantial enrichment of the preferred component by the process of rearranging the chain ends.

Finally, in Figure 6.2(c) we display the affect of changing the grafting density upon the chain rearrangement. Interestingly, with increasing grafting density, the enrichment in A chain exhibits a nonmonotonic variation (seen in the magnitude of the peaks of $\phi_{A,brush}(z)/f - \phi_{B,brush}(z)/(1-f)$ in the interfacial region). We note that in our previous work on random copolymer brushes in homopolymer melts (albeit for a smaller χN), we also found that the rearrangement effect behaved nonmonotonically by decreasing from $\sigma R_g^2/C = 1.22$ to $\sigma R_g^2/C = 2.45$, and then increasing again at $\sigma R_g^2/C = 4.89$. Since the chain rearrangement effects involve a complex interplay of many features, we

can only speculate that these nonmonotonic trends arise from a combination of the reduced interfacial widths between the melt polymer and the brush with increasing grafting density and the enrichment that can be achieved by rearranging the chain ends in such a region.

In summary, in this section we discussed the "chemical templating" phenomena arising in the brush copolymer due to the presence of a parallel aligned diblock copolymer. Explicitly, we demonstrated that chemical templating arises through a rearrangement of the chains to enrich the brush in the component of the diblock copolymer which is at the interface. The parametric dependencies of this chain rearrangement effect were shown to be consistent with the results observed earlier for the interface of a random copolymer brush and a homopolymer melt.

6.3.2 Templating of Perpendicular Morphologies

In contrast to the behavior discussed for the case of parallel lamella phases, templating of perpendicular morphologies is expected to be even richer due to the possibility of both normal and tangential inhomogeneities. Moreover, within the context of tangential inhomogeneities, two further situations may arise: (i) Inhomogeneities in the structure and heights of the grafted layer (referred to as "physical templating"); (ii) A compositional or chemical templating similar to that observed in the context of the lamella phases aligned in the parallel direction. Below we present evidence for the occurrence of both of these possibilities and discuss their dependence on different parameters of

the grafted layer.

In Figure 6.3(a) we display representative composition profiles of the A components in the diblock copolymer and the random copolymer brush for the case where the diblock copolymer lamellae are aligned in a perpendicular manner. The first observation we make is that the lamellae formed by the diblock copolymer are rounded at the edges in the region which are in contact with the brush. This feature is seen to manifest more clearly in the results displayed in Fig. 6.3(b) which depicts the total volume fractions of the diblock copolymer and the brush component. The latter quantifies the structure and height of the brush and is seen to display periodical inhomogeneities with peaks in the regions corresponding to the location of the interfaces in the diblock lamellae. Taken together, the preceding observations indicate a "physical templating" of the brush driven by the rearrangement of the grafted layer in an inhomogeneous manner to accumulate more material from the brush at the AB interface of the lamellae of the diblock copolymer.

Before we discuss the origins of the above behavior, we note another aspect of self-assembly in perpendicular alignment. Specifically, in the plot of the segmental enrichments (defined as $\phi_A/f - \phi_B/(1-f)$ of the brush component) displayed in Figure 6.3(c), it is seen that the composition profiles of the A and B components in the brush are both enriched in the regions where they are in contact with the respective phases. A more intriguing aspect of the above chemical templating behavior is in a comparison of the magnitudes of the enrichments observed in the interfacial region for perpendicularly

and parallel aligned lamellae. Explicitly, it is seen that for the perpendicular alignment the magnitude of A (and B) enrichment in the interfacial region is ~ 0.011, whereas, the enrichment is 0.008 in the corresponding result for parallel lamellae in Figure 6.2(a).

We hypothesize that the origins of all the observations above can be traced back to the statistics of the sequences in the grafted chains and how they rearrange their ends to reduce the enthalpic cost of the interface between the diblock copolymer lamella and the grafted layer. The presence of chemical templating of the diblock copolymer is easiest to understand as a generalization of the behavior seen for the parallel lamellae. Explicitly, the chain ends now rearrange so as to present an enriched phase of the appropriate component in the interface. In a similar manner, by rearranging its chain ends, the grafted layer can present "neutral" portions of the chains (i.e. which exhibit equal affinity to both A and B components) which can potentially reduce the energy costs at the interfaces of a diblock copolymer by acting like a surfactant. We believe that the latter mechanism is responsible for the "physical templating" seen at the interfacial locations of the diblock lamellae see in Figs. 6.3(a) and (b). This is also confirmed by the gaps seen in the enrichment plots displayed in Figs. 6.3(c), which are indicative of a lack of enrichment and a more uniform distribution of A and B monomers of the brush at the lamellar interfacial locations of the diblock.

What is the origin of the enhanced rearrangement in chemical templating for the perpendicular lamellae? We believe that this arises from a confor-

mational rearrangement of the chains. Explicitly, the grafted chains which are in contact the A portion of the block copolymer, and which are enriched in the B component have two options: (i) They can go to the interior of the layer, as they do in the case of parallel arrangement; or (ii) If they are sufficiently close to the B portion of the lamellae, then they can splay and contribute to the enrichment of B in the B portion. The interplay of these is dictated by a competition between the entropic costs of the conformation rearrangements and the enthalpic gain in the interface between the diblock copolymer and the grafted layer. We believe that this effect leads to an "enhanced" enrichment in the case of perpendicular lamellae.

One ramification of the above enhanced enrichment is that even when considered at the same conditions of the grafted copolymers, parallel and perpendicular lamellae exhibit different characteristics in the interfacial layer between the block copolymer component and the grafted polymer. Indeed, the perpendicular lamellae, being the beneficiary of enhanced interfacial enrichment, will have more favorable interfacial interactions with the grafted surface when considered relative to the parallel alignment. In the next section, we show this finding has important consequences for the stability of the perpendicularly aligned phases.

Additional evidence for the above mechanistic explanations is furnished by considering a more blocky random copolymer brush (while keeping f fixed at 0.5), depicted in Figures 6.4(a) - (c). We observe that the qualitative features of the morphologies in this case are very similar to that of $\lambda = 0$ shown

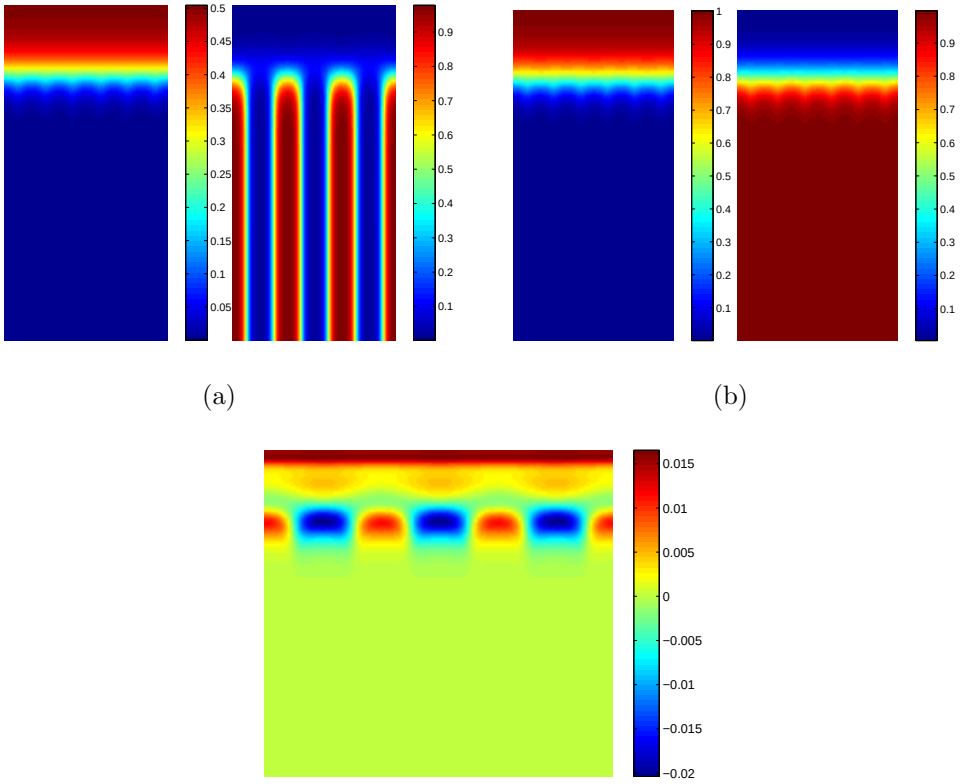

Figure 6.3: Intensity plot of (a) species A volume fraction in diblock copolymer, (b) total volume fraction and (c) chain rearrangement for a perpendicular lamellar morphology at $f_{brush} = 0.5$. $\sigma R_g^2/C = 2.45$, and $\lambda = 0$. Diblock composition $f_{diblock} = 0.5$ Chain lengths and segment interactions are defined by $\alpha = 1$ and $\chi N = 20$. Film thickness is $12.5R_g$, which is the location of the minimum in energy of parallel morphology for three lamellaes.

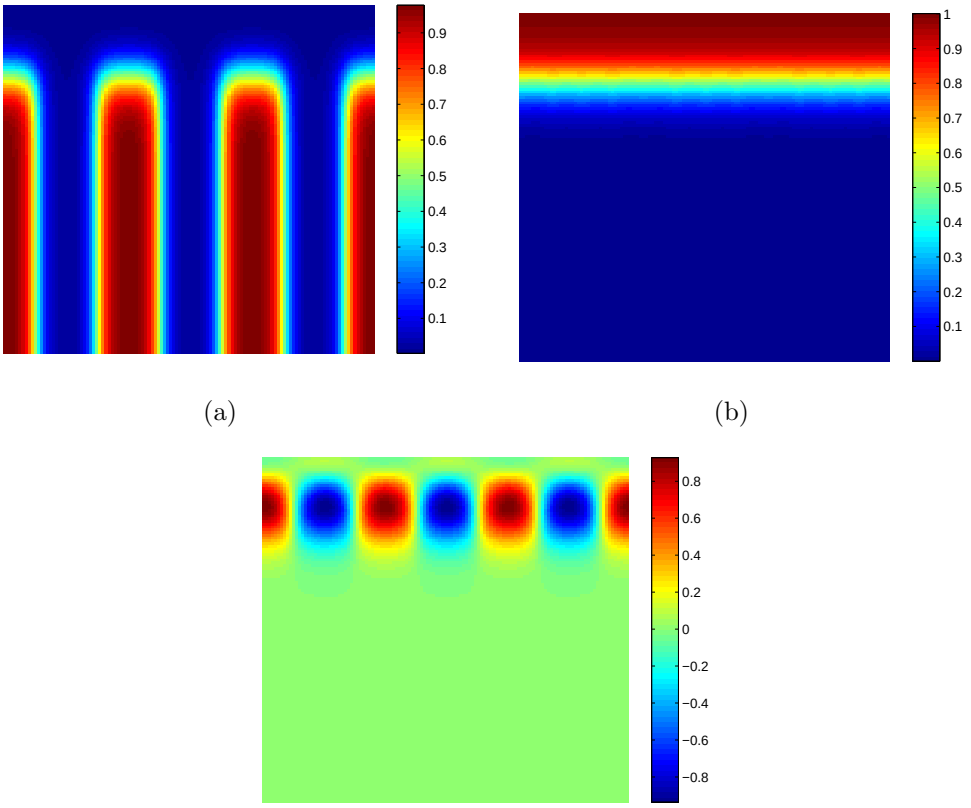

Figure 6.4: Intensity plot of (a) species A volume fraction in diblock copolymer, (b) total volume fraction, and (c) chain rearrangement for a perpendicular lamellar morphology at $\lambda = 0.9$. $\sigma R_g^2/C = 2.45$ and $f_{brush} = 0.5$. Diblock composition $f_{diblock} = 0.5$ Chain lengths and segment interactions are defined by $\alpha = 1$ and $\chi N = 20$. Film thickness is $12.5R_g$, which is the location of the minimum in energy of parallel morphology for three lamellaes.

in Figure 6.3. However, we note three features which distinguish systems with higher blockiness: (i) The magnitude of the physical templating effect seems diminished and the brush height becomes more uniform in the lateral direction (compare Figures 6.3(b) and 6.4(b)); (ii) The magnitude of the chemical templating becomes more pronounced for the blockier copolymers (compare Figures 6.3(c) and 6.4(c); (iii) The differences in the enrichment effect between the perpendicular and parallel phases become more pronounced. Explicitly, the magnitudes of the maximum enrichment are 0.916 and 0.622 for the perpendicular and parallel phases respectively.

The above observations are consistent with the mechanisms proposed in explaining Figure 6.3. First, we point out that increasing blockiness leads to chains which have longer sequences of A or B monomers (with however, the average over the different chains being maintained at $f = 0.5$), and hence less numbers of "neutral" sequences. Consequently, they are expected to be less efficient than the nonblocky chains ($\lambda = 0$, depicted in Fig 6.3) in modulating the interfacial cost of AB interfaces in diblock lamella, which explains (i) above. However, for the same preceding reason, blockier chains allows for an easier and more substantial chain rearrangement and enrichment at the interface, thereby explaining (ii) above. Finally, for the same reason, the conformational rearrangement of the chains (splaying) is expected to have a more significant effect at enhancing the interfacial enrichment, and is consistent with our observation (iii) above.

How do the above trends change for non symmetric ($f \neq 0.5$) grafted

chains? In Figure 6.5 we present results displaying the effect of f for a non-blocky ($\lambda = 0$) random copolymer. In comparing these pictures with the results depicted in 6.3, we observe the following features: (i) The diblock copolymer lamellae become asymmetric with the A segments of the diblock spreading more on the grafted layer, whereas the B segments reduce their contact with the brush; (ii) The height inhomogeneities in the brush become more pronounced, with the brush exhibiting *relatively* enhanced and lowered heights in regions respectively in contact with the A and B segments of the diblock copolymer; (iii) The rearrangement/chemical templating effects are seen to become more mitigated for the A component whereas it is enhanced for the B component. This is seen by comparing the magnitude of the positive values (representing the enrichment of A) which is 0.011 in Figure 6.3(c) and 0.077 in Fig. 6.5(c). On the other hand, the magnitude of the negative values (enrichment of B) in Figures 6.3(c) and 6.5(c) are 0.011 and 0.019 respectively.

Much of the above observations can be understood by noting that for $f > 0.5$ the grafted polymer has a higher fraction of A segments (if $f < 0.5$ there is a higher fraction of B segments). Consequently, the grafted surface is by itself preferable to the A segments of the block copolymers and not preferable to the B segments of the block copolymers. In view of this feature, it is not surprising that the lamellae of the diblock copolymers become asymmetric with an enhanced spreading of the A polymers ((i) above). However, unlike a hard surface with an inherent surface energy, grafted polymers can modulate the contact between the surface and the B component by an appro-

priate conformational rearrangements and redistribution of the segments. We believe that the preceding mechanism underlies observation (ii) above where the grafted chains compress themselves to bring more of their B segments in contact with the B phase of the diblock copolymer. The changes in the rearrangement plots and trends of (iii) can be understood by noting that since the brush is as a whole enriched in A segments, there is expected to be less driving force for chain rearrangement driven interfacial enrichment of A segments. Moreover, the magnitude of the A enrichment possible (relative to the average volume fraction of A) also diminishes with increasing f. In contrast, an opposite effect is at play for the B segments in the brush. Explicitly, the region of the brush which is in contact with the B segments of the diblock copolymer experience an unfavorable interaction and hence try to reduce the corresponding enthalpic costs by undergoing chain rearrangements to enrich the interfacial region in B segments. Moreover, the magnitude of the B enrichment possible (relative to the average volume fraction of B) also increases with increasing f. Together, the preceding effects manifest in the observation (iii) noted above.

In summary, the above morphological characteristics indicate novel physical and chemical templating arising during the perpendicular alignment of block copolymer lamellae. In the next section, we develop these considerations more quantitatively by considering the free energies of parallel and perpendicular alignment and the preferred equilibrium phases.

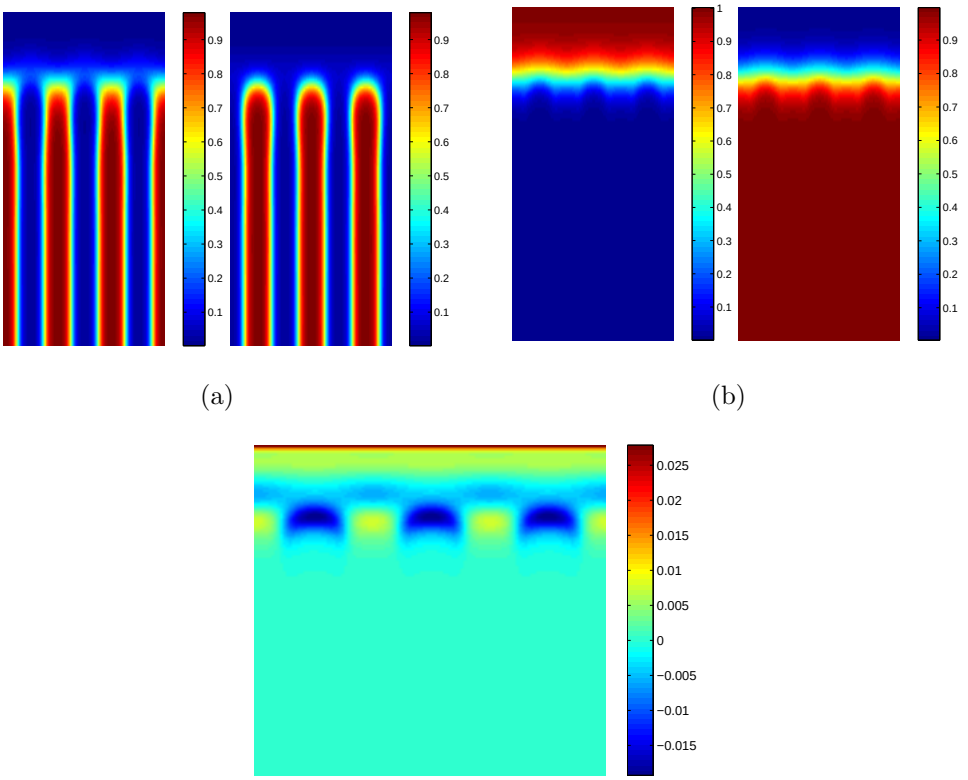

(a) (b)

(c)

Figure 6.5: Intensity plot of (a) species A (left) and B (right) volume fraction in diblock copolymer, (b) total volume fraction and (c) chain rearrangement for a perpendicular lamellar morphology at $f_{brush} = 0.6$. $\sigma R_g^2/C = 2.45$, and $\lambda = 0$. Diblock composition $f_{diblock} = 0.5$ Chain lengths and segment interactions are defined by $\alpha = 1$ and $\chi N = 20$. Film thickness is $12.5R_g$, which is the location of the minimum in energy of parallel morphology for 3 lamellaes.

6.4 Equilibrium Alignment and Neutral Windows

In this section, we use a more quantitative framework to examine the self-assembly characteristics of block copolymers on grafted random copolymer surfaces. To set the context for the manner in which we quantify the results, in Figure 6.6, we display the free energy per unit area (relative to the bulk value) of the random copolymer brush-diblock copolymer thin film system as a function of film thickness for the parallel and perpendicular morphologies for a specified set of parameters. The curves labeled $2, 2.5$, and 3 correspond to the number of parallel lamellae in the thickness D (which represents half the confinement width). Perpendicular morphologies are unaffected by the confinement thickness and hence their free energies are independent of thickness. On the other hand, we observe that the free energies for the parallel morphologies show an oscillatory trend as a function of film thickness. Such a behavior has been noted in many earlier studies of diblock copolymers, [138, 161, 210, 214] and can be understood as arising from a mismatch between the preferred lamellar domain spacing and the confinement thickness. Explicitly, upon increasing the confinement thickness beyond a value commensurate with the preferred lamella spacing, the chains in the lamella have to stretch to fill the space. The latter leads to entropic costs, which is reflected in the increasing portion of the free energies. However, beyond a certain thickness it becomes more beneficial for the lamellae to accommodate an additional layer (the next higher period) while compressing the chains to accommodate the mismatch between confinement thickness and the preferred lamella spacing.

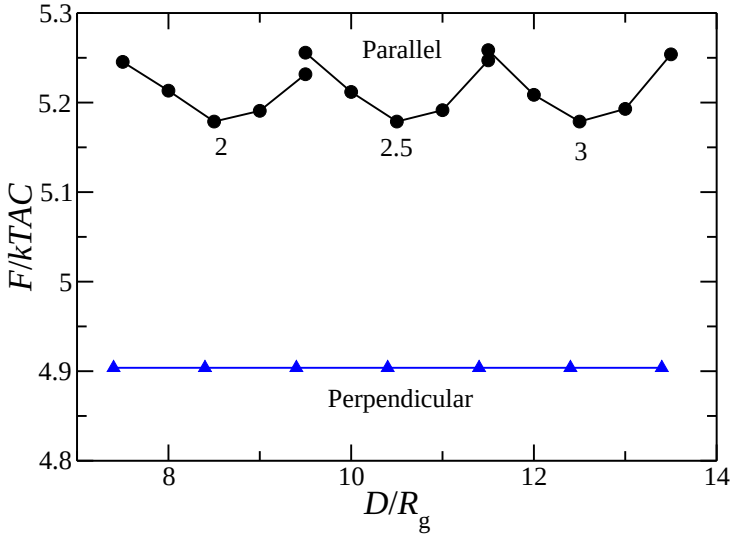

Figure 6.6: Free energies as a function of film thickness for a diblock copolymer film in contact with a neutral random copolymer brush-covered substrate. Brush parameters are $\sigma R_g^2/C = 2.45$, $f_{brush} = 0.5$, and $\lambda = 0$. Diblock composition $f_{diblock} = 0.5$ Chain lengths and segment interactions are defined by $\alpha = 1$ and $\chi N = 20$. Spacing = 4.0346121; $D_b = 4.029894158$.)

Beyond this point, increasing the confinement thickness relieves the compression and leads to the decreasing portion of the free energy. We note that for the conditions depicted in Figure 6.6 the bulk lamellar spacing is $2.05R_g$, which is identical to the distance between the minima noted for the parallel alignment. The latter demonstrates that in this case the random copolymer brush has no effect on the preferred spacing of the lamellae.

A more nontrivial and an important observation from the plot is that while the depicted conditions correspond to a situation where the grafted surface is "neutral" ($f = 0.5$) to both A and B components, the perpendicular

lamella structure seems to be the preferred alignment over the entire range of confinement thickness. In contrast for block copolymer melts confined by hard, *neutral* surfaces there is expected to be a degeneracy in the free energies of the parallel and perpendicular configurations of the lamellae when the confinement thicknesses are commensurate with the domain spacing. The origin of our result can be traced back to the morphological characteristics described in the previous section. Explicitly, we demonstrated that even for a grafting layer with "neutral" characteristics, perpendicular alignment of lamellae was accompanied by an *enhanced* (relative to parallel alignment) chemical enrichment in the brush. This self-assembly driven enrichment is in turn expected to lead to a more favorable interfacial energy between the A and B components of the diblock and their respective contacts with the grafted surface. Additionally, we also showed that there is also the possibility for a "physical templating" of the perpendicular diblock lamellae which reduces the interfacial costs in the diblock copolymer lamellae. We believe that the preceding factors together render the free energies of the perpendicularly aligned lamellae to be lower than the corresponding parallel ones.

With the above understanding, one may enquire what happens when the surface is made more preferential to one of the components. To address this issue, in Figure 6.7, we display the free energy plots for the above-discussed situation with however the composition of the grafted copolymer surface varied from 0.5 to 0.7 (we zoom in on the confinement thicknesses corresponding to three lamellae). As would be expected upon the rendering the surface to be

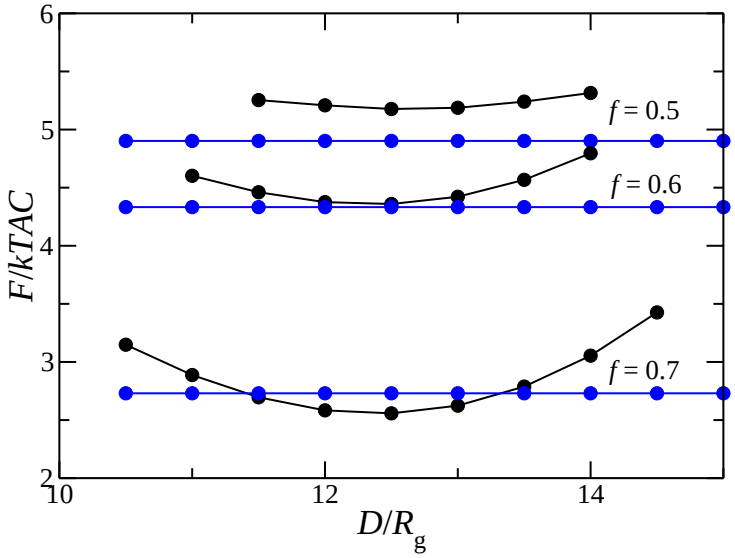

Figure 6.7: Free energies as a function of film thickness for a diblock copolymer film in contact with a neutral random copolymer brush-covered substrate for $f = 0.5, 0.6, and 0.7$. Brush parameters are $\sigma R_g^2/C = 2.45$, and $\lambda = 0$. Diblock composition $f_{diblock} = 0.5$ Chain lengths and segment interactions are defined by $\alpha = 1$ and $\chi N = 20$.)

selective, the free energy of the parallel alignment is seen to be lowered more when compared to the perpendicular alignment. [138, 161] It is seen that for $f = 0.6$, the perpendicular lamella is still the preferred morphology for all thicknesses. However, for $f = 0.7$ it is observed that the parallel alignment now becomes preferred for a range of thickness around its minima. Increasing f further (not shown) is expected to render the parallel lamellae to become the preferred phase for all thicknesses.

Much of the motivation for the present research derives from applications desiring the perpendicular alignment of the lamellar phases. Based on the above results, it is evident that there are two questions which relate to the stability of perpendicular phases: (i) For a given set of parameters, what is the composition of the random copolymer at which the parallel morphology becomes feasible? Explicitly, this quantifies the critical f_{crit} at which the minimum in the free energy curve for parallel alignment becomes lower than that for perpendicular alignment. This quantity is of significant interest for applications since it delineates the regime for which perpendicular morphologies are preferred independent of the thickness of the grafted layer. We quantify this by considering $\Delta F = F_{\parallel,min} - F_{\perp}$, where $F_{\parallel,min}$ denotes the free energy of the minimum in the parallel alignment; (ii) For $f < f_{\text{crit}}$ what is the range of confinement thickness over which the perpendicular lamellae are expected to be stable? For instance, in Figure 6.7, it is seen that even for $f = 0.7$, the perpendicular morphology can be achieved by an appropriate choice of the film thickness. We also present results for this thickness range (restricted to

$f \leq 0.7$) for different parameters. However, it is to be noted that such considerations would hold only for confined films. For free standing films (such as spun-cast) the system would prefer to form parallel morphologies with islands and holes corresponding to the distinct minima in the free energy curves.

Another issue we consider in the results below pertains to the question raised in the introduction, viz., whether the surface energies derived in our previous article, can indeed be used to understand the stability of the perpendicular morphologies on grafted surfaces. We note that for a symmetric diblock copolymer, it has been suggested that a key quantity determining the stabilities of parallel and perpendicular alignment of lamellae is:[138, 214]

$$\Delta\gamma = |\gamma_{AS} - \gamma_{BS}|$$

where γ_{AS} and γ_{BS} denote the interfacial energies of A and B polymers with the surface (in this case, the random copolymer brush). We address the connections between at two levels, viz., whether the quantitative values of $\Delta F = F_{\parallel,min} - F_{\perp}$ can actually be predicted from just the knowledge of $\Delta\gamma$. This is equivalent to addressing the issue whether the grafted copolymer surface can be replaced by a hard confining surface of equivalent surface energies. The results presented in Fig. 6.6 already points to nontrivial trends arising from templating effects, and so it would be of interest to see whether different parameters impact this correspondence. A second question is whether $\Delta\gamma$ can be used to deduce a qualitative measure of stability of perpendicular alignment. In other words, we ask whether there is a range of $\Delta\gamma$ in which

the perpendicular morphologies are universally more stable (independent of thickness) relative to the parallel ones. If indeed there is such a window, experimentalists can tune the surface conditions achieve the specified $\Delta\gamma$ and thereby achieve perpendicular alignment of lamellar morphologies. In the following section we present results for $\Delta\gamma$ alongside the ΔF to examine if such a relationship holds and to explore the correlations, if any, between the two quantities. (In Section 6.2.1, we briefly explain the methodology used to determine $\Delta\gamma$.)

6.4.1 Effect of grafted surface properties on the neutral window

In Figure 6.8(a) we display plots of the free energy differences ΔF as a function of f for different blockiness of the random copolymer. We observe that with an increase in the blockiness, the free energy differences between the parallel and the perpendicular phases increases for all values of f. This suggests that the perpendicular phases are expected to exhibit a greater regime of stability when the surface is grafted with blockier copolymers. The latter is also reflected in the thickness dependence of the stabilities of parallel and perpendicular morphologies for $f = 0.5$ and 0.6 depicted in Figs. 6.8(b) and (c). The preceding results are consistent with the observations we made in comparing the Figures 6.3(c) and 6.4(c), where it was demonstrated that the differences in the interfacial enrichment between the parallel and perpendicular phases becomes more pronounced with increasing blockiness. Due to such an effect, a more blockier grafted surface is expected to exhibit larger differences

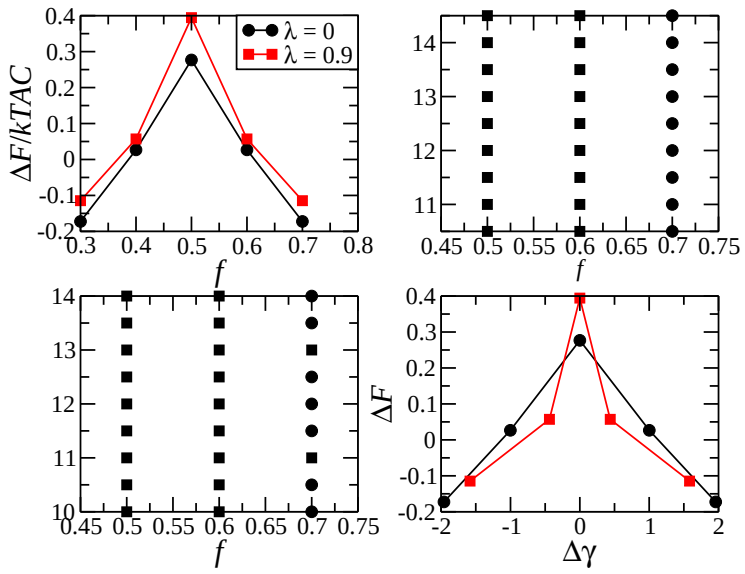

Figure 6.8: (a)Difference in free energy between parallel and perpendicular arrangement as a function of f for a diblock copolymer film in contact with a neutral random copolymer brush-covered substrate, for different values of λ. (b)-(c) Existence of perpendicular lamellae as a function of film thickness for a diblock copolymer film in contact with a neutral random copolymer brush-covered substrate, for (b) $\lambda = 0$ and (c) $\lambda = 0.9$. (d) ΔF as a function of $\Delta\gamma$ for different values of λ. Grafting density, $\sigma R_g^2/C = 2.45$. Diblock composition $f_{diblock} = 0.5$ Chain lengths and segment interactions are defined by $\alpha = 1$ and $\chi N = 20$)

between the self-assembly driven surface energies of perpendicular and parallel morphologies — which is consistent with the results of Figures 6.8(a) - (c).

In Figure 6.8(d) we display the free energy differences ΔF as a function $\Delta\gamma$ for the two different values of blockiness. It is evident that a unique correlation between ΔF and $\Delta\gamma$ does not hold for our system. The origin of this discrepancy can again be traced back to the above-discussed self-assembly driven modifications of interfacial energies which are not captured in the quantity $\Delta\gamma$.

In Figure 6.9 we display results for the situation when the grafting densities constitute the parameter which is varied (for a nonblocky random polymer, $\lambda = 0$). Unfortunately, due to numerical issues, we had to restrict our exploration in this case to only a limited set of grafting densities. Within the range of grafting densities we probed, it is seen that the lowest grafting density, $\sigma = 1.22$, has a broader neutral window (in the brush composition space), whereas $\sigma R_g^2/C = 2.45$ and $\sigma R_g^2/C = 3.67$ seem to have similar characteristics for the neutral window. These trends are also reflected in the thickness dependencies of the neutral window, which are displayed in Fig. 6.9(b) - (c). Interestingly, the changes in grafting density do not seem to have perceptible impact upon the free energy differences of neutral surfaces ($f = 0.5$). In Figure 6.9 (d) we compare ΔF to the differences in surface energies $\Delta\gamma$. Similar to the effect of blockiness, we observe that there is no unique correlation between ΔF and $\Delta\gamma$.

The results of Figure 6.9(a) - (c) can rationalized by going back to the

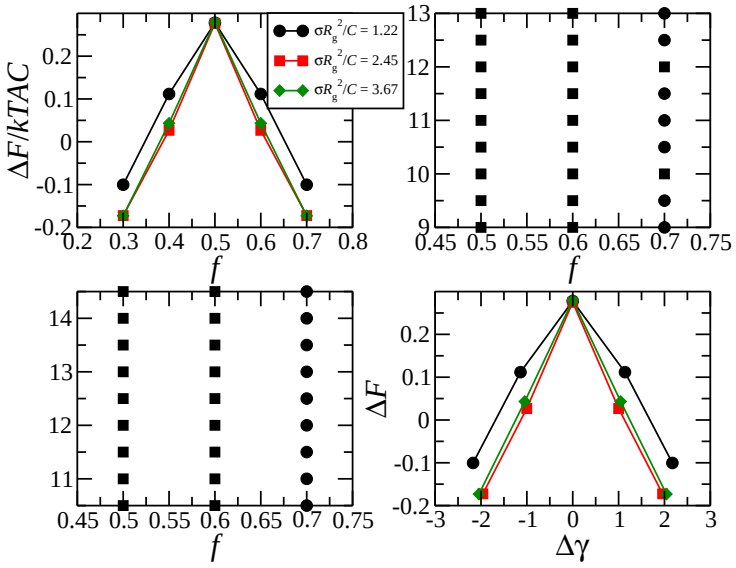

Figure 6.9: (a)Difference in free energy between parallel and perpendicular arrangement as a function of f for a diblock copolymer film in contact with a neutral random copolymer brush-covered substrate, for different values of grafting density, $\sigma R_g^2/C$. (b)-(c) Existence of perpendicular lamellae as a function of film thickness for a diblock copolymer film in contact with a neutral random copolymer brush-covered substrate, for (b) $\sigma R_g^2/C = 1.22$ and (c) $\sigma R_g^2/C = 2.45$. (d) ΔF as a function of $\Delta\gamma$ for different values of $\sigma R_g^2/C$. $\lambda = 0$. Diblock composition $f_{diblock} = 0.5$ Chain lengths and segment interactions are defined by $\alpha = 1$ and $\chi N = 20$)

origin of the free energy differences, namely the differences between the interfacial enrichments observed in the parallel and perpendicular alignment of the lamellae. We suggested that such differences were determined by an interplay of the entropic costs of splaying the chain and the enthalpic gain achievable by the enhanced enrichment. We speculate that beyond a certain grafting density σ, the entropic cost of splaying would become less sensitive to σ. Consequently, changing σ should have only little impact upon the differences in interfacial enrichments between parallel and perpendicular alignments.

Lastly, in Figure 6.10(a) - (d) we display the effect of varying the parameter α, which quantifies the relative number of segments in the diblock copolymer to that in the grafted polymer. We observe two main features in the results: (i) For $f = 0.5$, the ΔF values are largest for $\alpha = 1.5$ and decreases with decreasing α; and (ii) The window of brush compositions over which the perpendicular phase is stable is seen to have the maximum width for $\alpha = 0.75$ and to decrease with increasing α. To rationalize (i), we note that results presented in our earlier article have shown that larger αs in general lead to lower widths for the interface between the diblock copolymer and the brush layer. Such a scenario would allow for both easier and enhanced interfacial enrichment through conformational rearrangements of the chains. The latter is likely to enhance the differences in the self-assembly driven interfacial energies between parallel and perpendicular alignments, which is quantified by ΔF; To rationalize (ii), we note that the results of our previous article suggest that lower α systems are also expected to possess lower magnitudes of surface

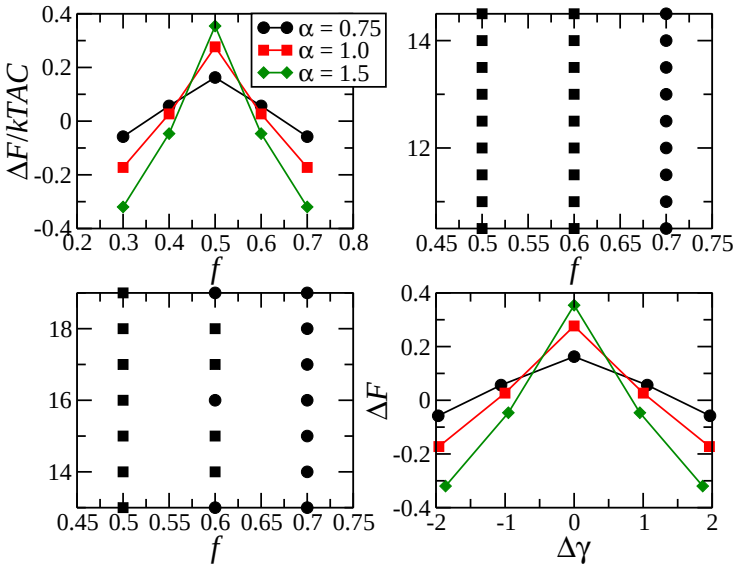

Figure 6.10: (a)Difference in free energy between parallel and perpendicular arrangement as a function of f for a diblock copolymer film in contact with a neutral random copolymer brush-covered substrate, for different values of α. (b)-(c) Existence of perpendicular lamellae as a function of film thickness for a diblock copolymer film in contact with a neutral random copolymer brush-covered substrate, for (b) $\alpha = 0.75$ and (c) $\alpha = 1.5$. (d) ΔF as a function of $\Delta\gamma$ for different values of α. $\sigma R_g^2/C = 2.45$. $\lambda = 0$. Diblock composition $f_{diblock} = 0.5$ Chain lengths and segment interactions are defined by $\chi N = 20$)

energies. Prior studies have shown [138, 214] that lower magnitudes of surface energies in general correlate with regions of stability for the perpendicular lamellae, a trend consistent with (ii).

Finally, we address whether indeed there is a universal range of $\Delta\gamma$ which can facilitate perpendicular alignment of lamellar morphologies. In Figure 6.11 we depict the $\Delta\gamma$ for the different systems we considered and indicate the stable morphology (based on whether ΔF is positive or negative). For the most part, this plot indicates that higher surface energies correspond to parallel morphologies, and vice versa. However, this correlation is seen to fail for more blockier grafted surfaces. Specifically, we observe a stable configuration of parallel alignment for low magnitudes of surface energies which occur at $f = 0.3$ and $f = 0.7$ for $\lambda = 0.9$. Based on these results, we conclude that in general the magnitude of $\Delta\gamma$ alone cannot be used to predict the alignment that will be stable in a diblock copolymer thin film.

6.5 Conclusions

In this article, we used SCFT to explore the phase behavior of a diblock copolymer thin film on top of a random copolymer brush. At the outset, we discussed the qualitative features of the morphologies formed in such systems. For parallel morphologies, we showed the occurrence of "chemical templating" in the grafted polymers, which manifests as an enrichment in the brush interfacial layer of the component of the diblock copolymer in contact. In the case of perpendicular alignment of the diblock copolymer, we demonstrated that

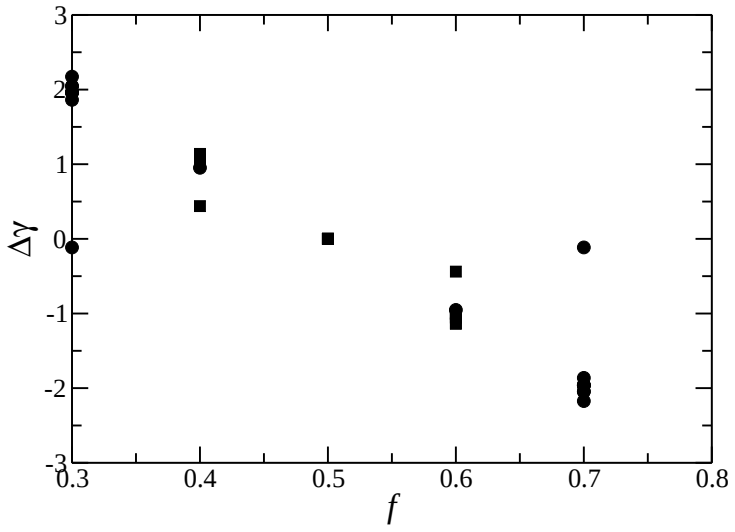

Figure 6.11: $\Delta\gamma$ as a function of f for all the parameters we studied. Squares correspond to points where the ΔF dictates that a perpendicular morphology will form and circles correspond to a parallel morphology.

there is an additional possibility of physical templating which leads to lateral inhomogeneities in the heights of the brush. Moreover, we also presented results and rationalized the existence of a more pronounced chemical templating effect during perpendicular alignment of lamellae.

We presented results for the free energy of the system and demonstrate that, as a function of film thickness, they exhibit trends that are consistent with previously shown results for parallel and perpendicular morphologies on hard surfaces. However, a key difference is a lack of degeneracy between the perpendicular and parallel alignments. Additionally, we explore the behavior of the neutral window and find that, in general, this window is larger for more blocky chains and for smaller values of σ and α. We also sought to assess whether knowledge of the surface energy between the brush and a homopolymer suffices to describe the free energy differences between the parallel and perpendicular alignments as well as their stabilities. We found a lack of correlation between our results for $\Delta\gamma$ and ΔF, which indicates that surface energy considerations alone cannot be used to make predictions about phase behavior of the diblock copolymer thin film. Further, we demonstrated that it is not possible to identify even a window of surface energy that exclusively produces perpendicular alignment of lamellae.

More broadly, the work presented in this article demonstrates that modeling the self-assembly of block copolymers necessitate a detailed treatment of the grafted layer which goes beyond simple surface energy considerations. It will be of interest to see whether such findings remain applicable for nonlamel-

lar phases of block copolymers as well as other kinds of multiblock copolymers used to create grafted surfaces.

Chapter 7

Summary and Future Work

In this chapter, we summarize the research done in this dissertation and provide several future directions for research on modeling water-soluable polymers, including modeling grafted water soluble polymers, exploring the effects of substrate and air interactions, and modeling the phase behavior of random-diblock copolymers.

7.1 Summary of Research

In this research we have developed self-consistent field theory models, scaling models, and strong stretching theory models to describe several systems involving polymers grafted to surfaces that have technologically relevant applications. By studying the structure, interfacial widths, interparticle potentials, and interfacial energies in the these systems, we have provided fundamental insight into the behavior and design of these systems as a function of paramters like grafting density, chain lengths, particle sizes, curvature, chemical interaction between dissimilar segments, and volume fractions.

7.2 Recommendations for Future Work

The modeling work done in this dissertation has several possible extensions, many of them related to the assumptions required to create the models and to additional ingredients that could be added to the models.

7.2.1 Modeling grafted water-soluble polymers

Although in this work we assumed that our grafted polymers were simple polymers, many biological applications involve the use of water soluable polymers such as polyethelene glycol (PEG), a polymer which has unique clustering properties associated with its hydrogen bonding that affect the way it behaves when grafted to a surface. Previous modeling work has successfully taken these properties into account through modified Flory models such as the n-cluster model. However, studies still need to be done on the effect of these unique properties on the interaction potentials between polymer-grafted surfaces, especially in the context of highly curved particles.

7.2.2 Modeling the effects of air and substrate surface interactions for patterning applications

Our results assume that there are no substrate-diblock or air-diblock interactions even though these are the interactions that induce the unfavorable formation of parallel lamellae. In making this assumption, our results seek to quantify the effects on the neutral window of the polymer-based parameters. Lifting this assumption is necessary to model the actual system, and it would

be interesting to explore whether, as we expect, there is a linear relationship between the surface energies with a potential included and those we calculated.

7.2.3 Exploring the phase behavior of random-block copolymers

Recent experimental efforts have explored the use of diblock copolymers in which one of the blocks is a random copolymer as a method of tuning the effective interaction between the blocks (usually modeled as χ independent of the chain length N). A melt of such chains is expected to have different phase behavior than its diblock copolymer counterpart, in particular because of the chain rearrangement affect that we showed exists in the random copolymers. The tools we have developed to model random copolymers would allow us to explore this phase diagram.

7.2.4 Exploring the phase behavior of thin films of assymetric diblock copolymer on random copolymer brushes

While our results in Chapter 6 focused on the phase behavior of symmetric, lamella-forming diblock copolymers ($f = 0.5$), varying the composition of the diblock copolymer is a key source of the rich phase behavior that has been demonstrated in diblock copolymer systems. The tools we have developed would allow us to study such systems, which have the potential to form spherical and cylindrical phases. In particular, the self-assembly of diblock copolymers into phases cylindrical phases finds application in electronic materials applications such as memory devices.

Bibliography

[1] *Numerical Recipes: The Art of Scientific Computing, Third Edition*. Cambridge University Press, 2007.

[2] Pinar Akcora, Hongjun Liu, Sanat K. Kumar, Joseph Moll, Yu Li, Brian C. Benicewicz, Linda S. Schadler, Devrim Acehan, Athanassios Z. Panagiotopoulos, Victor Pryamitsyn, Venkat Ganesan, Jan Ilavsky, Pappanan Thiyagarajan, Ralph H. Colby, and Jack F. Douglas. *Nature Materials*, 8(4):354–U121, 2009.

[3] M Alcoutlabi and GB McKenna. *J. Phys.: Condens. Matter*, 17:R461, 2005.

[4] S. Alexander. *Journal de Physique*, 38:983–987, 1977.

[5] Abraham Arceo, Luciana Meli, and Peter F. Green. *Nano Letters*, 8(8):2271–2276, August 2008.

[6] S Ata, M Muramatsu, J Takeda, T Ohdaira, R Suzuki, K Ito, Y Kobayashi, and T Ougizawa. *Polymer*, 50:3343, 2009.

[7] M Aubouy, GH Fredrickson, P Pincus, and E Raphael. *Macromolecules*, 28(8):2979–2981, APR 10 1995.

[8] A. C. Balazs and M. T. DeMeuse. *Macromolecules*, 22:4260, 1989.

[9] Anna C. Balazs, Isaac C. Sanchez, Irving R. Epstein, Frank E. Karasz, and William J. MacKnight. *Macromolecules*, 18:2188, 1985.

[10] R. C. Ball, J. F. Marko, S. T. Milner, and T. A. Witten. *Macromolecules*, 24:693–703, 1991.

[11] A Bansal, HC Yang, CZ Li, KW Cho, BC Benicewicz, SK Kumar, and LS Schadler. *Nature Materials*, 4(9):693–698, 2005.

[12] Amitabh Bansal, Hoichang Yang, Chunzhao Li, Rian C. Benicewicz, Sanat K. Kumar, and Linda S. Schadler. *J. Polym. Sci., Part B: Polym. Phys.*, 44(20):2944–2950, OCT 15 2006.

[13] J Baschnagel and F Varnik. *J. Phys.: Condens. Matter*, 17:R851, 2005.

[14] G Beaucage, R Composto, and RS Stein. *Journal of Polymer Science, Part B: Polymer Physics*, 31:319, 1993.

[15] M Bhattacharya, MK Sanyal, T Geue, and U Pietsch. *Physical Review E*, 71:041801, 2005.

[16] I Borukhov and L Leibler. *Macromolecules*, 35(13):5171–5182, JUN 18 2002.

[17] Itamar Borukhov and Ludwik Leibler. *Physical Review E*, 62:R41, 2000.

[18] Francoise Brochard-Wyart, Jean-Marc di Meglio, David Quere, and Pierre-Gilles de Gennes. *Langmuir*, 7:335, 1991.

[19] G. Brown, A. Chakrabarti, and J.F. Marko. *Europhysics Letters*, 25:239, 1994.

[20] G Brown, A Chakrabarti, and JF Marko. *Macromolecules*, 28:7817, 1995.

[21] H. R. Brown, K. Char, V. R. Deline, and P.F. Green. *Macromolecules*, 26:4155, 1993.

[22] I. Carmesin and K. Kremer. *Macromolecules*, 21:2819, 1988.

[23] Amitabha Chakrabarti and Raul Toral. *Macromolecules*, 23:2016–2021, 1990.

[24] K. Char, H. R. Brown, and V. R. Deline. *Macromolecules*, 26:4164, 1993.

[25] C Chevigny, J Jestin, D Gigmes, R Schweins, E Di-Cola, F Dalmas, D Bertin, and F Boue. *Macromolecules ASAP*, 2010.

[26] Terence Cosgrove, Timothy Heath, Boudewijin Van Lent, Frans Leermakers, and Jan Scheutjens. *Macromolecules*, 20:1692–1696, 1987.

[27] J. Crank and P. Nicolson. *Proc. Camb. Phil. Soc.*, 43:50–67, 1947.

[28] A Crosby. Private communication. 2011.

[29] M. Dadmun. *Macromolecules*, 29:3868, 1996.

[30] Chi-An Dai, Benita J. Dair, Kevin H. Dai, Christopher K. Ober, Edward J. Kramer, Chung-Yuen Hui, and Lynn W. Jelinski. *Physical Review Letters*, 73:2472, 1994.

[31] N. Dan and M. Tirrell. *Macromolecules*, 25:2890–2895, 1992.

[32] M. Daoud and J.P. Cotton. *Journal de Physique*, 43:531–538, 1982.

[33] P. G. de Gennes. *Macromolecules*, 13:1069–1075, 1980.

[34] P. G. de Gennes. *European Physical Journal E*, 2:201, 2000.

[35] GB DeMaggio, WE Frieze, DW Gidley, M Zhu, HA Hristov, and AF Yee. *Phys. Rev. Lett.*, 78:1524, 1997.

[36] FA Detcheverry, G Liu, PF Nealey, and JJ de Pablo. *Macromolecules*, 43:3446, 2010.

[37] FA Detcheverry, PF Nealey, and JJ de Pablo. *Macromolecules*, 43:6495, 2010.

[38] H. P. Deutsch and K. Binder. *Journal of Chemical Physics*, 94:1991, 1991.

[39] EA Di Marzio. *Journal of Chemical Physics*, 42:2101, 1965.

[40] Aui Dong, John F. Marko, and Thomas A. Witten. *Macromolecules*, 27:6428, 1994.

[41] F Drolet and GH Fredrickson. *Macromolecules*, 34:5317, 2001.

[42] Douglas Dukes, Yu Li, Sarah Lewis, Brian Benicewicz, Linda Schadler, and Sanat K. Kumar. *Macromolecules*, 43(3):1564–1570, FEB 9 2010.

[43] SR Edgecombe, JM Gardiner, and MW Matsen. *Macromolecules*, 35(16):6475–6477, JUL 30 2002.

[44] S F Edwards and K F Freed. *Journal of Physics A: General Physics*, 2:145–150, 1969.

[45] S.F. Edwards. *Proc. Phys. Soc.*, 85:613, 1965.

[46] S. A. Egorov. *J. Chem. Phys.*, 129(6):064901, 2008.

[47] CJ Ellison and JM Torkelson. *Nature Materials*, 2:695, 2003.

[48] PG Ferreira, A Ajdari, and L Leibler. *Macromolecules*, 31(12):3994–4003, JUN 16 1998.

[49] P.G. Ferreira and L. Leibler. *Journal of Chemical Physics*, 105:9362, 1996.

[50] TD Fornes, DL Hunter, and DR Paul. *Macromolecules*, 37(5):1793–1798, MAR 9 2004.

[51] JA Forrest, K Dalnoki-Veress, and JR Dutcher. *Physical Review E*, 56:5705, 1997.

[52] JA Forrest, K Dalnoki-Veress, JR Stevens, and JR Dutcher. *Physical Review Letters*, 77:2002, 1996.

[53] GH Fredrickson. *The Equilibrium Theory of Inhomogeneous Polymers*. Oxford University Press, 2006.

[54] Glenn H. Fredrickson, Venkat Ganesan, and Francois Drolet. *Macromolecules*, 35:16–39, 2002.

[55] Glenn H. Fredrickson, Scott T. Milner, and Ludwik Leibler. *Macromolecules*, 25:6341, 1992.

[56] DS Fryer, RD Peters, EJ Kim, JE Tomaszewski, JJ de Pablo, PF Nealey, CC White, and WL Wu. *Macromolecules*, 34:5627, 2001.

[57] V. Ganesan, C. J. Ellison, and V. Pryamitsyn. Mean-field models of structure and dispersion of polymer-nanoparticle mixtures. *Soft Matter*, 6:4010, 2010.

[58] T. Garel, D. A. Huse, S. Leibler, and H. Orland. *Europhysics Letters*, 8:9, 1989.

[59] C Gay. *Macromolecules*, 30(19):5939–5943, SEP 22 1997.

[60] C Gay and E Raphael. *Journal de Physique II*, 6(5):587–591, MAY 1996.

[61] S Ge, L Guo, MH Rafailovich, J Sokolov, RM Overney, C Buenviaje, DG Peiffer, and SA Schwarz. *Langmuir*, 17:1687, 2001.

[62] Dilip Gersappe and Anna C. Balazs. *Physical Review E*, 52:5061, 1995.

[63] Dilip Gersappe, Michael Fasolka, Rafel Israels, and Anna C. Balazs. *Macromolecules*, 28:4753, 1995.

[64] Dilip Gersappe, Weixiong Li, and Anna C. Balazs. *Journal of Chemical Physics*, 99:7209, 1993.

[65] EP Giannelis, R Krishnamoorti, and E Manias. Polymer-silicate nanocomposites: Model systems for confined polymers and polymer brushes. In *Polymers in Confined Environments*, volume 138 of *Advances in Polymer Science*, pages 107–147. Springer-Verlag Berlin, 1999.

[66] David L. Green and Jan Mewis. *Langmuir*, 22(23):9546–9553, NOV 7 2006.

[67] Gary S. Grest. *J. Chem. Phys.*, 105(13):5532–5541, 1996.

[68] Y Grohens, M Brogly, C Labbe, MO David, and J Schulze. *Langmuir*, 14:2929, 1998.

[69] N Grossiord, J Loos, O Regev, and CE Koning. *Chemistry of Materials*, 18(5):1089–1099, MAR 7 2006.

[70] Sujin Ham, Changhak Shin, Eunhye Kim, Du Yeol Ryu, Unyong Jeong, Thomas P. Russell, and Craig J. Hawker. *Macromolecules*, 41:6431, 2008.

[71] E Han, KO Stuen, M Leolukman, CC Liu, PF Nealey, and P Gopalan. *Macromolecules*, 42:4896, 2009.

[72] Eungnak Han, Karl O. Stuen, Young-Hye La, Paul F. Nealey, and Padma Gopalan. *Macromolecules*, 41:9090, 2008.

[73] G.R. Harper, M.C. Davies, S.S. Davis, Th.F. Tadros, D.C. Taylor, M.P. Irving, and J.A Waters. *Biomaterials*, 12:695 – 700, 1991.

[74] Shane E. Harton and Sanat K. Kumar. *J. Polym. Sci., Part B: Polym. Phys.*, 46(4):351–358, FEB 15 2008.

[75] Ryuichi Hasegawa, Yuji Aoki, and Masao Doi. *Macromolecules*, 29:6656–6662, 1996.

[76] E Helfand. *Macromolecules*, 25(6):1676–1685, MAR 16 1992.

[77] G Henn, DG Bucknall, M Stamm, P Vanhoorne, and R Jerome. *Macromolecules*, 29:4305, 1996.

[78] J Hilding, EA Grulke, ZG Zhang, and F Lockwood. *Journal of Dispersion Science and Technology*, 24(1):1–41, 2003.

[79] E. Huang, S. Pruzinsky, T.P. Russell, J Mays, and C.J. Hawker. *Macromolecules*, 32:5299, 1999.

[80] E. Huang, T.P. Russell, C. Harrison, P.M. Chaikin, R.A. Register, C.J Hawker, and J Mays. *Macromolecules*, 31:7641, 1998.

[81] L. Illum and S.S. Davis. *FEBS Letters*, 167:79 – 82, 1984.

[82] Jacob Israelachvili. *Intermolecular and Surface Forces*. Academic Press, 1991.

[83] Arthi Jayaraman and Kenneth S. Schweizer. *Macromolecules*, 41(23):9430–9438, DEC 9 2008.

[84] Arthi Jayaraman and Kenneth S. Schweizer. *Macromolecules*, 42(21):8423–8434, NOV 10 2009.

[85] Shengxiang Ji, Wen Liao, and Paul F. Nealey. *Macromolecules*, 43:6919, 2010.

[86] RL Jones, L Kane, and RJ Spontak. *Chem. Eng. Sci.*, 51:1365, 1996.

[87] O Kahle, U Wielsch, H Metzner, J Bauer, C Uhlig, and C Zawatzki. *Thin Solid Films*, 313-314:803, 1998.

[88] T Kajiyama, K Tanaka, N Satomi, and A Takahara. *Macromolecules*, 31:5150, 1998.

[89] T Kajiyama, K Tanaka, and A Takahara. *Polymer*, 39:4665, 1998.

[90] S. Y. Kamath and M. D. Dadmun. *Macromolecular Theory and Simulations*, 14:519, 2005.

[91] T Kanaya, T Miyazaki, H Watanabe, K Nishida, H Yamano, S Tasaki, and DB Bucknall. *Polymer*, 44:3769, 2003.

[92] S Kawana and RAL Jones. *Physical Review E*, 63:021501, 2001.

[93] JL Keddie, RAL Jones, and RA Cory. *Europhysics Letters*, 27:59, 1994.

[94] JL Keddie, RAL Jones, and RA Cory. *Faraday Discuss.*, 98:219, 1994.

[95] T Kerle, R Yerushalmi-Rozen, and J Klein. *Macromolecules*, 31:422, 1998.

[96] B. Kim, D. Y. Ryu, V. Pryamitsyn, and V. Ganesan. Dewetting of pmma on ps-brush substrates. *Macromolecules*, 42(20):7919–7923, October 2009.

[97] J. U. Kim and M. W. Matsen. *European Physical Journal E*, 23:135–144, 2007.

[98] Jaeup U. Kim and Mark W. Matsen. *Macromolecules*, 41:246–252, 2008.

[99] Jaeup U. Kim and Mark W. Matsen. *Macromolecules*, 41:4435–4443, 2008.

[100] Jaeup U. Kim and Ben O'Shaughnessy. *Macromolecules*, 39:413–425, 2006.

[101] Jenny Kim and Peter F. Green. *Macromolecules*, 43(3):1524–1529, FEB 9 2010.

[102] JH Kim, J Jang, DY Lee, and WC Zin. *Macromolecules*, 35:311, 2001.

[103] JH Kim, J Jang, and WC Zin. *Langmuir*, 16:4064, 2000.

[104] JH Kim, J Jang, and WC Zin. *Langmuir*, 17:2703, 2001.

[105] S Kim, CB Roth, and JM Torkelson. *Journal of Polymer Science Part B: Polymer Physics*, 46:2754, 2008.

[106] J. Klos and T. Pakula. *J. Chem. Phys.*, 118(16):7682–7689, 2003.

[107] J Klos and T Pakula. *Macromolecules*, 37(21):8145–8151, OCT 19 2004.

[108] Nikhil A. Koratkar, Jonghwan Suhr, Amit Joshi, Ravi S. Kane, Linda S. Schadler, Pulickel M. Ajayan, and Steve Bartolucci. *Applied Physics Letters*, 87(6):063102, 2005.

[109] JM Kropka, V Pryamitsyn, and V Ganesan. *Phys. Rev. Lett.*, 101:075702, 2008.

[110] Pik-Yin Lai. *Journal of Chemical Physics*, 100:3351, 1994.

[111] Jin Ho Lee, Hai Bang Lee, and Joseph D. Andrade. *Progress in Polymer Science*, 20:1043 – 1079, 1995.

[112] Michelle D. Lefebvre, Christine M. Dettmer, Rachel L. McSwain, Chen Xu, Jonathan R. Davila, Russell J. Composto, SonBinh T. Nguyen, and Kenneth R. Shull. *Macromolecules*, 38:10494, 2005.

[113] L Leibler, A Ajdari, A Mourran, G Coulon, and D Chatenay. Wetting of grafted polymer surfaces by compatible chains. In Teramoto, A and Kobayashi, M and Norisuye, T, editor, *Ordering in Macromolecular Systems*, pages 301–311. Springer-verlag, Berlin, 1994.

[114] L Leibler and A Mourran. *MRS Bulletin*, 22(1):33–37, JAN 1997.

[115] B. Van Lent, R. Israels, J. M. H. M. Scheutjens, and G. J. Fleer. *Journal of Colloid and Interface Science*, 137(2):380 – 394, 1990.

[116] C. N. Likos, H. Löwen, M. Watzlawek, B. Abbas, O. Jucknischke, J. Allgaier, and D. Richter. *Phys. Rev. Lett.*, 80:4450–4453, May 1998.

[117] Eric K. Lin and Alice P. Gast. *Macromolecules*, 29:390–397, 1996.

[118] JEG Lipson and ST Milner. *European Physical Journal B*, 72:133, 2009.

[119] Y Liu, MH Rafailovich, J Sokolov, SA Schwarz, and S Bahal. *Macromolecules*, 29:899, 1996.

[120] Y Liu, MH Rafailovich, J Sokolov, SA Schwarz, X Zhong, A Eisenberg, EJ Kramer, BB Sauer, and S Satija. *Phys. Rev. Lett.*, 73:440, 1994.

[121] D Long, A Ajdari, and L Leibler. *Langmuir*, 12:1675, 1996.

[122] D Long, A Ajdari, and L Leibler. *Langmuir*, 12:5221, 1996.

[123] D Long and F Lequeux. *European Physical Journal E*, 4:371, 2001.

[124] Vladimir I. Lozinsky, Irina A. Simenel, Valentina K. Kulakova, Elena A. Kurskaya, Tatyana A. Babushkina, Tamara P. Klimova, Tatyana V. Burova, Alexander S. Dubovik, Valerij Ya. Grinberg, Igor Yu. Galaev, Bo Mattiasson, and Alexei R. Khokhlov. *Macromolecules*, 36:7308, 2003.

[125] JH Maas, GJ Fleer, FAM Leermakers, and MA Cohen Stuart. *Langmuir*, 18:8871, 2002.

[126] JH Maas, FAM Leermakers, GJ Fleer, and MA Cohen Stuart. *Macromol. Symp.*, 191:69, 2003.

[127] Luis G. MacDowell and Marcus Muller. *J. Chem. Phys.*, 124(8):084907, 2006.

[128] Ravish Malik, Carol K. Hall, and Jan Genzer. *Macromolecules*, 43:5149, 2010.

[129] P Mansky, Y Liu, E Huang, TP Russell, and CJ Hawker. *Science*, 275(5305):1458–1460, MAR 7 1997.

[130] P. Mansky and T.P Russell. *Macromolecules*, 30:6810, 1997.

[131] J. F. Marko and T. A. Witten. *Macromolecules*, 25:296, 1992.

[132] JI Martin and ZG Wang. *Journal of Physical Chemistry*, 99(9):2833–2844, MAR 2 1995.

[133] M. W. Matsen. *Journal of Chemical Physics*, 117:2351, 2002.

[134] M. W. Matsen. *Journal of Chemical Physics*, 121:1938, 2004.

[135] M. W. Matsen. *J. Chem. Phys.*, 122(14):144904, 2005.

[136] M. W. Matsen and J. M. Gardiner. *J. Chem. Phys.*, 115(6):2794–2804, 2001.

[137] M. W. Matsen and J. M. Gardiner. *Journal of Chemical Physics*, 118:3775, 2003.

[138] MW Matsen. *Journal of Chemical Physics*, 106:7781, 1997.

[139] M.W. Matsen and G.H. Griffiths. *The European Physical Journal E*, 29:219, 2009.

[140] MW Matsen and M Schick. *Macromolecules*, 27:187, 1994.

[141] MW Matsen and RB Thompson. *Journal of Chemical Physics*, 111:7139, 1999.

[142] J Mattsson, JA Forrest, and L Borjesson. *Physical Review E*, 62:5187, 2000.

[143] JD McCoy and JG Curro. *Journal of Chemical Physics*, 116:9154, 2002.

[144] Maura McEwan and David Green. *Soft Matter*, 5(8):1705–1716, 2009.

[145] Luciana Meli, Abraham Arceo, and Peter F. Green. *Soft Matter*, 5(3):533–537, 2009.

[146] Dong Meng and Qiang Wang. *Soft Matter*, 6:5819, 2010.

[147] S. T. Milner, T. A. Witten, and M. E. Cates. *Macromolecules*, 21:2610–2619, 1988.

[148] Scott T. Milner and Glenn H. Fredrickson. *Macromolecules*, 28:7953, 1995.

[149] T Miyazaki, K Nishida, and T Kanaya. *Physical Review E*, 69:061803, 2004.

[150] Mohammad Moniruzzaman and Karen I. Winey. *Macromolecules*, 39(16):5194–5205, AUG 8 2006.

[151] TL Morkved, M Lu, AM Urbas, EE Ehrichs, HM Jaeger, P Mansky, and TP Russell. *Science*, 273:931, 1996.

[152] Michael Murat and Gary S. Grest. *Macromolecules*, 22:4054–4059, 1989.

[153] Michael Murat and Gary S. Grest. *Macromolecules*, 24:704–708, 1991.

[154] B Narayanan and V Ganesan. *Phys. Fluids*, 18:042109, 2006.

[155] B Narayanan, VA Pryamitsyn, and V Ganesan. *Macromolecules*, 37:10180, 2004.

[156] WJ Ortis, JH van Zanten, WL Wu, and SK Satija. *Phys. Rev. Lett.*, 71:867, 1993.

[157] Donald E. Owens III and Nicholas A. Peppas. *International Journal of Pharmaceutics*, 307:93–102, 2006.

[158] T Pakula, D Vlassopoulos, G Fytas, and J Roovers. *Macromolecules*, 31(25):8931–8940, DEC 15 1998.

[159] C Pastorino, K Binder, and M Muller. *Macromolecules*, 42:401, 2008.

[160] Galen T. Pickett. *Journal of Chemical Physics*, 118:3898, 2003.

[161] GT Pickett and AC Balazs. *Macromolecules*, 30:3097, 1997.

[162] GT Pickett, TA Witten, and SR Nagel. *Macromolecules*, 26:3194, 1993.

[163] DJ Pochan, EK Lin, SK Satija, and WL Wu. *Macromolecules*, 34:3041, 2001.

[164] I. I. Potemkin. *Macromolecules*, 37:3505, 2004.

[165] RD Priestley, LJ Broadbelt, JM Torkelson, and K Fukao. *Physical Review E*, 75:061806, 2007.

[166] V Pryamitsyn and V Ganesan. *Macromolecules*, 43:5851, 2010.

[167] Victor Pryamitsyn and Venkat Ganesan. *Macromolecules*, 39:8499–8510, 2006.

[168] Victor Pryamtisyn, Venkat Ganesan, Athanassios Z. Panagiotopoulos, Hongjun Liu, and Sanat K. Kumar. Modeling the anisotropic self-assembly of spherical polymer-grafted nanoparticles. *The Journal of Chemical Physics*, 131(22):221102, 2009.

[169] E Raphael, P Pincus, and GH Fredrickson. *Macromolecules*, 26(8):1996–2006, APR 12 1993.

[170] G Reiter, P Auroy, and L Auvray. *Macromolecules*, 29(6):2150–2157, MAR 11 1996.

[171] G Reiter and R Khanna. *Phys. Rev. Lett.*, 85:5599, 2000.

[172] GS Reiter, P Auroy, and L Auvray. *Europhysics Letters*, 33:29, 1996.

[173] C Ren, K Chen, and YQ Ma. *Journal of Chemical Phyics*, 122:154904, 2005.

[174] Jiunn-Ren Roan and Toshihiro Kawakatsu. *The Journal of Chemical Physics*, 116:7283–7294, 2002.

[175] JF Rong, ZH Jing, HQ Li, and M Sheng. *Macromolecular Rapid Communications*, 22(5):329–334, MAR 26 2001.

[176] R Ruiz, H Kang, FA Detcheverry, E Dobisz, CS Kercher, TR Albrecht, JJ de Pablo, and PF Nealey. *Science*, 321:936, 2008.

[177] GM Russo, GP Simon, and L Incarnato. *Macromolecules*, 39(11):3855–3864, MAY 30 2006.

[178] T Sato, H Watanabe, K Osaki, and ML Yao. *Macromolecules*, 29(11):3881–3889, MAY 20 1996.

[179] N Satomi, A Takahara, and T Kajiyama. *Macromolecules*, 32:4474, 1999.

[180] Arezou Seifpour, Philip Spicer, Nitish Nair, and Arthi Jayaramana. *The Journal of Chemical Physics*, 132:164901, 2010.

[181] A. N. Semenov. *Macromolecules*, 26:2273, 1993.

[182] James J. Semler, Young K. Jhon, Alan Tonelli, Martin Beevers, Ramanan Krishnamoorti, and Jan Genzer. *Advanced Materials*, 19:2877, 2007.

[183] M Shah and V Ganesan. *Journal of Chemical Physics*, 130:054904, 2009.

[184] M Shah and V Ganesan. *Macromolecules*, 43:543, 2010.

[185] Kenneth R. Shull, Edward J. Kramer, Kenneth R. Shull'tt, and Edward J. Kramer. *Macromolecules*, 23:4780, 1990.

[186] KR Shull. *Macromolecules*, 25:2122, 1992.

[187] KR Shull. *Faraday Discuss.*, 98:203–217, 1994.

[188] A Sikorski, A Kolinski, and J Skolnick. *Macromolecular Theory and Simulations*, 3(4):715–729, JUL 1994.

[189] L Singh, PJ Ludovice, and CL Henderson. *Thin Solid Films*, 449:231, 2004.

[190] Archie P. Smith, Amit Sehgal, Jack F. Douglas, Alamgir Karim, and Eric J. Amis. *Macromolecular Rapid Communications*, 24:131, 2003.

[191] Grant D. Smith and Dmitry Bedrov. *Langmuir*, 25(19):11239–11243, OCT 6 2009.

[192] LH Sterling, editor. *Introduction to Physical Polymer Science*. John Wiley and Sons, Inc, 2001.

[193] Gert Storm, Sheila O. Belliot, Toos Daemen, and Danilo D. Lasic. *Advanced Drug Delivery Reviews*, 17:31 – 48, 1995.

[194] MP Stoykovich, M Muller, SO Kim, HS Harun, EW Edwards, JJ de Pablo, and PF Nealey. *Science*, 308:1442, 2005.

[195] L. Anderson Strickland, Carol K. Hall, and Jan Genzer. *Macromolecules*, 42:9063, 2009.

[196] Alberto Striolo and S. A. Egorov. *J. Chem. Phys.*, 126(1), JAN 7 2007.

[197] Hyo Seon Suh, Huiman Kang, Paul F. Nealey, and Kookheon Char. *Macromolucules*, 43:4744, 2010.

[198] M. Surve, V. Pryamitsyn, and V. Ganesan. Depletion and pair interactions of proteins in polymer solutions. *Journal of Chemical Physics*, 122(15):154901, April 2005.

[199] M. Surve, V. Pryamitsyn, and V. Ganesan. Nanoparticles in solutions of adsorbing polymers: Pair interactions, percolation, and phase behavior. *Langmuir*, 22(3):969–981, January 2006.

[200] M. Surve, V. Pryamitsyn, and V. Ganesan. Polymer-bridged gels of nanoparticles in solutions of adsorbing polymers. *Journal of Chemical Physics*, 125(6):064903, August 2006.

[201] M. Surve, V. Pryamitsyn, and V. Ganesan. Dispersion and percolation transitions of nanorods in polymer solutions. *Macromolecules*, 40(2):344–354, January 2007.

[202] RS Tate, DS Fryer, S Pasqualini, MF Montague, JJ de Pablo, and PF Nealey. *Journal of Chemical Physics*, 115:9982, 2001.

[203] T Thurn-Albrecht, J Schotter, GA Kastle, N Emley, T Shibauchi, L Krusin-Elbaum, K Guarini, CT Black, MT Tuominen, and TP Russell. *Science*, 290:2126, 2000.

[204] JA Torres, PF Nealey, and JJ de Pablo. *Phys. Rev. Lett.*, 85:3221, 2000.

[205] David Trombly and Venkat Ganesan. *J. Polym. Sci., Part B: Polym. Phys.*, 47(24, Sp. Iss. SI):2566–2577, DEC 15 2009.

[206] DM Trombly, V Pryamitsyn, and V Ganesan. *Journal of Chemical Physics*, 134:154903, 2011.

[207] TM Truskett and V Ganesan. *Journal of Chemical Physics*, 119:1897, 2003.

[208] Y Tsori and D Andelman. *Macromolecules*, 36:8560, 2003.

[209] O. K. C. Tsui, T. P. Russell, and C. J. Hawker. *Macromolecules*, 34:5535, 2001.

[210] MS Turner. *Physical Review Letters*, 69:1788, 1992.

[211] JH van Zanten, WE Wallace, and WL Wu. *Physical Review E*, 53:R2053, 1996.

[212] A Voronov and O Shafranska. *Langmuir*, 18:4471, 2002.

[213] WE Wallace, JH van Zanten, and WL Wu. *Physical Review E*, 52:R3329, 1995.

[214] DG Walton, GJ Kellogg, AM Mayes, P Lambooy, and TP Russell. *Macromolecules*, 27:6225, 1994.

[215] Q Wang. *Macromolecular Theory and Simulations*, 14:96, 2005.

[216] Q Wang, SK Nath, MD Graham, PF Nealey, and JJ de Pablo. *Journal of Chemical Physics*, 112:9996, 2000.

[217] Q Wang, PF Nealey, and JJ de Pablo. *Macromolecules*, 34:3458, 2001.

[218] Q Wang, PF Nealey, and JJ de Pablo. *Macromolecules*, 36:1731, 2003.

[219] Q Wang, Y Qiliang, PF Nealey, and JJ de Pablo. *Journal of Chemical Physics*, 112:450, 2000.

[220] Q Wang, Q Yan, PF Nealey, and JJ de Pablo. *Macromolecules*, 33:4512, 2000.

[221] S.C. Warren, L.C. Messina, L.S. Slaughter, Kamperman, Zhou M., S.M. Gruner, F.J. DiSalvo, and U. Wiesner. *Science*, 320:1748, 2008.

[222] H Watanabe. *Acta Polymerica*, 48(7):215–233, JUL 1997.

[223] H Watanabe and Y Matsumiya. *Macromolecules*, 38(9):3808–3819, MAY 3 2005.

[224] C. M. Wijmans and E. B. Zhulina. *Macromolecules*, 26:7214–7224, 1993.

[225] CM Wijmans, EB Zhulina, and GJ Fleer. *Macromolecules*, 27(12):3238–3248, JUN 6 1994.

[226] D.R.M. Williams and P.A. Pincus. *Europhysics Letters*, 24:29–34, 1993.

[227] T. A. Witten and P. A. Pincus. *Macromolecules*, 19:2509–2513, 1986.

[228] WL Wu, JH van Zanten, and WJ Ortis. *Macromolecules*, 28:771, 1995.

[229] L Xie, GB DeMaggio, WE Frieze, J DeVries, DW Gidley, HA Hristov, and AF Yee. *Phys. Rev. Lett.*, 74:4947, 1995.

[230] J Xu, F Qiu, H Zhang, and Y Yang. *J. Polym. Sci., Part B: Polym. Phys.*, 44:2811–2820, 2006.

[231] X Ye, BJ Edwards, and B Komami. *Macromolecules*, 43:9594, 2010.

[232] C. Yeung, Anna C. Balazs, and David Jasnow. *Macromolecules*, 25:1357, 1992.

[233] X Zhang, FK Lee, and OKC Tsui. *Macromolecules*, 41:8148, 2008.

[234] E. B. Zhulina, O. V. Borisov, and L. Brombacher. *Macromolecules*, 24:4679–4690, 1991.

[235] E. B. Zhulina, O. V. Borisov, V. A. Pryamitsyn, and T. M. Birshtein. *Macromolecules*, 24:140–149, 1991.

[236] EB Zhulina and A Halperin. *Macromolecules*, 25:5730, 1992.

[237] Ekaterina Zhulina and Anna C. Balazs. *Macromolecules*, 29:2667, 1996.

[238] Ekaterina B. Zhulina, Oleg V. Borisov, and Victor A. Priamitsyn. *Journal of Colloid and Interface Science*, 137:495 – 511, 1990.

Vita

David Matthew Trombly was born in Woodland, CA on 19 August 1982, and grew up in the nearby town of Davis. He received his Bachelor of Science degree in Chemical Engineering from the University of California, Davis in 2006. He began his graduate studies in Chemical Engineering at the University of Texas at Austin in August 2006.

Permanent address: 214 Jalisco Pl.
Davis, CA 95616

This dissertation was typeset with LaTeX[†] by the author.

[†]LaTeX is a document preparation system developed by Leslie Lamport as a special version of Donald Knuth's TeX Program.